

50280

50280/

1133

ACTA UNIVERSITATIS SZEGEDIENSIS

ACTA PHYSICA ET CHEMICA

50280

NOVA SERIES

TOMUS XXII

FASCICULI 1-4

AUSHAF 22 (1-4) 1-136 (1976)

HU ISSN 0001-6721



SZEGED, HUNGARIA
1976

50280

ACTA UNIVERSITATIS SZEGEDIENSIS

ACTA PHYSICA ET CHEMICA

NOVA SERIES

TOMUS XXII

FASCICULI 1—4

AUSHAF 22 (1—4) 1—136 (1976)

HU ISSN 0001—6721



SZEGED, HUNGARIA
1976

Adiuvantibus

M. BARTÓK, L. CSÁNYI, J. CSÁSZÁR, P. FEJES, F. GILDE, P. HUHN,
I. KETSKEMÉTY, F. MÁRTA, L. SZALAY et F. SZÁNTÓ

Redigit

KÁLMÁN KOVÁCS

Edit

Facultas Scientiarum Naturalium Universitatis Szegediensis de
Attila József nominatae

Editionem curant

J. ANDOR, L. BALÁSPIRI, I. BÁRDI, G. BERNÁTH, E. BOGA,
J. SCHNEIDER et Á. SÜLI

Nota

Acta Phys. et Chem. Szeged

Szerkeszti

KOVÁCS KÁLMÁN

A szerkesztőbizottság tagjai:

BARTÓK M., CSÁNYI L., CSÁSZÁR J., FEJES P., GILDE F., HUHN P.,
KETSKEMÉTY I., MÁRTA F., SZALAY L. és SZÁNTÓ F.

Kiadja

a József Attila Tudományegyetem Természettudományi Kara
(Szeged, Aradi vértanúk tere 1.)

Szerkesztőbizottsági titkárok:

ANDOR J., BALÁSPIRI L., BÁRDI I., BERNÁTH G., BOGA E.,
SCHNEIDER J. és SÜLI Á.

Kiadványunk rövidítése:

Acta Phys. et Chem. Szeged

MULTIPLE SCATTERING $X\alpha$ TREATMENT OF SCATTERING STATES OF CLUSTERS

By

I. K. GYÉMÁNT, M. G. BENEDICT, GY. PAPP

Institute of Theoretical Physics, Attila József University, Szeged

and

B. VASVÁRI

Central Research Institute for Physics, Budapest

(Received February 1, 1976)

The multiple scattering $X\alpha$ method seems to be an appropriate tool to handle scattering states of clusters. We formulate the solution of the scattering problem in the language used by Johnson to determine bound states of clusters.

The $X\alpha$ potential approximation combined with the multiple scattering method has turned out to be a very effective and successful computational scheme in determining bound states of polyatomic molecules [1]. JOHN and ZISCHE [2, 3] have shown how to treat scattering states of clusters by this multiple scattering (MS) method, but the equations they derived can be applied only for potentials constant outside the — not necessarily spherically symmetric — muffin tin regions (no Watson sphere). This restriction, however, can be removed as DILL and DEHMER and ZIESCHE have recently pointed out [4, 5]. We want to show in this paper, that with a slight modification of the existing computer programs [6] phase shifts of clusters with Watson sphere can be determined. Note that the method of JOHNSON and that of JOHN and ZIESCHE are equivalent.

First we summarize the MS method in the muffin tin approximation [1]. The space is partitioned into regions of three types:

- (I) Atomic region, consisting of atomic spheres containing an atomic nucleus at their center \vec{R}_p ($p=1, 2, \dots, N$). In the p -th atomic sphere of radius b_p the potential V_p is taken to be spherically symmetric.
- (III) Outer region, defined by $|\vec{r}-\vec{R}_0| \geq b_0$, where b_0 is the radius of the so called Watson sphere containing the atomic region and centered at \vec{R}_0 . The potential V_0 in this region is spherically symmetric.
- (II) Interatomic region, bounded by regions (I) and (III). In this region the volume averaged potential is \bar{V} .

The one-electron wave functions of the cluster are the solutions of the Schrödinger equation

$$[\Delta + k^2 - V(\vec{r})]\psi = 0 \quad (1)$$

where $k^2 = E$ and $V(\vec{r})$ is the spherically or volume averaged cluster potential.

Within the p -th atomic sphere the solution can be expanded into partial waves

$$\psi^p(\vec{r}_p) = \sum_L C_L^p R_L^p(k; r_p) Y_L(\hat{r}_p) \quad (0 \leq r_p \leq b_p) \quad (2)$$

where $\vec{r}_p = \vec{r} - \vec{R}_p$, $L \equiv (l, m)$ and the functions R_L^p are solutions of the radial equation

$$\left[-\frac{1}{r^2} \frac{d}{dr} r^2 \frac{d}{dr} + \frac{l(l+1)}{r^2} + V^p(r) - k^2 \right] R_L^p(k; r) = 0 \quad (3)$$

These solutions can be obtained by outward numerical integration as they must be regular at the center $r=0$. In the outer region the cluster wave functions can be written in the form

$$\psi^0(\vec{r}_0) = \sum_L D_L^0 R_L^0(k; r_0) Y_L(\hat{r}_0) \quad (b_0 \leq r_0) \quad (4)$$

where $\vec{r}_0 = \vec{r} - \vec{R}_0$, and the functions R_L^0 satisfy the radial equation (3), but with $V_0(r)$ instead of $V_p(r)$. For bound states the functions R_L^0 must decay exponentially at large distances, so that R_L^0 can be generated by inward numerical integration.

In the interatomic region we can write the solution of Eq(1) in the form

$$\psi_{II}(\vec{r}) = \sum_p \sum_L A_L^p F_L(\kappa r_p) Y_L(\hat{r}_p) + \sum_L B_L^0 J_L(\kappa r_0) Y_L(\hat{r}_0) \quad (5)$$

where $\kappa = \sqrt{|E - \bar{V}|}$ and

$$F_L = \begin{cases} k_l^1, & E < \bar{V} \\ n_l, & E > \bar{V} \end{cases}; \quad J_L = \begin{cases} i_l, & E < \bar{V} \\ j_l, & E > \bar{V} \end{cases} \quad (6)$$

(Here we have used Bessel functions j_l, n_l, i_l, k_l^1 , as they were used in [1].)

Requiring the continuity of the wave functions and their first derivatives, we are led to a system of linear homogeneous equations [1]:

$$\begin{aligned} \sum_{p'} \sum_{L'} [T^{-1}(E)]_{LL'}^{pp'} A_{L'}^{p'} + \sum_{L'} S_{LL'}^{p_0}(E) B_{L'}^{p_0} &= 0 \\ \sum_{p'} \sum_{L'} S_{LL'}^{p_0}(E) A_{L'}^{p'} + \sum_{L'} \delta_{LL'} [g_L^0(E)]^{-1} B_{L'}^{p_0} &= 0 \end{aligned} \quad (7)$$

in which $[T^{-1}(E)]_{LL'}^{pp'} = \delta_{pp'} \delta_{LL'} [t_L^p(E)]^{-1} + (1 - \delta_{pp'}) G_{LL'}^{pp'}(E)$

$$g_L^0(E) = \frac{[F_L, R_L^0]_{b_p}}{[J_L, R_L^0]_{b_0}} \quad t_L^p(E) = \frac{[J_L, R_L^p]_{b_p}}{[F_L, R_L^p]_{b_p}}$$

$$G_{LL'}^{pp'}(E) = 4\pi \sum_{L''} s(L'', L, L'; E) I_{L''}(L, L') F_{L''}(\kappa R_{pp'}) Y_{L''}(\hat{R}_{pp'})$$

$$S_{LL'}^{p_0}(E) = 4\pi \sum_{L''} s(L'', L, L'; E) I_{L''}(L, L') J_{L''}(\kappa R_{p_0}) Y_{L''}(\hat{R}_{p_0})$$

Here $s(L'', L, L'; E) = \begin{cases} (-1)^{l+l'}, & E < \bar{V} \\ i^{l-l'-l''}, & E > \bar{V} \end{cases}$

$$[J_l, R_l^p]_{b_p} = \left(J_l(\chi r) \frac{dR_l^p}{dr} - R_l^p \frac{dJ_l(\chi r)}{dr} \right)_{r=b_p}$$

$$\bar{R}_{pp'} = \bar{R}_{p'} - \bar{R}_p; \quad \bar{R}_{p0} = \bar{R}_0 - \bar{R}_p$$

and $I_{L'}(L; L')$ are the Gaunt integrals. The continuity requires also

$$C_L^p = (\chi b_p^2 \sigma_l(E) [J_l, R_l^p]_{b_p})^{-1} A_L^p; \quad \sigma_l(E) = \begin{cases} (-1)^{l+l'}, & E < \bar{V} \\ 1, & E > \bar{V} \end{cases} \quad (8)$$

$$D_L^0 = (-\chi b_0^2 \sigma_l(E) [F_l, R_l^0]_{b_0})^{-1} B_L^0;$$

These equations have been programmed and used very efficiently in SCF calculations treating localized electronic charge distribution of clusters [1].

In the case of scattering states ($E > 0$), the only difference is in the boundary conditions satisfied by the functions R_l^0 at large distances. If the potential $V_0(r_0)$ tends to zero sufficiently rapidly as r_0 tends to infinity, or, to be more definite, V_0 vanishes outside a sphere of radius R

$$V_0(r_0) = 0 \quad r_0 > R > b_0.$$

DEMCOV and RUDAKOV [7] have shown, that the asymptotic behaviour of the solution of Eq. (1) can be characterised by the formula

$$\psi(r \rightarrow \infty) \sim \sum_L D_L^0 [j_l(kr_0) - \text{tg } \delta n_l(kr_0)] \psi_L(f_0), \quad (9)$$

where δ is the phase shift of the cluster. It can be seen, that the appropriate solution of the radial equation (3) in region $r_0 \cong R$ is

$$R_l^0(r_0) = j_l(kr_0) - \text{tg } \delta n_l(kr_0), \quad (10)$$

and in region $b_0 \cong r_0 \cong R$

$$R_l^0(r_0) = u_l(r_0) - \text{tg } \delta v_l(r_0) \quad b_0 \cong r_0 \cong R, \quad (11)$$

where $u_l(r)$ and $v_l(r)$ are determined by inward numerical integration with the following starting values at $r_0 = R$:

$$u_l(R) = j_l(kR), \quad v_l(R) = n_l(kR),$$

$$\frac{du_l}{dr}(R) = \left. \frac{dj(kR)}{dr} \right|_{r=R}, \quad \frac{dv_l}{dr}(R) = \left. \frac{dn_l(kr)}{dr} \right|_{r=R}$$

Because the phase shift δ enters Eq. (7) via

$$g_l^0(E, \delta) = \frac{[n_l(\chi r), R_l^0]_{b_0}}{[j_l(\chi r), R_l^0]_{b_0}} = \frac{[n_l, u_l]_{b_0} - \text{tg } \delta [n_l, v_l]_{b_0}}{[j_l, u_l]_{b_0} - \text{tg } \delta [j_l, v_l]_{b_0}}, \quad (12)$$

the secular determinant with constant energy E will not be zero except at certain values δ_λ of the phase shift. So we obtain a set of solutions $\{A_{l\lambda}^p, B_{l\lambda}^0\}_\lambda$ corresponding to δ_λ . In this way the solutions ψ_λ of Eq. (1) can be obtained. Knowing the eigen

phase shifts δ_λ and amplitudes $D_{l\lambda}^0$ we can express, for example, the scattering amplitude of the cluster [7]:

$$f(k, k') = \frac{4\pi}{2i} \sum_{\lambda} (e^{2i\delta_\lambda} - 1) A_{\lambda}^*(k) Y_{\lambda}(k'),$$

where

$$A_{\lambda}(k) = \frac{1}{\cos \delta_{\lambda}} \sum_L (-i)^L D_{L\lambda}^0 Y_L(k)$$

We hope that the little modification of existing computer programs needed to get phase shifts δ_λ , allows to treat with this method physical problems in which scattering states are of importance.

References

- [1] Johnson, K. H.: In Advances in Quantum Chemistry Vol. 7, p. 143.
- [2] John, W., P. Ziesche: Phys. stat. sol. (b) 47, 555 (1971).
- [3] Ziesche, P.: Phys. C. 7, 1085 (1974).
- [4] Dill, D., J. L. Dehmer: J. Chem. Phys. 61, 692 (1974).
- [5] Ziesche, P., W. John: TU Dresden, Inf. 05—31—75, 06—32—75, 05—33—75.
- [6] Liberman, D., J. R. Barta: Multiple scattering Program Description (1973) I. B. M. Thomas Watson Research Center
- [7] Demkov, Rudakov: ZSETF 59, 2035 (1970).

ИССЛЕДОВАНИЕ СВОБОДНЫХ СОСТОЯНИЙ КЛАСТЕРОВ МЕТОДОМ МНОГОКРАТНОГО РАССЕЯНИЯ

И. К. Дьемант, М. Г. Бенедикт, Г. Пapp и Б. Вашвари

Метод многократного рассеяния вместе с методом X_α представляется пригодным для исследования свободных состояний кластеров. Мы сформулировали проблемы рассеяния на языке примененным Джонсоном для определения связанных состояний кластеров.

INTEGRAL EXPRESSIONS FOR $(nl|n'l')$ WITH $n, n' = 3, 4$

By

V. MARÁZ

Institute of Theoretical Physics, Attila József University,

Szeged

(Received February 1, 1976)

In this paper we give integral expressions for overlap integrals $(nl|n'l')$ with $n, n' = 3, 4$ using SLATER type orbitals for $3d, 4s$ and $4p$ atomic orbitals and an approximate function for the radial part of $4s$ and $4p$.

In LCAO—MO calculations on polynuclear complexes of transition metal ions have to be calculated overlap integrals between $2s, 2p, 3d, 4s$ and $4p$ atomic orbitals. From these integrals the expressions of $(nl|n'l')$ with $n=2, 3, 4; n'=2, 3$ are available in literature [1-4] but expressions of the other integrals — to our knowledge — have not been published until now. As these integrals are important in theoretical investigations of polynuclear complexes and similar molecular problems, we give in the following expressions for these integrals using SLATER type orbitals.

The calculation of overlap integrals

The radial part of SLATER type orbitals is of the form

$$r^{n^*-1} \cdot e^{-\alpha r},$$

where

$$\alpha = \frac{Z - \sigma}{n^* a_0};$$

n^* is the effective principal quantum number and $Z - \sigma$ is the effective nuclear charge. If the principal quantum number is $n=1, 2, 3, 4, \dots$, n^* has the following values: $n^*=1, 2, 3, 3.7, \dots$. The constant α can be determined with the help of SLATER's rules.

The overlap integrals of the real SLATER type orbitals can be divided into three classes:

1. The overlap integrals $(nl|n'l')$ with $n=2, 3; n'=2, 3$ can be calculated in elliptical coordinates (μ, ν, φ) defined by

$$\mu = \frac{r+r'}{R}, \quad \nu = \frac{r-r'}{R}, \quad \varphi = \varphi',$$

where $1 \leq \mu \leq \infty$, $-1 \leq v \leq 1$, $0 \leq \varphi \leq 2\pi$ and the meaning of r , r' , φ and R can be seen in Fig. 1 (the coordinate system (2) is left-handed).

In these elliptical coordinates the overlap integrals (3d, 2s), (3d, 2p) and (3d, 3d) can be expressed by the integrals

$$A_n(a) = \int_1^\infty \mu^n e^{-a\mu} d\mu$$

$$B_n(b) = \int_{-1}^1 v^n e^{-bv} dv$$

where $a = \frac{R}{2}(\alpha + \beta)$, $b = \frac{R}{2}(\alpha - \beta)$ and α , β are orbital exponents. The values of $A_n(a)$ and $B_n(b)$ for various a and b can be found for example in [5] but it is inconvenient

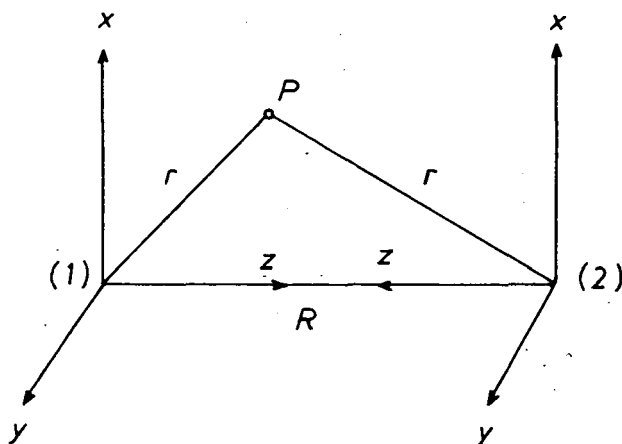


Fig. 1

to use this table in practice. It seems more practical to calculate these integrals with the help of the following recurrence relations:

$$A_n = \frac{1}{a} [nA_{n-1} + e^{-a}],$$

$$B_n = \frac{1}{b} [nB_{n-1} + (-1)^n e^b - e^{-b}].$$

2. The overlap integrals $(nl|n'l')$ with $n=4$; $n'=2, 3$ can be expressed with the help of integrals

$$I(n|y \pm x) = \frac{(n|y \pm x)!}{(y \pm x)^{n+1}}, \quad G(n|y+x) = \frac{\Gamma(n)}{(y+x)^n},$$

where $x = \alpha R$, $y = \beta R$ and

$$(n|y \pm x)! = \int_0^{y \pm x} t^n e^{-t} dt, \quad \Gamma(n) = \int_0^{\infty} t^{n-1} e^{-t} dt.$$

For the calculation of these integrals it is necessary to know the values of the incomplete Γ -function, which are available in [6].

3. The overlap integrals $(nl|n'l')$ with $n, n'=4$ cannot be expressed by any closed formulas. For this reason we approximated the radial part of $4s$ and $4p$ by the function

$$\tilde{\psi} = \sum_{k=1}^4 c_k r^k e^{-\alpha' r}$$

where c_k -s and α' are constants. These constants can be determined in various ways, for example under the condition

$$\int (\psi - \tilde{\psi})^2 dV = \min.$$

From this condition for c_k -s (if $\alpha' = \alpha_{4s}$), we get for the Co atom the following results:

$$c_1 = -0.047\ 530\ 507,$$

$$c_2 = 0.360\ 145\ 640,$$

$$c_3 = 0.728\ 294\ 860,$$

$$c_4 = -0.041\ 616\ 865.$$

Naturally the coefficients c_k -s depend on α . We intend to determine these c_k -s and α' for all transition elements.

Using the approximate function, the overlap integrals $(4s, 4s)$, $(4s, 4p)$, $(4p, 4p)$ as well as $(nl|n'l')$ with $n=4$; $n'=2, 3$ can already be expressed with integrals $A_n(a)$ and $B_n(b)$.

Expressions for integrals

$$1. (3d_{xy}, 3d_{xy}) = (3d_{x^2-y^2}, 3d_{x^2-y^2}) =$$

$$= \frac{1}{6} \frac{(ab)^{3.5}}{128} \{A_6 B_0 - 2A_6 B_2 + A_6 B_4 - 2A_4 B_0 + 3A_4 B_2 - A_4 B_4 + \\ + A_2 B_0 - 3A_2 B_4 + 2A_2 B_6 - A_0 B_2 + 2A_0 B_4 - A_0 B_6\}$$

$$2. (3d_{xz}, 3d_{xz}) = (3d_{yz}, 3d_{yz}) =$$

$$= \frac{2}{3} \frac{(ab)^{3.5}}{128} \{-A_6 B_2 + A_6 B_4 + A_4 B_0 - A_4 B_6 - A_2 B_0 + A_2 B_6 + A_0 B_2 - A_0 B_4\}$$

$$3. (3d_{z^2}, 3d_{z^2}) =$$

$$= \frac{1}{9} \frac{(ab)^{3.5}}{128} \{A_6 B_0 - 6A_6 B_2 + 9A_6 B_4 - 6A_4 B_0 + 3A_4 B_2 - 9A_4 B_6 + \\ + 9A_2 B_0 - 3A_2 B_4 + 6A_2 B_6 - 9A_0 B_2 + 6A_0 B_4 - A_0 B_6\}$$

4. $(4s, 3d_{zs}) = \frac{2^{1.7}}{3(7.4)^{0.7}} \frac{y^{4.2}}{x^{3.5}} \times$
 $\times e^x [(360 - 360x + 192x^2 - 72x^3 + 24x^4 - 8x^5) \{G(4.7|y+x) -$
 $- I(3.7|y+x)\} + (360x - 360x^2 + 192x^3 - 72x^4 + 24x^5) \{G(5.7|y+x) -$
 $- I(4.7|y+x)\} + (144x^2 - 144x^3 + 72x^4 - 24x^5) \{G(6.7|y+x) -$
 $- I(5.7|y+x)\} + (24x^3 - 24x^4 + 8x^5) \{G(7.7|y+x) - I(6.7|y+x)\}] +$
 $+ e^{-x} [(360 + 360x + 192x^2 + 72x^3 + 24x^4 + 8x^5) \{I(3.7|y-x) -$
 $- G(4.7|y+x)\} - (360x + 360x^2 + 192x^3 + 72x^4 + 24x^5) \{I(4.7|y-x) +$
 $+ G(5.7|y+x)\} + (144x^2 + 144x^3 + 72x^4 + 24x^5) \{I(5.7|y-x) -$
 $- G(6.7|y+x)\} - (24x^3 + 24x^4 + 8x^5) \{I(6.7|y-x) + G(7.7|y+x)\}]$
5. $(4p_x, 3d_{xz}) = (4p_y, 3d_{yz}) = \frac{2^{1.7}}{(7.4)^{0.5}} \frac{y^{4.2}}{x^{3.5}} \times$
 $\times \{e^x [(720 - 720x + 312x^2 - 72x^3 + 8x^4) \{I(2.7|y+x) - G(3.7|y+x)\} +$
 $+ (720x - 720x^2 + 312x^3 - 72x^4 + 8x^5) \{I(3.7|y+x) - G(4.7|y+x)\} +$
 $+ (312x^2 - 312x^3 + 128x^4 - 24x^5) \{I(4.7|y+x) - G(5.7|y+x)\} +$
 $+ (72x^3 - 72x^4 + 24x^5) \{I(5.7|y+x) - G(6.7|y+x)\} +$
 $+ (8x^4 - 8x^5) \{I(6.7|y+x) - G(7.7|y+x)\}] +$
 $+ e^{-x} [(720 + 720x + 312x^2 + 72x^3 + 8x^4) \{G(3.7|y+x) - I(2.7|y-x)\} +$
 $+ (720x + 720x^2 + 312x^3 + 72x^4 + 8x^5) \{G(4.7|y+x) + I(3.7|y-x)\} +$
 $+ (312x^2 + 312x^3 + 128x^4 + 24x^5) \{G(5.7|y+x) - I(4.7|y-x)\} +$
 $+ (72x^3 + 72x^4 + 24x^5) \{G(6.7|y+x) + I(5.7|y-x)\} +$
 $+ (8x^4 + 8x^5) \{G(7.7|y+x) - I(6.7|y-x)\}]$
6. $(4p_x, 3d_{zs}) = \frac{\sqrt{3}}{3} \frac{2^{0.7}}{(7.4)^{0.5}} \frac{y^{4.2}}{x^{4.5}} \times$
 $\times \{e^x [(15120 - 15120x + 7440x^2 - 2400x^3 + 576x^4 - 112x^5 + 16x^6) \{I(2.7|y+x) -$
 $- G(3.7|y+x)\} + (15120x - 15120x^2 + 7440x^3 - 2400x^4 + 576x^5 - 112x^6 +$
 $+ 16x^7) \{I(3.7|y+x) - G(4.7|y+x)\} + (6480x^2 - 6480x^3 + 3168x^4 -$
 $- 1008x^5 + 240x^6 - 48x^7) \{I(4.7|y+x) - G(5.7|y+x)\} + (1440x^3 -$
 $- 1440x^4 + 688x^5 - 208x^6 + 46x^7) \{I(5.7|y+x) - G(6.7|y+x)\} +$
 $+ (144x^4 - 144x^5 + 64x^6 - 16x^7) \{I(6.7|y+x) - G(7.7|y+x)\}] +$
 $+ e^{-x} [(15120 + 15120x + 7440x^2 + 2400x^3 + 576x^4 + 112x^5 + 16x^6) \{G(3.7|y+x) -$
 $- I(2.7|y-x)\} + (15120x + 15120x^2 + 7440x^3 + 2400x^4 + 576x^5 + 112x^6 +$
 $+ 16x^7) \{G(4.7|y+x) + I(3.7|y-x)\} + (6480x^2 + 6480x^3 + 3168x^4 +$
 $+ 1008x^5 + 240x^6 + 48x^7) \{G(5.7|y+x) - I(4.7|y-x)\} + (1440x^3 +$
 $+ 1440x^4 + 688x^5 + 208x^6 + 46x^7) \{G(6.7|y+x) + I(5.7|y-x)\} +$
 $+ (144x^4 + 144x^5 + 64x^6 + 16x^7) \{G(7.7|y+x) - I(6.7|y-x)\}]$

$$\begin{aligned}
 7. \quad (4s, 4s) &= 2\pi \left(\frac{R}{2}\right)^5 N_{4s}(\alpha) N_{4s}(\beta) \times \\
 &\times \{a_1 b_1 [A_4 B_0 - 2A_2 B_2 + A_0 B_4] + \\
 &+ a_1 b_2 \frac{R}{2} [A_5 B_0 - A_4 B_1 - 2A_3 B_2 + 2A_2 B_3 + A_1 B_4 - A_0 B_5] + \\
 &+ a_1 b_3 \left(\frac{R}{2}\right)^2 [A_6 B_0 - 2A_5 B_1 - A_4 B_2 + A_3 B_3 - A_2 B_4 - 2A_1 B_5 + A_0 B_6] + \\
 &+ a_1 b_4 \left(\frac{R}{2}\right)^3 [A_7 B_0 - 3A_6 B_1 + A_5 B_2 + 5A_4 B_3 - 5A_3 B_4 - A_2 B_5 + 3A_1 B_6 - A_0 B_7] + \\
 &+ a_2 b_1 \frac{R}{2} [A_5 B_0 + A_4 B_1 - 2A_3 B_2 - 2A_2 B_3 + A_1 B_4 + A_0 B_5] + \\
 &+ a_2 b_2 \left(\frac{R}{2}\right)^2 [A_6 B_0 - 3A_4 B_2 + 3A_2 B_4 - A_0 B_6] + \\
 &+ a_2 b_3 \left(\frac{R}{2}\right)^3 [A_7 B_0 - A_6 B_1 - 3A_5 B_2 + 3A_4 B_3 + 3A_3 B_4 - 3A_2 B_5 - A_1 B_6 + A_0 B_7] + \\
 &+ a_2 b_4 \left(\frac{R}{2}\right)^4 [A_8 B_0 - 2A_7 B_1 - 2A_6 B_2 + 6A_5 B_3 - 6A_4 B_5 + 2A_2 B_6 + 2A_1 B_7 - A_0 B_8] + \\
 &+ a_3 b_1 \left(\frac{R}{2}\right)^2 [A_6 B_0 + 2A_5 B_1 - A_4 B_2 - 4A_3 B_3 - A_2 B_4 + 2A_1 B_5 + A_0 B_6] + \\
 &+ a_3 b_2 \left(\frac{R}{2}\right)^3 [A_7 B_0 + A_6 B_1 - 3A_5 B_2 - 3A_4 B_3 + 3A_3 B_4 + 3A_2 B_5 - A_1 B_6 - A_0 B_7] + \\
 &+ a_3 b_3 \left(\frac{R}{2}\right)^4 [A_8 B_0 - 4A_6 B_2 + 6A_4 B_4 - 4A_2 B_6 + A_0 B_8] + \\
 &+ a_3 b_4 \left(\frac{R}{2}\right)^5 [A_9 B_0 - A_8 B_1 - 4A_7 B_2 + 4A_6 B_3 + 6A_5 B_4 - 6A_4 B_5 - 4A_3 B_6 + 4A_2 B_7 + \\
 &\quad + A_1 B_8 - A_0 B_9] + \\
 &+ a_4 b_1 \left(\frac{R}{2}\right)^3 [A_7 B_0 + 3A_6 B_1 + A_5 B_2 - 5A_4 B_3 - 5A_3 B_4 + A_2 B_5 + 3A_1 B_6 + A_0 B_7] + \\
 &+ a_4 b_2 \left(\frac{R}{2}\right)^4 [A_8 B_0 + 2A_7 B_1 - 2A_6 B_2 - 6A_5 B_3 + 6A_4 B_5 + 2A_2 B_6 - 2A_1 B_7 - A_0 B_8] + \\
 &+ a_4 b_3 \left(\frac{R}{2}\right)^5 [A_9 B_0 + A_8 B_1 - 4A_7 B_2 - 4A_6 B_3 + 6A_5 B_4 + 6A_4 B_5 - 4A_3 B_6 - 4A_2 B_7 + \\
 &\quad + A_1 B_8 + A_0 B_9] + \\
 &+ a_4 b_4 \left(\frac{R}{2}\right)^6 [A_{10} B_0 - 5A_9 B_2 + 10A_6 B_4 - 10A_4 B_6 + 5A_2 B_8 - A_0 B_{10}] \}
 \end{aligned}$$

$$\begin{aligned}
 8. \quad (4s, 4p_2) &= 2\pi \left(\frac{R}{2}\right)^5 N_{4s}(\alpha) N_{4p_2}(\beta) \times \\
 &\times \{a_1 b_1 [-A_4 B_1 + A_3 B_0 - A_3 B_2 + A_2 B_1 + A_2 B_3 - A_1 B_2 + A_1 B_4] +
 \end{aligned}$$

$$\begin{aligned}
& + a_1 b_2 \frac{R}{2} [-A_5 B_1 + A_4 B_0 + 2A_3 B_3 - 2A_2 B_2 - A_1 B_5 + A_0 B_4] + \\
& + a_1 b_3 \left(\frac{R}{2}\right)^2 [-A_6 B_1 + A_5 B_0 + A_5 B_2 - A_4 B_1 + 2A_4 B_3 - 2A_3 B_2 - 2A_3 B_4 + \\
& \quad + 2A_2 B_3 - A_2 B_6 + A_1 B_4 + A_1 B_6 - A_0 B_6] + \\
& + a_1 b_4 \left(\frac{R}{2}\right)^3 [-A_7 B_1 + A_6 B_0 + 2A_6 B_2 - 2A_5 B_1 + A_5 B_3 - A_4 B_2 - 4A_4 B_4 + 4A_3 B_3 + \\
& \quad + A_3 B_5 - A_2 B_4 + 2A_2 B_6 - 2A_1 B_5 - A_1 B_7 + A_0 B_6] + \\
& + a_2 b_1 \frac{R}{2} [-A_5 B_1 + A_4 B_0 - 2A_4 B_2 + 2A_3 B_1 + 2A_2 B_4 - 2A_1 B_3 + A_1 B_5 - A_0 B_4] + \\
& + a_2 b_2 \left(\frac{R}{2}\right)^2 [-A_6 B_1 + A_5 B_0 - A_5 B_2 + A_4 B_1 + 2A_4 B_3 - 2A_3 B_2 + 2A_3 B_4 - 2A_2 B_3 - A_2 B_6 + \\
& \quad + A_1 B_4 - A_1 B_6 + A_0 B_5] + \\
& + a_2 b_3 \left(\frac{R}{2}\right)^3 [-A_7 B_1 + A_6 B_0 + 3A_5 B_3 - 3A_4 B_2 - 3A_3 B_5 + 3A_2 B_4 + A_1 B_7 - A_0 B_6] + \\
& + a_2 b_4 \left(\frac{R}{2}\right)^4 [-A_8 B_1 + A_7 B_0 + A_7 B_2 - A_6 B_1 + 3A_6 B_3 - 3A_5 B_2 - 3A_5 B_4 + \\
& \quad + 3A_4 B_3 - 3A_4 B_5 + 3A_3 B_4 + 3A_3 B_6 - 3A_2 B_5 + A_2 B_7 - A_1 B_6 - A_1 B_8 + A_0 B_7] + \\
& + a_3 b_1 \left(\frac{R}{2}\right)^2 [-A_6 B_1 + A_5 B_0 - 3A_5 B_2 + 3A_4 B_1 - 2A_4 B_3 + 2A_3 B_2 + 2A_3 B_4 - 2A_2 B_3 + \\
& \quad + 3A_2 B_5 - 3A_1 B_4 + A_1 B_6 - A_0 B_6] + \\
& + a_3 b_2 \left(\frac{R}{2}\right)^3 [-A_7 B_1 + A_6 B_0 - 2A_6 B_2 + 2A_5 B_1 + A_5 B_3 - A_4 B_2 + 4A_4 B_4 - 4A_3 B_3 + \\
& \quad + A_3 B_5 - A_2 B_2 - 2A_2 B_6 + 2A_1 B_5 - A_1 B_6 + A_1 B_7 + A_0 B_6] + \\
& + a_3 b_3 \left(\frac{R}{2}\right)^4 [-A_8 B_1 + A_7 B_0 - A_7 B_2 + A_6 B_1 + 3A_6 B_3 - 3A_5 B_2 + 3A_5 B_4 - 3A_4 B_3 - 3A_4 B_6 + \\
& \quad + 3A_3 B_4 - 3A_3 B_6 + 3A_2 B_5 + A_2 B_7 - A_1 B_6 - A_0 B_7] + \\
& + a_3 b_4 \left(\frac{R}{2}\right)^5 [-A_9 B_1 + A_8 B_0 + 4A_7 B_3 - 4A_6 B_2 - 6A_5 B_5 + 6A_4 B_4 + 4A_3 B_7 - 4A_2 B_6 - \\
& \quad - A_1 B_9 + A_0 B_8] + \\
& + a_4 b_1 \left(\frac{R}{2}\right)^3 [-A_7 B_1 + A_6 B_0 - 4A_6 B_2 + 4A_5 B_1 - 5A_5 B_3 + 5A_4 B_2 + 5A_3 B_5 - 5A_2 B_4 + 4A_2 B_6 - \\
& \quad - 4A_1 B_5 + A_1 B_7 - A_0 B_6] + \\
& + a_4 b_2 \left(\frac{R}{2}\right)^4 [-A_8 B_1 + A_7 B_0 - 3A_7 B_2 + 3A_6 B_1 - A_6 B_3 + A_5 B_2 + 5A_5 B_4 - 5A_4 B_3 + \\
& \quad + 5A_4 B_5 - 5A_3 B_4 - A_3 B_6 + A_2 B_5 - 3A_2 B_7 + 3A_1 B_6 - A_1 B_8 + A_0 B_7] +
\end{aligned}$$

$$\begin{aligned}
 &+ a_4 b_3 \left(\frac{R}{2} \right)^5 [-A_9 B_1 + A_9 B_0 - 2A_3 B_2 + 2A_7 B_1 + 2A_7 B_3 - 2A_6 B_2 + 6A_5 B_4 - 6A_5 B_3 - 6A_4 B_6 + \\
 &\quad + 6A_3 B_5 - 2A_3 B_7 + 2A_2 B_6 + 2A_2 B_8 - 2A_1 B_7 + A_1 B_9 - A_0 B_8] + \\
 &+ a_4 b_4 \left(\frac{R}{2} \right)^6 [-A_{10} B_1 + A_9 B_0 - A_9 B_2 + A_8 B_1 + 4A_8 B_3 - 4A_7 B_2 + 4A_7 B_4 - 4A_6 B_3 - 6A_6 B_5 + \\
 &\quad + 6A_5 B_4 - 6A_5 B_6 + 6A_4 B_5 + 4A_4 B_7 - 4A_3 B_6 + 4A_3 B_8 - 4A_2 B_7 - A_2 B_9 + \\
 &\quad + A_1 B_8 - A_1 B_{10} + A_0 B_9] \}
 \end{aligned}$$

$$\begin{aligned}
 9. \quad (4p_x, 4p_x) = (4p_y, 4p_y) = \pi \left(\frac{R}{2} \right)^5 N_{4p_x}(\alpha) N_{4p_x}(\beta) \times \\
 \times \{ a_1 b_1 [A_4 B_0 - A_4 B_2 - A_2 B_0 + A_2 B_4 + A_0 B_2 - A_0 B_4] + \\
 + a_1 b_2 \frac{R}{2} [A_5 B_0 - A_5 B_2 - A_4 B_1 + A_4 B_3 - A_3 B_0 + A_3 B_4 + A_2 B_1 - A_2 B_5 + A_1 B_2 - \\
 \quad - A_1 B_4 - A_0 B_3 + A_0 B_5] + \\
 + a_1 b_3 \left(\frac{R}{2} \right)^2 [A_6 B_0 - A_6 B_2 - 2A_5 B_1 + 2A_5 B_3 - A_4 B_0 + A_4 B_2 + 2A_3 B_1 - 2A_3 B_5 - A_2 B_4 + \\
 \quad + A_2 B_6 - 2A_1 B_3 + 2A_1 B_5 + A_0 B_4 - A_0 B_6] + \\
 + a_1 b_4 \left(\frac{R}{2} \right)^3 [A_7 B_0 - A_7 B_2 - 3A_6 B_1 + 3A_6 B_3 - A_5 B_0 + 3A_5 B_2 - 2A_5 B_4 + 3A_4 B_1 - A_4 B_3 - \\
 \quad - 2A_4 B_5 - 2A_3 B_2 - A_3 B_4 + 3A_3 B_6 - 2A_2 B_3 + 3A_2 B_5 - A_2 B_7 + 3A_1 B_4 - \\
 \quad - 3A_1 B_6 + A_0 B_7] + \\
 + a_2 b_1 \frac{R}{2} [A_5 B_0 - A_5 B_2 + A_4 B_1 - A_4 B_3 - A_3 B_0 + A_3 B_4 - A_2 B_1 + A_2 B_5 + \\
 \quad + A_1 B_2 - A_1 B_4 + A_0 B_3 - A_0 B_5] + \\
 + a_2 b_2 \left(\frac{R}{2} \right)^2 [A_6 B_0 - A_6 B_2 - A_4 B_0 - A_4 B_2 + 2A_4 B_4 + 2A_2 B_2 - A_2 B_4 - A_2 B_6 - \\
 \quad - A_0 B_4 + A_0 B_6] + \\
 + a_2 b_3 \left(\frac{R}{2} \right)^3 [A_7 B_0 - A_7 B_2 - A_6 B_1 + A_6 B_3 - A_5 B_0 - A_5 B_2 + 2A_5 B_4 + 2A_3 B_2 - \\
 \quad - A_3 B_4 - A_3 B_6 + A_4 B_1 + A_4 B_3 - 2A_4 B_5 - 2A_2 B_3 + A_2 B_5 + A_2 B_7 - \\
 \quad - A_1 B_4 + A_1 B_6 + A_0 B_5 - A_0 B_7] + \\
 + a_3 b_4 \left(\frac{R}{2} \right)^4 [A_8 B_0 - A_8 B_2 - 2A_7 B_1 + 2A_7 B_3 - A_6 B_0 + A_6 B_4 + 2A_5 B_1 + 2A_5 B_3 - \\
 \quad - 4A_5 B_5 + A_4 B_2 - 2A_4 B_4 + A_4 B_6 - 4A_3 B_3 + 2A_3 B_5 + 2A_3 B_7 + A_2 B_4 - \\
 \quad - A_2 B_6 + 2A_1 B_5 - 2A_1 B_7 - A_0 B_6 + A_0 B_8] + \\
 + a_3 b_1 \left(\frac{R}{2} \right)^3 [A_6 B_0 - A_6 B_2 + 2A_5 B_1 - 2A_5 B_3 - A_4 B_0 + A_4 B_2 - 2A_3 B_1 + 2A_3 B_5 - A_2 B_4 +
 \end{aligned}$$

$$\begin{aligned}
& + A_2 B_6 + 2A_1 B_3 - 2A_1 B_6 + A_0 B_4 - A_0 B_6] + \\
& + a_3 b_2 \left(\frac{R}{2}\right)^3 [A_7 B_0 - A_7 B_2 + A_6 B_1 - A_6 B_3 - A_5 B_2 + 2A_5 B_4 - A_4 B_1 - A_4 B_3 + 2A_4 B_5 + \\
& + 2A_3 B_2 - A_3 B_4 - A_3 B_6 + 2A_2 B_3 - A_2 B_5 - A_2 B_7 - A_1 B_4 + A_1 B_6 - A_0 B_5 + \\
& + A_0 B_7 + A_0 B_9] + \\
& + a_3 b_3 \left(\frac{R}{2}\right)^4 [A_8 B_0 - A_8 B_2 - A_6 B_0 - 2A_6 B_2 + 3A_6 B_4 + 3A_4 B_2 - 3A_4 B_6 - 3A_2 B_4 + \\
& + 2A_2 B_6 + A_2 B_8 + A_0 B_6 - A_0 B_8] + \\
& + a_3 b_4 \left(\frac{R}{2}\right)^5 [A_9 B_0 - A_9 B_2 - A_3 B_1 + A_8 B_3 - A_7 B_0 - 2A_7 B_2 + 3A_7 B_4 + A_6 B_1 + 2A_6 B_3 - \\
& - 3A_6 B_5 + 3A_5 B_2 - 3A_5 B_6 - 3A_4 B_3 + 3A_4 B_7 - 3A_3 B_4 + 2A_3 B_6 + \\
& + A_2 B_8 + 3A_2 B_5 - 2A_2 B_7 - A_2 B_9 + A_1 B_6 - A_1 B_8 - A_0 B_7 + A_0 B_9] + \\
& + a_4 b_1 \left(\frac{R}{2}\right)^3 [A_7 B_0 - A_7 B_2 + 3A_6 B_1 - 3A_6 B_3 - A_5 B_0 + 3A_5 B_2 - 2A_5 B_4 - 2A_3 B_2 - A_3 B_4 + \\
& + 3A_3 B_6 + 2A_2 B_3 - 3A_2 B_5 + A_2 B_7 - 3A_4 B_1 + A_4 B_3 + 2A_4 B_5 + 3A_1 B_4 - \\
& - 3A_1 B_6 + A_0 B_5 - A_0 B_7] + \\
& + a_4 b_2 \left(\frac{R}{2}\right)^4 [A_8 B_0 - A_8 B_2 + 2A_7 B_1 - 2A_7 B_3 - A_6 B_0 + A_6 B_4 - 2A_5 B_1 - 2A_5 B_3 + \\
& + 4A_5 B_5 + A_4 B_2 - 2A_4 B_4 + A_4 B_6 + 4A_3 B_3 - 2A_3 B_5 - 2A_3 B_7 + A_2 B_4 - \\
& - A_2 B_8 - 2A_1 B_5 + 2A_1 B_7 - A_0 B_6 + A_0 B_8] + \\
& + a_4 b_3 \left(\frac{R}{2}\right)^5 [A_9 B_0 - A_9 B_2 + A_8 B_1 - A_8 B_3 - A_7 B_0 - 2A_7 B_2 + 3A_7 B_4 - A_6 B_1 - \\
& - 2A_6 B_3 + 3A_6 B_5 + 3A_5 B_2 - 3A_5 B_6 + 3A_4 B_3 - 3A_4 B_7 - 3A_3 B_4 + \\
& + 2A_3 B_6 + A_3 B_8 - 3A_2 B_5 + 2A_2 B_7 + A_2 B_9 + A_1 B_6 - A_1 B_8 + A_0 B_7 - A_0 B_9] + \\
& + a_4 b_4 \left(\frac{R}{2}\right)^6 [A_{10} B_0 - A_{10} B_2 - A_8 B_0 - 3A_8 B_2 + 4A_8 B_4 + 4A_6 B_2 + 2A_6 B_4 - 6A_6 B_6 - \\
& - 6A_4 B_4 + 2A_4 B_6 + 4A_4 B_8 + 4A_2 B_6 - 3A_2 B_8 - A_2 B_{10} - A_0 B_8 + A_0 B_{10}]
\end{aligned}$$

$$\begin{aligned}
10. (4p_z, 4p_z) &= 2\pi \left(\frac{R}{2}\right)^5 N_{4p_z}(\alpha) N_{4p_z}(\beta) \times \\
&\times \{a_1 b_1 [-A_4 B_2 + A_2 B_0 + A_2 B_4 - A_0 B_2] + \\
&+ a_1 b_2 \frac{R}{2} [-A_5 B_2 + A_4 B_3 + A_3 B_0 + A_3 B_4 - A_2 B_1 - A_2 B_5 - A_1 B_2 + A_0 B_3] + \\
&+ a_1 b_3 \left(\frac{R}{2}\right)^2 [-A_6 B_2 + 2A_5 B_3 + A_4 B_0 - 2A_3 B_1 - 2A_3 B_5 + A_2 B_6 + 2A_1 B_3 - A_0 B_4] + \\
&+ a_1 b_4 \left(\frac{R}{2}\right)^3 [-A_7 B_2 + 3A_6 B_3 + A_5 B_0 - 2A_5 B_4 - 3A_4 B_1 - 2A_4 B_5 + 2A_3 B_2 + 3A_3 B_6 +
\end{aligned}$$

$$\begin{aligned}
& +2A_2B_3 - A_2B_7 - 3A_1B_4 + A_0B_5] + \\
& + a_2 b_1 \frac{R}{2} [-A_5B_2 - A_4B_3 + A_3B_4 + A_2B_1 - A_1B_2 - A_0B_3 + A_2B_5 + A_3B_0] + \\
& + a_2 b_2 \left(\frac{R}{2}\right)^2 [-A_6B_2 + A_4B_0 + 2A_4B_4 - 2A_2B_2 - A_2B_6 + A_0B_4] + \\
& + a_2 b_3 \left(\frac{R}{2}\right)^3 [-A_7B_2 + A_6B_3 + A_5B_0 + 2A_5B_4 - A_4B_1 - 2A_4B_5 - 2A_3B_2 - A_3B_6 + \\
& + 2A_2B_3 + A_2B_7 + A_1B_4 - A_0B_5] + \\
& + a_2 b_4 \left(\frac{R}{2}\right)^4 [-A_8B_2 + 2A_7B_3 + A_6B_0 + A_6B_4 - 2A_5B_1 - 4A_5B_5 - A_4B_2 + A_4B_6 + 4A_3B_3 + \\
& + 2A_3B_7 - A_2B_4 - A_2B_8 - 2A_1B_5 + A_0B_6] + \\
& + a_3 b_1 \left(\frac{R}{2}\right)^2 [-A_6B_2 - 2A_5B_3 + A_4B_0 + 2A_3B_1 + 2A_3B_6 + A_2B_6 - 2A_1B_3 - A_0B_4] + \\
& + a_3 b_2 \left(\frac{R}{2}\right)^3 [-A_7B_2 - A_6B_3 + A_5B_0 + 2A_5B_4 + A_4B_1 + 2A_4B_5 - 2A_3B_2 - A_3B_6 - 2A_2B_3 - \\
& - A_2B_7 + A_1B_4 + A_0B_5] + \\
& + a_3 b_3 \left(\frac{R}{2}\right)^4 [-A_8B_2 + A_6B_0 + 3A_6B_4 - 3A_4B_2 - 3A_4B_6 + 3A_2B_4 + A_2B_8 - A_0B_6] + \\
& + a_3 b_4 \left(\frac{R}{2}\right)^5 [-A_9B_2 + A_8B_3 + A_7B_0 + 3A_7B_4 - A_6B_1 - [3A_6B_5 - 3A_5B_2 - 3A_5B_6 + 3A_4B_3 + \\
& + 3A_4B_7 + 3A_3B_4 + A_3B_8 - 3A_2B_5 - A_2B_9 - A_1B_6 + A_0B_7] + \\
& + a_4 b_1 \left(\frac{R}{2}\right)^3 [-A_7B_2 - 3A_6B_3 + A_5B_0 - 2A_5B_4 + 3A_4B_1 + 2A_4B_5 + 2A_3B_2 + 3A_3B_6 - \\
& - 2A_2B_3 + A_2B_7 - 3A_1B_4 - A_0B_5] + \\
& + a_4 b_2 \left(\frac{R}{2}\right)^4 [-A_8B_2 - 2A_7B_3 + A_6B_0 + A_6B_4 + 2A_5B_1 + 4A_5B_5 - A_4B_2 + A_4B_6 - \\
& - 4A_3B_3 - 2A_3B_7 - A_2B_4 - A_2B_8 + 2A_1B_5 + A_0B_6] + \\
& + a_4 b_3 \left(\frac{R}{2}\right)^5 [-A_9B_2 - A_8B_3 + A_7B_0 + 3A_7B_4 + A_6B_1 + 3A_6B_5 - 3A_5B_2 - 3A_5B_6 - \\
& - A_4B_3 - 3A_4B_7 + 3A_3B_4 + A_3B_8 + 3A_2B_5 + A_2B_9 - A_1B_6 - A_0B_7] + \\
& + a_4 b_4 \left(\frac{R}{2}\right)^6 [-A_{10}B_2 + A_8B_0 + 4A_8B_4 - 4A_6B_2 - 6A_6B_6 + 6A_4B_4 + 4A_4B_8 - \\
& - 4A_2B_6 - A_2B_{10} + A_0B_8]
\end{aligned}$$

References

- [1] *Mulliken, R. S., C. A. Rieke, D. Orloff, H. Orloff*: J. Chem. Phys. 17, 1248 (1949).
- [2] *Jaffé, H. H.*: J. Chem. Phys. 21, 198, 258 (1953).
- [3] *Preuss, H.*: Integraltafeln zur Quantenchemie, Springer Verl., Berlin, 1957.
- [4] *Gilde, F. J.*: Acta Phys. et Chem. Szeged 7, 83 (1961).
- [5] *Miller, J. J. M. Gerhauser, F. A. Matsen*: Quantum Chemistry Integrals and Tables, University of Texas Press, Austin, 1959.
- [6] *Pearson, K.*: Tables of the Incomplete Γ -function, Ed: K. Pearson, London, 1922.

ИНТЕГРАЛЬНЫЕ ВЫРАЖЕНИЯ ДЛЯ $(nl|n'l')$ с $n, n' = 3, 4$

В. Мараз

Представлены интегральные выражения для интеграла перекрытия $(nl|n'l')$ с $n, n' = 3, 4$ с помощью орбиталей типа СЛЕТЕРА для атомных орбиталей $3d, 4s$ и $4p$, и приближительная функция для радиальной части $4s$ и $4p$.

TRANSFER OF ELECTRONIC EXCITATION ENERGY IN PROTEIN-DETERGENT SOLUTIONS

By

E. VOZÁRY and L. SZALAY

Institute of Biophysics, Attila József University, Szeged

(Received February 6, 1976)

The electronic absorption spectra of mixtures of lysozyme and triton *X*-100 are additive, those of albumin and triton are non-additive in the concentration range of $2 \cdot 10^{-6}$ – $8 \cdot 10^{-4}$ *M* protein and $2 \cdot 10^{-5}$ – $8 \cdot 10^{-3}$ *M* detergent. In both cases there is an overlap of absorption and fluorescence spectra which leads to transfer of electronic excitation from the detergent to the protein. The dependence of transfer frequency on the distance (*R*) follows an R^{-8} -law for the transfer from triton to lysozyme and an R^{-5} -law for the other case. The activity of lysozyme increases by about 60% in the presence of triton.

Introduction

Photochemical processes of photosynthesis are often investigated on chloroplast fractions obtained by treating chloroplast suspensions with detergents [1–3]. The sizes and properties of the particles forming the fractions depend highly on the characteristics of the detergent and on its concentration. The absorption of light at 280 nm in these systems is often measured in order to determine their protein contents [3]. However, this method can only be applied if the detergents used for the treatment have no absorption at 280 nm. In general, this is not the case, e.g. triton *X*-100 has two bands, at 275 nm and 285 nm [4].

The detergents may interact with the particle fractions and may even be incorporated [3], leading to changes in their properties. To permit conclusions concerning the true properties of the particles, the interactions between detergents and proteins and those between detergents and pigments have to be known.

Interactions between pigments and detergents have been investigated by several authors [5–7], and the results provide a broad outline of these interactions. Interactions between proteins and detergents have also been investigated for a long time, but a comprehensive picture of these interactions has still not been obtained. The effects caused by detergents have been studied by measuring the absorption [8, 9] and fluorescence [9, 10], if the detergent has no absorption and fluorescence in the wavelength range of the proteins. However, if protein and detergent absorb in the same wavelength range, but the maximum of the detergent fluorescence lies at a shorter wave than that of the protein excitation, energy transfer from the detergent to the protein becomes possible in mixed solutions. The transfer efficiency depends on the distance (concentration of the components). This dependence may render it possible to characterize the interaction between the proteins and detergents. The aim of this paper is to study the action of triton *X*-100 on lysozyme and albumin.

Materials and methods

The hen ovalbumine lysozyme was a lyophilized, three times crystallized commercial product (Nutritional Biochemical Corporation, Cleveland). Its activity was 6000–10 000 unit/mg. The human serum albumin (Reanal) and *Micrococcus lysodeikticus* (Worthington Biochemical Corporation, Freehold, New Jersey) used as substrate for activity measurements were also commercial products. Triton X-100 (Rohm and Haas, Co.) is a non-ionic detergent; its micelles are formed by about 100 molecules [11], and its critical micelle concentration (c.m.c.) is $3 \cdot 10^{-4} M$ [4]. The protein and detergent were dissolved in phosphate buffer of pH=7. The concentrations of albumin, lysozyme and triton X-100 solutions were varied from $2 \cdot 10^{-6} M$ to $8 \cdot 10^{-4} M$, from $2 \cdot 10^{-6} M$ to $6 \cdot 10^{-4} M$ and from $2 \cdot 10^{-5} M$ to $8 \cdot 10^{-3} M$, respectively. In all mixed solutions the concentration of triton X-100 was 10 times greater than that of the proteins.

The absorption and fluorescence spectra were measured with an Optica Milano CF4DR recording spectrophotometer and a Perkin—Elmer MPF-3, spectrofluorimeter, respectively. The fluorescence spectra were corrected for the reabsorption of fluorescence and for the spectral sensitivity of the detector [12]. The layer thickness was selected after BUDÓ and KETSKEMÉTY [13] so that the secondary fluorescence was negligible.

The activity of lysozyme was measured spectrophotometrically with a method by SHUGAR [14].

The absolute quantum yields were determined after DOMBI [15], allowance being made, however, for the different geometry.

Results and discussion

Absorption spectra. Fig. 1 shows that in a mixture of lysozyme and triton the absorption of the mixed solution is the sum of the absorptions of the components, while in a mixture of albumin and triton the additivity does not hold in the short-wave region of absorption. This suggests the existence of some interaction between albumin and triton. This behavior was independent of the concentration in the range studied.

Fluorescence spectra. The relative absorption and fluorescence spectra of lysozyme and triton are presented in Fig. 2. There is a comparatively strong overlap (shaded area) between the fluorescence spectrum of triton and the absorption spectrum of lysozyme. A similar overlap occurs in the case of albumin and triton. This overlap permits the transfer of excitation energy from triton to lysozyme or albumin.

Fig. 3 shows the spectral distribution of the fluorescence of a mixture of lysozyme and triton and that of the components in arbitrary units. It can be seen that the intensity of the fluorescence of triton at 305 nm is decreased in the mixture; in other words, the fluorescence spectra are not additive. The same applies in the case of albumin and triton. This indicates that the excitation energy is partly transferred to the proteins (acceptors) from the detergent (donor). In order to determine the transfer efficiency, the expected contribution of the fluorescence of the components to the total fluorescence must be considered.

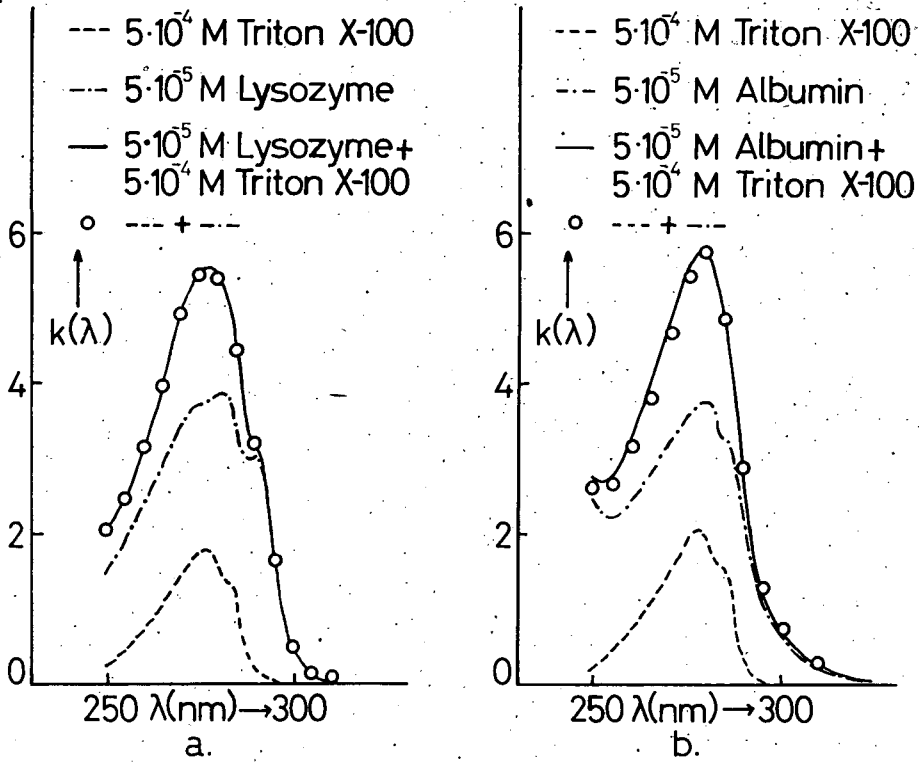


Fig. 1.

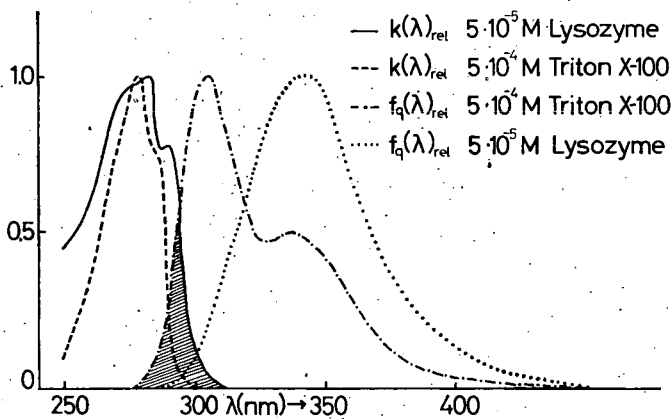


Fig. 2

Determination of the transfer efficiency: A relation between the quantum distribution function $f(\lambda')$ of the fluorescence of a mixed solution consisting of two components and the quantum distribution spectra of the fluorescence of the components, $f_1(\lambda')$ and $f_2(\lambda')$, is known for the case when there is no energy transfer between the components:

$$f(\lambda) = \frac{f_1(\lambda)k_1(\lambda)\mu_1(\lambda) + f_2(\lambda)k_2(\lambda)\eta_2(\lambda)}{k_1(\lambda)\eta_1(\lambda) + k_2(\lambda)\eta_2(\lambda)}, \quad (1)$$

where $k_1(\lambda)$ and $\eta_1(\lambda)$, and $k_2(\lambda)$ and $\eta_2(\lambda)$ are the absorption coefficients and the absolute quantum yields of the first and the second component, respectively, at the exciting wavelength λ [15].

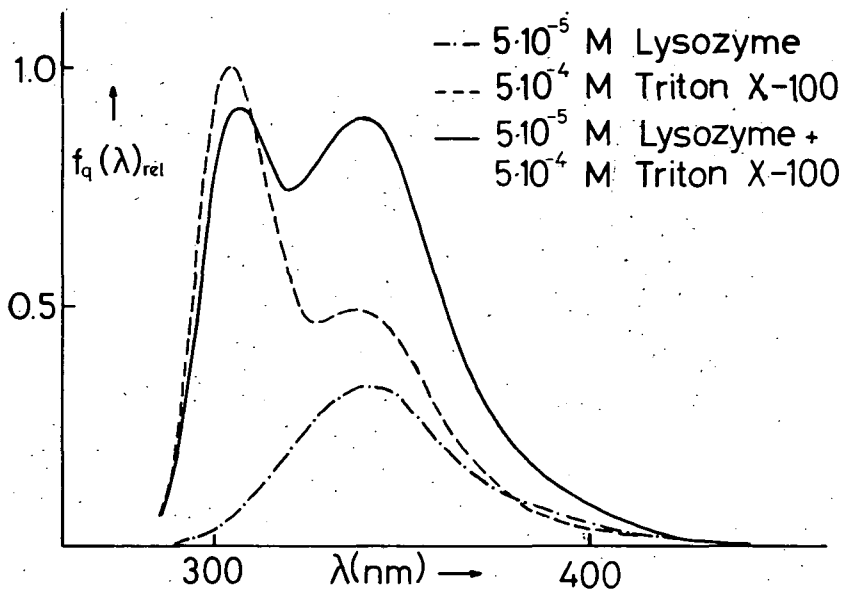


Fig. 3

In Fig. 4 the calculated and measured functions $f(\lambda')$ are plotted for mixed solutions containing albumin-triton (Fig. 4b) and lysozyme-triton (Fig. 4a). The difference between the calculated and measured spectra is related to the energy transfer.

The efficiency of transfer is given by the general relation [16]

$$f = \frac{(R_0/R)^j}{(R_0/R)^j + 1}, \quad (2)$$

where j is the exponent of the distance-dependence (if $j=6$, the interaction is of inductive resonance type), R is the distance between the molecules, and R_0 is the critical distance, at which the probability of transfer is equal to that of radiative deactivation of the primarily excited molecule.

From data obtained experimentally:

$$f = \frac{I_{\text{mix}}(\lambda) - I_A(\lambda) - I_D(\lambda)}{\frac{k_D(\lambda_{\text{exc}})}{k_A(\lambda_{\text{exc}})} I_A(\lambda) - I_D(\lambda)}, \quad (3)$$

where $I_{\text{mix}}(\lambda)$, $I_D(\lambda)$ and $I_A(\lambda)$ are the fluorescence intensities (corrected for reabsorption) of the mixture and solutions containing only the donor molecule and acceptor

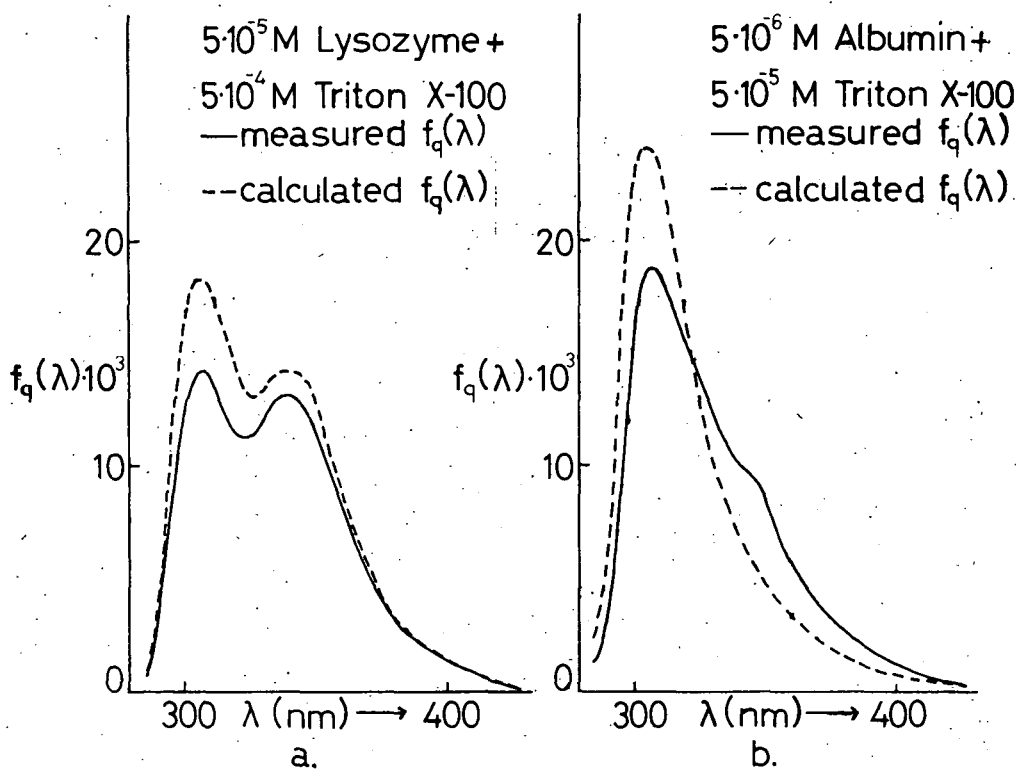


Fig. 4

molecule, respectively; λ denotes the wavelength at the maximum of the fluorescence spectrum of the donor; $k_D(\lambda_{\text{exc}})$ and $k_A(\lambda_{\text{exc}})$ are the absorption coefficients of solutions containing only the donor and the acceptor molecules respectively; and λ_{exc} is the wavelength of excitation [17].

With values of f calculated with (3) for mixtures of different concentrations, the function $\lg(f^{-1}-1)$ was determined and plotted as a function of $\lg R$ for lysozyme-triton (Fig. 5a) and albumin-triton (Fig. 5b) systems.

The calculation of the average distance R between donor and acceptor molecules can be omitted, because the ratio of these distances in solutions with different

concentrations is equal to the ratio of the distances between donor molecules in these solutions. Therefore, in Fig. 5 R is the distance between the donor molecules in mixed solutions. R was calculated from the relationship $R^3 = 3000/4\pi Nc$, where c is the molar concentration of the pigment, and N is Avogadro's number [12].

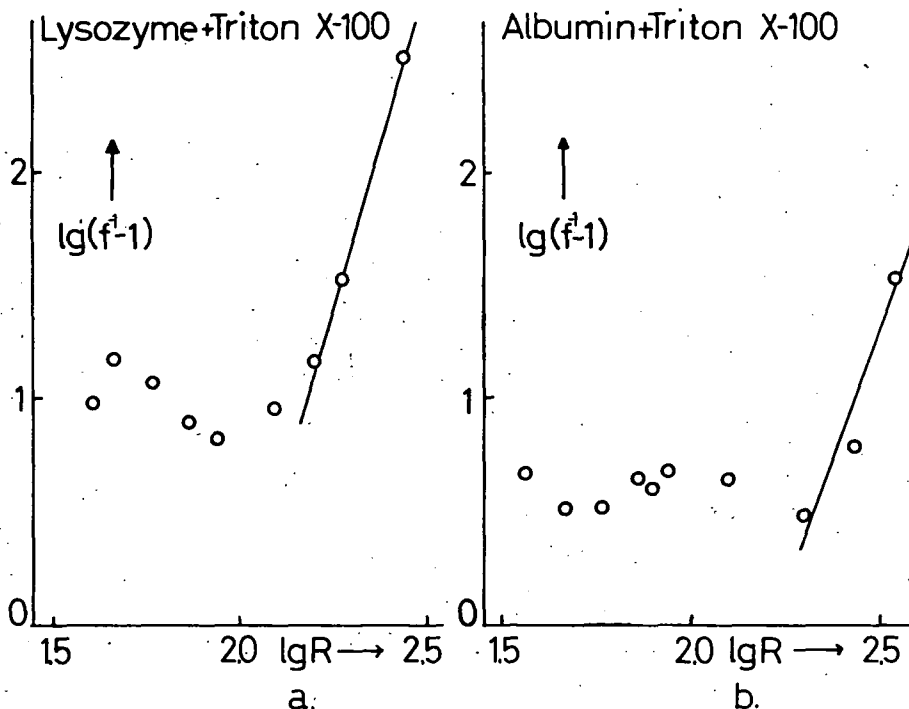


Fig. 5

At low concentrations the function $\lg(f^{-1}-1)$ is linear, the slope being $j \approx 5$ in the albumin-triton system (Fig. 5b). This points to the existence of a stronger interaction than that of inductive resonance. Since albumin molecules have about 5 places to bind triton molecules at a molar ratio triton:albumin=10 [8], the bondings here may give the possibility for this phenomenon. In lysozyme-triton systems (Fig. 5a) $j \approx 6$, i.e. the energy transfer takes place by inductive resonance.

At higher concentrations, above the critical micelle concentration, the number of free detergent molecules is constant. The efficiency of energy transfer should increase with increasing protein concentration, if the transfer were to take place from free detergent molecules. This increase was, however, not observed, the efficiency showing practically no concentration-dependence. Therefore, it has to be assumed that the protein molecules interact with micelles, similarly as was found in the system of tween 20—lysozyme [10]. In Fig. 6 the ratio of the activities measured in the presence and absence of triton is plotted as a function of the logarithmic detergent concentration. When a great number of micelles are present, the activity of lysozyme

increases by about 60%. Formally we can think that the lysozyme molecule interacting with the micelles is oriented in such a way that its active part becomes more accessible for the substrate. An alternative explanation is offered by assuming the weakening of the β -1,4 glycoside linkages of the substrate due to the detergent, which would cause the lysis to become quicker.

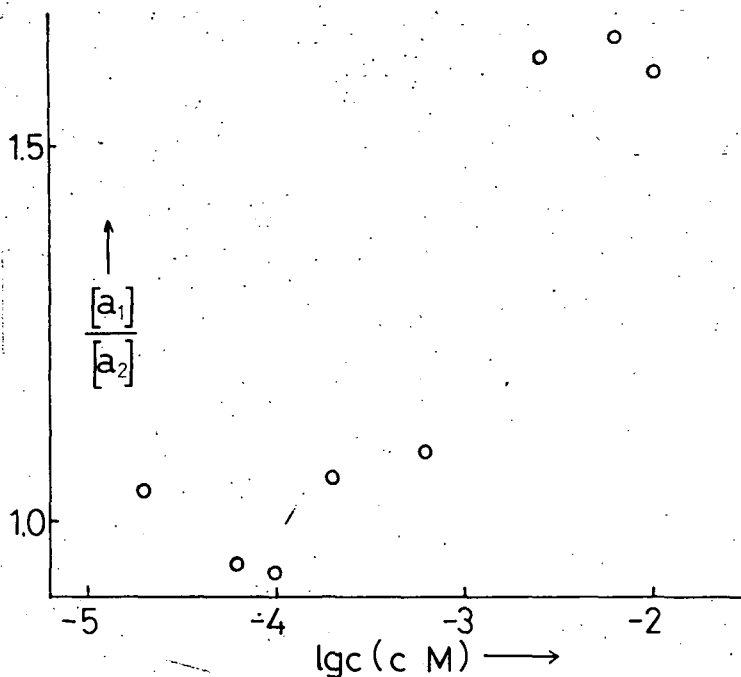


Fig. 6

References

- [1] Ogawa, T., L. P. Vernon: BBA 180, 334 (1969).
- [2] Thornber, J. P., J. M. Olson: Photochem. Photobiol. 14, 329 (1971).
- [3] Fehér, G.: Photochem. Photobiol. 14, 373 (1971).
- [4] Gratzner, W. B., G. H. Beaven: J. Phys. Chem. 73, 2270 (1969).
- [5] Krasnovsky, A. A.: Biophys. J. 12, 749 (1972).
- [6] Brashnikov, B. I., A. K. Chibisov: Biofizika 18, 747 (1973).
- [7] Massini, P., G. Voorn: BBA 153, 589 (1968).
- [8] Green, F. A.: J. Coll. Interf. Sci. 35, 481 (1971).
- [9] Cowgill, R. W.: Arch. Biochem. Biophys. 104, 84 (1964).
- [10] Bernath, F. R., W. R. Vieth: Biotechnol. Bioenerg. 14, 737 (1972).
- [11] Dwiggin, C. W., Jr., R. J. Bolen, H. N. Dunning: J. Phys. Chem. 64, 1175 (1964).
- [12] Förster, Th.: Fluoreszenz Organischer Verbindungen, Vandenhoeck und Ruprecht, Göttingen, 1951.
- [13] Budó Á., I. Ketskeméty: J. Chem. Phys. 25, 595 (1956).
- [14] Shugar, D.: BBA 8, 302 (1952).

- [15] *Dombi, J.*: Lumineszkáló keverék oldatokban lejátszódó energiaátadásokról. (About Energy Transfers in Luminescent Mixed-solutions; Candidate Thesis in Hungarian) Szeged, (1967).
- [16] *Streyer, L., R. P. Haugland*: Proc. Nat. Acad. Sci. US 58, 719 (1967).
- [17] *Bauer, R. K., L. Szalay, E. Tombácz*: Biophys. J. 12, 73 (1972).

ПЕРЕНОС ЭНЕРГИИ ЭЛЕКТРОННОГО ВОЗБУЖДЕНИЯ
В РАСТВОРАХ ПРОТЕИНА—ДЕТЕРГЕНТА

Э. Возари и Л. Салаи

Для системы лизоцим-третон X—100 характерно, что спектры поглощения аддитивны, тогда как в случае альбумин-третон X—100 аддитивность не выполняется при концентрации белков $2 \cdot 10^{-6}$ — $8 \cdot 10^{-4}$ М и третона $2 \cdot 10^{-5}$ — $8 \cdot 10^{-3}$ М. В обеих системах вследствие перекрытия спектров поглощения и флуоресценции происходит передача энергии электронного возбуждения от третона на белок. Зависимость переноса энергии от расстояния молекул третона X—100 и белка в растворах лизоцима и альбумина описывается закономерностью R^{-6} и R^{-5} , соответственно. Установлено, что ферментная активность лизоцима в растворах третона X—100 увеличивается на 60% .

CONCENTRATION DEPOLARIZATION BY EXCITATION TRANSFER. SELFQUENCHING CONSIDERATIONS

By

C. BOJARSKI and R. BUJKO

Institute of Physics, Technical University, Gdańsk

(Received January 5, 1976)

A generalization of photoluminescence concentration depolarization worked out by FÖRSTER and ORE for the case of concentration quenching by nonluminescent dimers was made.

The obtained expression for emission anisotropy was compared with experimental results. It was found, that the generalized FÖRSTER-ORE theory can be applied to a wider range of concentration, first of all to the case of systems with a low value of dimerization constant.

1. Introduction

In the majority of the existing theories on photoluminescence concentration depolarization (PLCD) of isotropic solutions, photoluminescence concentration quenching (PLCQ) is either completely neglected or taken into account only approximately [1-15].¹

The PLCD theories which do not take self-quenching into consideration describe the experimental results correctly only for not large concentration ranges of dye molecules. In the range of high concentrations photoluminescence depolarization is smaller than that predicted by these theories. The most noticeable lack of agreement with experiment of these theories is seen in the case of the systems in which repolarization takes place². In the past attempts were made to generalize FÖRSTER-ORE's as well as JABLONSKI's theories for the case of self-quenching [4-8, 13, 14, 17]. SZALAY [6, 7] and KAWSKI [5] have succeeded in obtaining a better agreement of the FÖRSTER-ORE theory with experiment by replacing the reduced concentration γ appearing in the theory by an expression of type $\sqrt{\eta(\gamma)} \cdot \gamma$, where $\eta(\gamma)$ denotes the photoluminescence (PL) quantum yield. A procedure of this kind is, however, not adequate to the quenching mechanisms accepted at present³, because it treats all the forms of quenching in a summary way.

¹ In [1-3] a review of the existing PLCD theories and a discussion as to the accepted simplifying assumptions is presented.

² This phenomenon observed for the first time by FEOFILOV and SVESHNIKOV [16] has been proved by SZALAY *et al.* [17] as well as by others [18-20]).

³ These are [22-24]: (1) non-active absorption by non-luminescent dimers; (2) non-radiative energy transfer from excited monomers to dimers in one or many steps; (3) excitation energy degradation during its transfer between monomers.

Let us add that the non-active absorption of exciting light by dimers does not affect the observed PL polarization. The generalizations of the PLCD theory made by JABŁOŃSKI, presented in [8, 17], are of similar character. The FÖRSTER-ORE PLCD theory has recently been generalized by CRAVER and KNOX [11], who in their theory took into account the angular factor appearing in the expression for rate constant of non-radiative excitation energy transfer and also took into account the participation of the molecules D_1 and D_2 — the nearest neighbours of molecules D_0 , primarily excited by light absorption in the process of excitation energy migration. A generalization of the FÖRSTER-ORE theory for the case of PL-quenching by dimers seems to be equally useful. The aim of the present work is to take into consideration the quenching conditioned by the non-radiative energy transfer from excited monomers D^* to dimers D_{II} both in a single and in several steps in the mentioned FÖRSTER-ORE theory.

2. The effect of self-quenching on emission anisotropy

Let us assume, similarly as in [13], that non-radiative energy transfer from excited monomers to non-excited ones causes merely depolarization, while energy transfer to dimers causes PL selfquenching. Moreover, assuming that PL self-quenching leading to a drop of quantum yield η/η_0 causes parallel changes in the lifetime of molecules D in excited state, that is

$$\frac{\eta}{\eta_0} = \frac{\tau}{\tau_0}, \quad (1)$$

then, in conformity with PERRIN [25], changes in emission anisotropy can be described as:

$$\frac{r_0}{r} = 1 + \left(\frac{r_0}{r'} - 1 \right) \frac{\eta}{\eta_0}, \quad (2)$$

where r , introduced by Jabłoński in [26], connects the emission anisotropy (EA) with the polarization degree (P) by the relation

$$r = \frac{2P}{3-P}, \quad (3)$$

in which r is the emission anisotropy dependent on dimer and monomer concentrations c'' and c' respectively, r' denotes (EA) dependent only on c' and r_0 the ground anisotropy. We assume that concentration changes in emission anisotropy r'/r_0 are determined by the expression obtained by ORE [27]

$$\frac{r'}{r_0} = \int_0^\infty \frac{\xi^2(\xi^2 + \gamma_D^2) \exp(-\xi) d\xi}{(\xi^2 + \gamma_D^2)^2 - \gamma_D^4 \exp\left(-\frac{11\xi}{16}\right)} \quad (4)$$

and the changes of quantum yield η/η_0 are described by FÖRSTER's formula [28] taking into account a single-step mechanism of excitation transfer:

$$\frac{\eta}{\eta_0} = 1 - f(\gamma_{D_{II}}) = 1 - \sqrt{\pi} \gamma_{D_{II}} \exp(\gamma_{D_{II}}^2) [1 - \operatorname{erf}(\gamma_{D_{II}})]. \quad (5)$$

Here ξ is the mean number of luminescent molecules in the volume of a sphere of radius R , γ_D and $\gamma_{D_{II}}$ denote reduced concentrations of monomers and dimers, respectively, at which

$$\gamma_D = \frac{\sqrt{\pi}}{2} \frac{c'}{c'_0}; \quad \gamma_{D_{II}} = \frac{\sqrt{\pi}}{2} \frac{c''}{c''_0}; \quad (6)$$

where c'_0 and c''_0 are critical concentrations for non-radiative excitation transfer from D^* to D and from D^* to D_{II} , respectively.

In Fig. 1 the theoretical courses of r/r_0 determined by formula (2) are presented, taking into account expressions (4) and (5) for r'/r_0 and η/η_0 , respectively. The computations were made for several values of the dimensionless constant $\mathcal{K}_\gamma = \gamma_{D_{II}}/\gamma_D^2$, which is connected with dimerization constant $K = c''/c'^2$ by the equation

$$\mathcal{K}_\gamma = \frac{2Kc'_0{}^2}{\sqrt{\pi} c''_0}. \quad (7)$$

The values of the reduced concentrations γ_D and $\gamma_{D_{II}}$ were calculated for each particular \mathcal{K}_γ from relation

$$\gamma_D = \alpha\gamma, \quad \gamma_{D_{II}} = (1 - \alpha)\gamma, \quad (8)$$

where

$$\alpha = \frac{\sqrt{1 + 4\mathcal{K}_\gamma} - 1}{2\mathcal{K}_\gamma}, \quad (9)$$

$$\gamma = \gamma_D + \gamma_{D_{II}} \quad (10)$$

As seen from the figure, all curves for $\mathcal{K}_\gamma > 0$ exhibit maxima, the position of which depends on the value of \mathcal{K}_γ . Similar results [13] were obtained from an analogous generalization of JABŁOŃSKI's PLCD theory. In [13] we compared JABŁOŃSKI's theory with the experimental results concerning the concentration changes of emission anisotropy of rhodamin 6 G in glycerin-water solutions and we found a good agreement of theory with experiment in the range of low and moderate concentrations and an approximate agreement in the range of high concentrations.

A comparison was made for the values of critical concentrations c'_0 and c''_0 , found on the basis of spectroscopic investigations ($\kappa_{\text{theor}} = \frac{c'_0}{c''_0} = 1.29$) and for values

c'_0 and c''_0 ($\kappa_{\text{exp}} = \frac{c'_0}{c''_0} = 4.75$) obtained by comparing the appropriate experimental results with JABŁOŃSKI's theoretical expressions describing the concentration changes of r/r_0 and η/η_0 . The mentioned agreement of theory with experiment was obtained for κ_{theor} , but for κ_{exp} the deviations of the experimental points from the theoretical curve in the range of high concentrations were very big. In [13] we proved that the difference between the values κ_{theor} and κ_{exp} resulted from the fact that in

the theoretical expression for η/η_0 given by JABŁOŃSKI the multi-step mechanism of non-radiative excitation energy transfer from monomers to dimers had been neglected.

Also Eq. (5) takes into account only the single-step mechanism of energy transfer from D^* to D_{II} . Recently we have worked out the PLCQ theory which takes into consideration the multi-step mechanism of energy transfer. For the quantum yield we obtained expression [23]

$$\frac{\eta}{\eta_0} = \frac{1-f(\gamma)}{1-\alpha f(\gamma)} \quad (11)$$

which in the case of $\gamma_D \ll \gamma_{D_{II}}$ becomes Eq. (5). Substituting in Eq. (2) formulas (4) and (11) for r'/r_0 and η/η_0 and taking into account (8) we obtain:

$$\frac{r}{r_0} = 1 + \left\{ \int_0^\infty \frac{\xi^2 [\xi^2 + (\alpha\gamma)^2] \exp(-\xi) d\xi}{[\xi^2 + (\alpha\gamma)^2]^2 - (\alpha\gamma)^4 \exp\left(-\frac{11\xi}{16}\right)} \right\}^{-1} - 1 \cdot \frac{1-f(\gamma)}{1-\alpha f(\gamma)} \quad (12)$$

When dimers do not appear in solution ($\alpha \rightarrow 1$), Eq. (12) becomes (4), but in the case when $\gamma_{D_{II}} \gg \gamma_D$,

$$\alpha \rightarrow 0 \quad \text{and} \quad r/r_0 \rightarrow 1.$$

In Fig. 1 the curves determined by Eq. (12) for several values of \mathcal{K}_γ , are plotted with dashed lines. They also exhibit minima and, moreover, in the range of highest concentrations, the higher their courses are in relation to the corresponding solid curves, the lower is the value of \mathcal{K}_γ . In this figure the Förster-Ore curve corresponding to $\mathcal{K}_\gamma = 0$ is also plotted and, in distinction from the other curves, it tends asymptotically to zero for $\gamma \rightarrow \infty$.

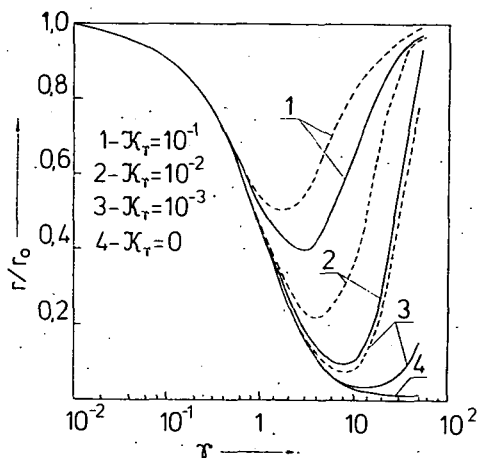


Fig. 1. Theoretical curves of concentration changes in emission anisotropy
 ——— computed on the basis of (2), (4) and (5)
 - - - - - computed on the basis of (12)

3. Comparison with experiment and final remarks

In Fig. 2 the experimental results referring to PL concentration depolarization of the systems listed in Table I are compared with formula (2), taking into account Eqs. (4) and (5), and with formula (12). The best agreement of experimental results with theory in the range of low and moderate concentrations was obtained for much higher values of η_0 than in the Refs. quoted in column 8 of Table I, (comp. columns 3 and 9) and thus for other values of constants \mathcal{K}_γ , c'_0 and c''_0 ⁴. Table II contains the parameter values indispensable for the comparison of theory with experiment. Column 6 gives also the values $\kappa_{\text{theor}} = (c'_0/c''_0)_{\text{theor}}$ found on the basis of spectroscopic investigations, and columns 15, 16, 17 the values κ_{exp}^* and κ_{exp}^{**} obtained by comparison of the experimental results with theoretical curves. Values of c'_0 were found by comparing the experimental results r/r_0 with Eq. (4) and c''_0 values by comparing the experimental η/η_0 with Eq. (5) and with Eq. (11), respectively; (the corresponding values are marked by c_0^{**} and c_0^{***}).

The concentrations c_0^{***} listed in columns 12 and 13, respectively, were found for the values $\alpha_0 = 1$ and $\alpha_0 < 1$ assumed in formula (11), *i. e.* neglecting and taking into account the PL monomer quenching⁵. The comparison of values κ_{theor} with values κ_{exp}^* and κ_{exp}^{**} proves the best agreement of value κ_{exp}^{**} from columns 17 with κ_{theor} . This means that correct values of $c_{0\text{exp}}^{**}$ are obtained by comparing the experimental results of η/η_0 not with Eq. (5) but with Eq. (11) for $\alpha_0 < 1$. Even for $\alpha_0 = 1$ expr. (11) gives more correct values of c_0^{***} than expr. (5) (comp. values κ_{theor} and κ_{exp}^{**} from column 16).

Hence it can be concluded that in PL concentration quenching the basic role can be ascribed to the multi-step mechanism of non-radiative excitation energy transfer to dimers; also the mechanism of monomer quenching cannot be neglected. From Fig. 2 we see that in the range of highest concentrations the experimental points deviate from both the solid curves and the dashed ones in the case of all the systems investigated, differing by the value of dimerization constant. In the mentioned range of concentrations γ the solid curves determined by expressions (2), (4) and (5) lie distinctly below the experimental results (except the case of system III). A similar regularity could be found [13] in the case of the generalization of JABŁOŃSKI's PLCD theory, the point of which was the role of self-quenching conditioned by the presence of dimers in solution. Still a further generalization of the mentioned theory, in which both dimer and monomer quenching was taken into account, gave better agreement with experiment chiefly in the case of systems of low dimerization constant value. In the case of systems with high value of \mathcal{K}_γ , this agreement was slightly improved. It is to be expected that taking monomer self-quenching into account in the actually discussed FÖRSTER-ORE theory could bring an analogous improvement of the agreement between theory and experiment in the case of the results presented in Fig. 2.

The dashed curves determined by expr. (12) in which η/η_0 was replaced by formula (11) lie distinctly above the experimental points in the range of highest

⁴ Because $\mathcal{K}_\gamma \sim \eta_0^{-1/2}$ and $c_0 \sim \eta_0^{-1/2}$; comp. also footnote 1 in [20].

⁵ Concrete values of α_0 to which the c_0^{***} listed in column 13 correspond have been taken from the Refs. quoted in Table I.

Table I

1	2	3	4	5	6	7	8	9	10	11	12	13	14	15	16	17
System	η'	η_0	C_0'	C_0''	\times theor	K	Ref	η_0	C_0'	C_0''	C_0'''	C_0''''	K_γ	\times_{exp}^*	\times_{exp}'''	\times_{exp}''''
	P	—	10^{-3} M/L		—	l/M			10^{-3} M/L							
I. Na-FL/GW — Na-fluorescein in glycerin-water solutions	3.3	0.88	4.67	3.28	1.426	0.065	[19]	1.4	3.704	0.13	1.25	3.31	0.0004	28.49	2.963	1.410
II. Na-FL/GW — Na-fluorescein in glycerin-water solutions	0.43	0.6	6.06	4.25	1.427	0.54	[19]	0.83	5.15	0.071	2.33	4.80	0.005	72.577	2.211	1.262
III. Ac/GM — Acri- flavine in glycerin- methanol solutions	3.9	0.417	10.1	10.1	1	12	[20]	0.66	8.02	4.8	10.32	13.28	0.14	1.67	0.777	0.760
IV. R6G/GW — Rhodamin 6 G in glycerin-water solutions	5.3	0.6	3.47	2.68	1.29	11.1	[18]	0.82	2.965	0.886	1.99	2.94	0.06	2.63	1.49	1.180
V. R6G/GE — Rhodamin 6 G in glycerin-ethanol solutions	5.85	0.7	3.94	2.67	1.475	1	[29]	2.21	2.22	0.34	1.513	2.66	0.004	6.54	1.467	1.479
VI. RB/GW — Rhodamin B in glycerin-water solutions	7.4	0.7	2.83	2.22	1.276	0.23	[30]	1.52	1.93	0.06	0.47	2.10	0.0007	32.17	4.106	1.349

concentrations. In this case, taking into account the monomer quenching would even more increase the divergence between theory and experiment.

An approximate description of the experimental results can thus be obtained by applying expr. (5) in PERRIN's formula (2) and taking into account the energy transfer from D^* to D_{II} in one step⁶.

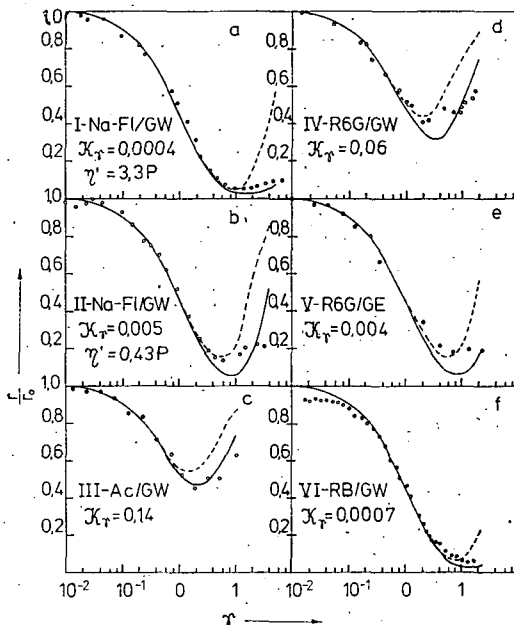


Fig. 2. Comparison of the generalized FÖRSTER-ORE theory with experimental results; ——— and ——— theoretical curves determined by equations (12) and (2), (4), (5) respectively; \circ are experimental points Fig. *a* and *b*: Na-fluorescein in glycerin-water solutions of 3,3 P and 0,45 P viscosities, respectively; Fig. *c*: acriflavine in glycerin-methanol solutions; Fig. *d*: rhodamin 6 G in glycerin—water solutions; Fig. *e* rhodamin 6 G in glycerin—ethanol solutions; Fig. *f*: rhodamin B in glycerin—water solutions.

This is so because the migration of excitation energy in a system of molecules D has already been taken into account in the expression for r'/r_0 appearing in (2). We should state that the generalization of the FÖRSTER-ORE PLCD theory for the case of quencing by dimers allows to apply this theory to a wider range of concentrations, first of all to systems of low dimerization constant value. In strongly dimerizing systems and in ranges of high concentrations this theory does not fully describe the experimental results (there is only a qualitative agreement as to the repolarization effect). The reasons of the mentioned disagreement can be numerous; among others, the assumption (1) as to parallel lifetime and quantum yield changes

⁶ Molecules D^* can be excited both by light absorption and as a result of excitation energy transfer.

is not generally valid, neither is the assumption of the independence of depolarization and self-quenching process. Let us add that the PLCD theory worked out by one of the authors [31] allows to describe correctly all the experimental results quoted in the present work in the whole range of concentrations [18–20, 29–31].

* * *

This work was supported by the Polish Academy of Sciences within the Project PAN—3.2.07.

References

- [1] *Knox, R. S.*: Physica 39, 361 (1968).
- [2] *Sarheuskij, A. M., A. N. Sevtschenko*: Anisotropija pogloschenija i ispuskanija sveta molekulami, Mińsk, 1971.
- [3] *Ore, A., E. L. Eriksen*: Phys. Norveg. 5, 57 (1971).
- [4] *Bojarski, C.*: Ann. Physik Leipzig 8, 402 (1961).
- [5] *Kawski, A.*: Z. Naturforsch. 18a, 966 (1963).
- [6] *Szalay, L.*: Ann. Physik Leipzig 14, 221 (1964).
- [7] *Szalay, L.*: Acta Phys. Polon. 26, 511 (1964).
- [8] *Kawski, A.*: Proceedings of the International Conference on Luminescence, Budapest, 1966, p. 292.
- [9] *Eriksen, E. L.*: Phys. Norveg. 2, 203 (1967).
- [10] *Dale, R. E., R. K. Bauer*: Acta Phys. Polon. A40, 853 (1971).
- [11] *Crauer, F. W., R. S. Knox*: Molec. Phys. 22, 385 (1971).
- [12] *Jabłoński, A.*: Acta Phys. Polon. A41, 85 (1972).
- [13] *Bojarski, C., J. Dudkiewicz, H. Pruszek*: Acta Phys. et Chem. Szeged 18, 3 (1972).
- [14] *Bojarski, C., J. Dudkiewicz*: Acta Phys. et Chem. Szeged 19, 15 (1973).
- [15] *Hemenger, R. P., R. P. Pearlstein*: J. Chem. Phys. 59, 4064 (1973).
- [16] *Feofilov, P. P., B. J. Sveshnikov*: J. exp. theor. Phys. 10, 1372 (1940).
- [17] *Szalay, L., B. Sárkány, E. Tombácz*: Acta Phys. et Chem. Szeged 11, 21 (1965).
- [18] *Bojarski, C., J. Dudkiewicz*: Z. Naturforsch. 26a, 1028 (1971).
- [19] *Bojarski, C., J. Dudkiewicz*: Z. Naturforsch. 27a, 1751 (1972).
- [20] *Bojarski, C., J. Dudkiewicz, A. Bujko*: Acta Phys. et Chem. Szeged 20, 267 (1974).
- [21] *Förster, Th.*: Fluoreszenz Organischer Verbindungen, Vandenhoeck und Ruprecht, Göttingen, 1951.
- [22] *Levshin, V. L.*: Izv. Akad. Nauk USSR, ser. fiz. 25, 540 (1963).
- [23] *Bojarski, C., J. Domsta*: Acta Phys. Hung. 30, 145 (1971).
- [24] *Makshantsev, B. I.*: Izv. Akad. Nauk USSR, ser. fiz. 36, 1082 (1972).
- [25] *Perrin, F.*: J. Physique Radium 7, 390 (1926).
- [26] *Jabłoński, A.*: Acta Phys. Polon. 16, 471 (1957).
- [27] *Ore, A.*: J. Chem. Phys. 31, 442 (1959).
- [28] *Förster, Th.*: Z. Naturforsch. 4a, 321 (1949).
- [29] *Bojarski, C., G. Obermueller*: Acta Phys. Polon., in press.
- [30] *Bojarski, C., A. Bujko, J. Dudkiewicz, J. Kuśba, G. Obermueller*: Acta Phys. Polon. A45, 71 (1974).
- [31] *Bojarski, C.*: J. Luminescence 5, 413 (1972).

КОНЦЕНТРАЦИОННАЯ ДЕПОЛЯРИЗАЦИЯ ПОСРЕДСТВОМ ПЕРЕНОСА ЭНЕРГИИ. УЧЕТ САМОТУШЕНИЯ

Ч. Боярски и Р. Буйко

Проведено обобщение теории концентрационной деполаризации фотоллюминесценции, разработанной Ферстером и Оре, на случай концентрационного тушения неллюминесцирующими димерами. Полученное выражение для анизотропии эмиссии сравнено с экспериментальными результатами. Установлено, что теория Ферстера–Оре может быть применена для более широкой области концентрации, особенно в случае систем с низким значением константы димеризации.

О ПРИРОДЕ ФОТОПРОДУКТОВ ГЕНЕРИРУЮЩИХ КРАСИТЕЛЕЙ

Л. КОЗМА, Э. ФАРКАШ, И. КЕЧКЕМЕТИ и М. МОЛНАР

Институт экспериментальной физики университета им. А. Йожефа, г. Сегед

(Поступило в редакцию 1 февраля 1976 г.)

В настоящей работе представлены результаты исследований проведенных для изучения спектроскопических свойств продуктов фотореакций родаминовых красителей. Фракции разделены хроматографическим методом и измерены их спектры поглощения и люминесценции. На основе экспериментальных данных найдены условия возникновения фотопродуктов и их влияние на генерацию.

В ряде работ показано, что фотопродукты, возникающие в генерирующих растворах при накачке мощными световыми импульсами, в значительной мере изменяют параметры излучения лазеров. Несмотря на то, что этот вопрос достаточно изучен, до сих пор не известна основная природа происходящих фотохимических процессов, спектрофотометрические характеристики возникающих продуктов и их влияние на работу лазера [1].

Цель настоящей работы — определить условия возникновения в растворе фотопродуктов, разделить их и измерить люминесцентные-спектроскопические характеристики. Исследовались два родаминовых красителя, широко используемых в лазерах: родамин 6Ж и родамин Б производства фирмы Merck.

В предыдущих работах [2] мы показали, что при облучении раствора мощным светом импульсных ламп возникает фотопродукт, поглощающий в длинноволновом краю полосы поглощения красителя родамина 6Ж. Анализ экспериментально полученных спектров при разных интенсивностях накачки позволил определить истинный спектр исходного красителя, однако из-за малой интенсивности полосы поглощения фотопродуктов эту полосу не могли полностью разделить расчетами. Спектр люминесценции фотопродуктов изучался при антистоксовом возбуждении в полосе поглощения родамина 6Ж.

Хроматографическое разделение компонентов красителей дает возможность детально изучить компоненты красителей. С этой целью мы разделили на компоненты заводские препараты на хроматографической колонне [3]. В обоих красителях получено несколько компонентов, из которых один составляет около 97%, 5—6 других компонентов составляют сравнительно большее количество, а остальные фракции встречаются в ничтожно малых количествах. Компоненты, присутствующие в самом большом количестве, разделили путем хроматографий, перекристаллизовали их и приготовили растворы для спектрофотометрических измерений. Спектры поглощения и люминесценции компонентов родамина 6Ж и родамина Б приведены на рисунках 1—4; данные, относящиеся к компонентам, представлены в таблице. Изображенные спектры

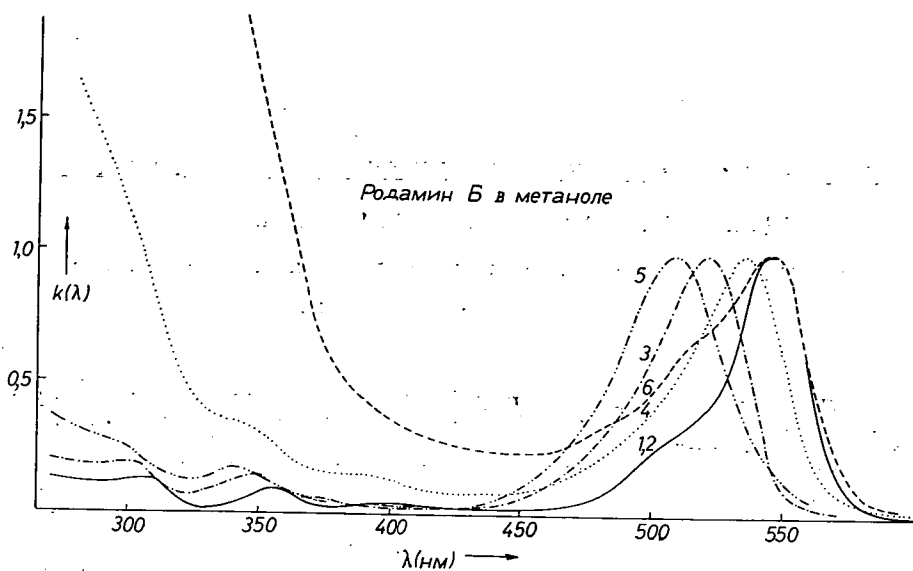


Рис. 1

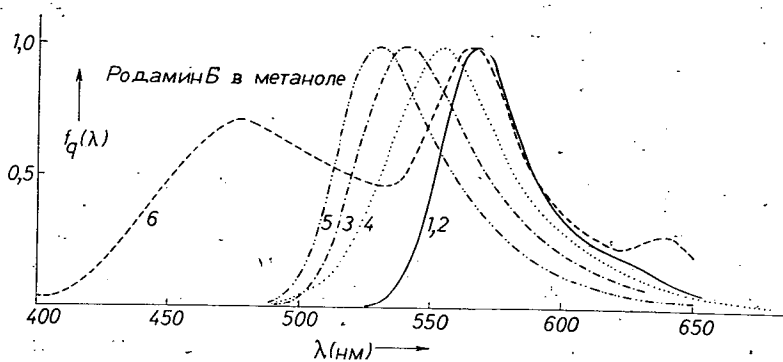


Рис. 2

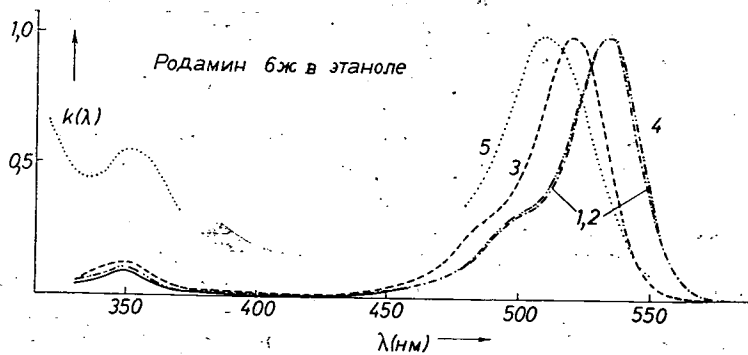


Рис. 3

нормированы в максимумах длинноволновой полосы поглощения и люминесценции. Растворителем служили этиловый и метиловый спирты без уксусной кислоты, т. к. в предыдущих исследованиях кислота усиливала фотореакции, что усложняло происходящие процессы.

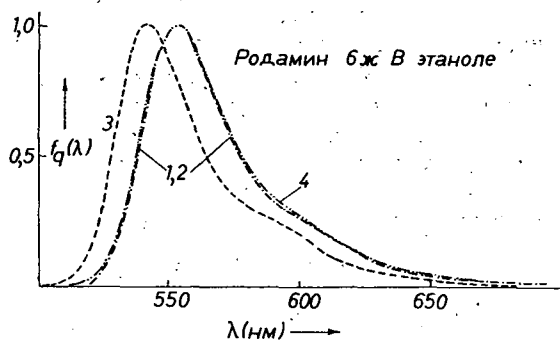


Рис. 4

Родамин Б в метаноле

Таблица 1

Родамин 6Ж в этаноле

№	Родамин Б в метаноле			Родамин 6Ж в этаноле				
	Количество (%)	$\lambda_{\text{в}}$ (нм)	$\lambda_{\text{погл. макс}}$ (нм)	$\lambda_{\text{люм. макс}}$ (нм)	Количество (%)	$\lambda_{\text{в}}$ (нм)	$\lambda_{\text{погл. макс}}$ (нм)	$\lambda_{\text{люм. макс}}$ (нм)
1	—	350	545	568	—	470	535	553
2	98	350	545	568	97	470	535	553
3	1	350	520	540	1	470	520	540
4	0,2	480	535	555	1	470	535	553
5	0,2	350	508	530	1	—	510	—
6	0,3	350	545	475 565				

Числа, поставленные возле кривых и в таблице, обозначают очередность компонентов, которая составлялась по сравнительному количеству веществ. Число 1 обозначает спектры неочищенного вещества, а число 2 — спектры главного компонента, который представляет собой чистое вещество родамина 6Ж и родамина Б. Так как главные компоненты достигают 97—98% в смеси, их спектры на рисунках практически не отличаются от спектров неочищенных веществ. Видно, что в большинстве случаев спектры компонентов в значительной мере сдвинуты к спектрам главного компонента. Надо подчеркнуть, что некоторые компоненты очень сильно поглощают в ультрафиолетовой области. Из этого следует, что эти фракции, хотя и содержащиеся в малых количествах, увеличивают мощность поглощения в ультрафиолетовой области не-

разделенного вещества, т. е. могут быть полезными в работе лазеров на красителях. На хроматографической колонне (адсорбент Al_2O_3 , растворитель — смесь бензола (40%) и этанола (60%)) полученная фракция часто не оказывается однородной. Так например, у родамина 6Ж 3 из 4 фракций вместе разделяются на колонне, а при тонкослойной хроматографии (киселгэль; бензол (40%), этанол (60%)) они хорошо разделяются. Шестой компонент родамина Б далее разделить не смогли, а спектр его люминесценции показывает неоднородность.

Детальное изучение продолжалось на растворах родамина 6Ж. В работе [2] проводились расчеты по методу Аленцева для вычисления спектра чистого родамина 6Ж из спектров растворов, содержащих разные количества фотопродуктов. Было показано, что экспериментально измеренные спектры, изображенные полулогарифмически, при малых частотах отклоняются от линейного хода, и отклонения увеличиваются с ростом интенсивности облучения, т. е. с увеличением количества фотопродуктов. В то же время функция $\lg \frac{\epsilon(\nu)}{\nu}$ для вычисленного спектра главного компонента оказалась линейной.

Главный компонент перекристаллизовали, затем приготавливался раствор.

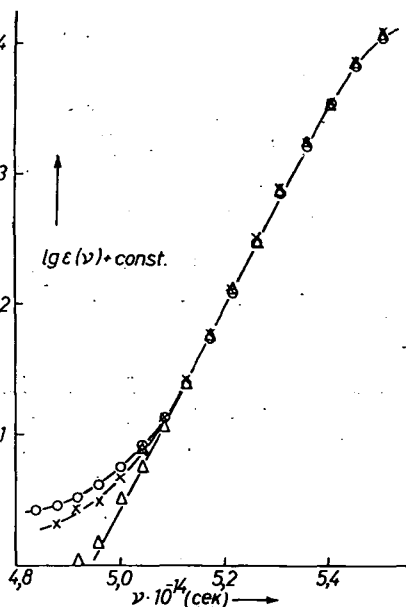


Рис. 5

Однородность красителя проверялась тонкослойной хроматографией, затем измерялся его спектр поглощения. Логарифмы полученных коэффициентов поглощения приведены на рис. 5. треугольниками, где для сравнения показана кривая, относящаяся к неочищенному красителю (кресты). Видно, что экспериментальный спектр главного компонента имеет такой же линейный ход, как и вычисленный в [2]. Из этого можно сделать вывод о том, что главный компонент можно считать чистым, а приготовленный из него раствор — однокомпонентным. Раствор главного компонента помещался в кювету лазера и накачивался вспышками двух импульсных ламп типа ИФП 5000. Электрическая энергия одной вспышки составляла 640 дж, раствор облучался 20 вспышками. После этого измерялся спектр поглощения, на основе которого получена функция $\lg \frac{\epsilon(\nu)}{\nu}$, изображенная на рис. 5 кружками. Видно, что при малых частотах

спектр поглощения $\left(\lg \frac{\epsilon(\nu)}{\nu}\right)$ облученного раствора главного компонента отклоняется от линейного хода. Это говорит о появлении в растворе фотопродуктов.

Хроматографическим методом не смогли отделить один компонент, спектр поглощения которого находится в длинноволновом краю спектра поглощения

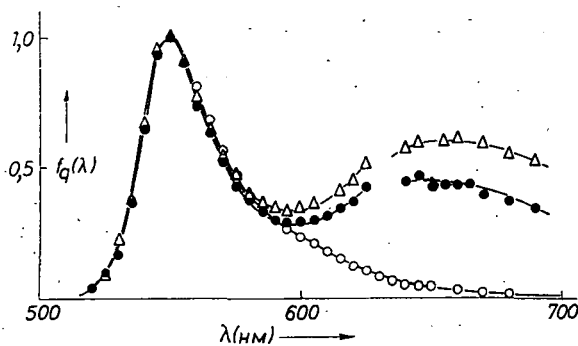


Рис. 6

родамина 6Ж. Количество этого вещества очень мало, но его поглощение соизмеримо с поглощением родамина 6Ж в этой области. Это очевидно из рисунка 6, где сплошная кривая изображает спектр флуоресценции родамина 6Ж при стоксовом возбуждении ($\lambda = 470$ нм), а треугольники — спектр неочищенного компонента, черные кружки — спектры главного компонента при возбуждении газовым лазером He-Ne ($\lambda = 632,8$ нм) [4]. Видно, что очистка уменьшает количество компонента, поглощающего и излучающего в красной области спектра. Из этих данных следует, что этот и главный компоненты не разделяются при этих условиях хроматографирования.

Для анализа спектров применялось универсальное соотношение Степанова [5], которое в логарифмическом виде дает линейную функцию в случае, если исследованное вещество состоит только из одного компонента. Кривые универсального соотношения $F(\nu)$ представлены на рис. 7 для главного компонента родамина 6Ж, где показаны кривые для неочищенного родамина 6Ж (кресты) и главного компонента до облучения (треугольники) и после облучения (кружки). Кривые показывают присутствие различных фракций в неочищенном веществе после облучения и в главном компоненте, в котором до облучения имелся только один сорт люми-

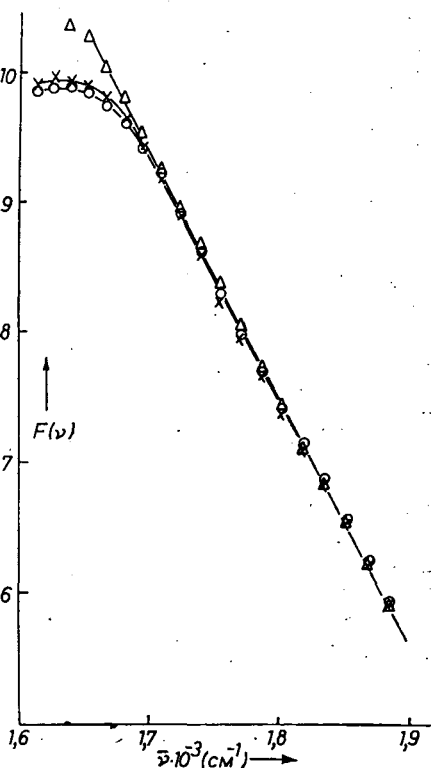


Рис. 7

несцирующих молекул. В работе [6] детально изучена связь между спектрами люминесценции и тепловым излучением, а также показана важная роль различных факторов. По выше показанным данным, раствор главного компонента можно считать однокомпонентным, поэтому представляет интерес изучение

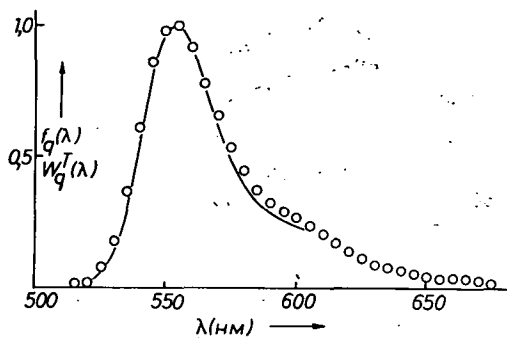


Рис. 8

отношения спектров флуоресценции и теплового излучения. Рис. 8 показывает спектры $f_q(\lambda)$ (кружки) и $W_q^T(\lambda)$ (сплошная кривая) для раствора главного компонента родамина 6Ж. При расчете функции $W_q^T(\lambda)$ использовалось значение температуры T , найденного из наклона кривой $F(\nu)$, которое оказалось равным 327°K (температура опыта была 298°K). Сравнительно большое значение вычисленной температуры и хорошее совпадение хода кривых $f_q(\lambda)$ и $W_q^T(\lambda)$, вычисленных с этими

значениями T , подтверждает предположение о локальном нагревании люминесцирующих центров во время возбужденного состояния. В этом случае, как показывает анализ спектров, на ход $F(\nu)$ примеси не влияют.

Проводились следующие эксперименты: главный компонент, не разделившийся при хроматографии, облучался в кристаллической фазе и в растворе, затем вновь была снята хроматограмма. Оказалось, что в обоих случаях появляются те же компоненты, которые содержались и в заводских препаратах. Также обнаружилось, что без интенсивной накачки через несколько дней появляются фотопродукты в растворе в условиях падения на него света лаборатории. Это явление не наблюдается, если раствор содержится в темноте.

На основе показанных данных и наших предыдущих результатов можно сделать следующие выводы: заводские препараты родаминовых красителей содержат различные примеси, которые являются продуктами фотореакций. Хроматографическим методом можно разделить главный компонент в чистом виде, в котором через некоторое время вновь возникают примеси под влиянием облучения. Фотопродукты, спектры которых находятся недалеко от спектров основного вещества, не ухудшают генерацию, т. к. с их присутствием раствор является смешанным и, следовательно, параметры генерации улунашаются [7]. Существует фотопродукт, который поглощает в области генерации основного вещества, поэтому этот компонент примесей увеличивает потери генерации. Так как спектры этого компонента в значительной мере сдвинуты в отношении спектра родамина 6Ж и его количество очень мало, при изучении спектров главного компонента влияние этих примесей не заметно, поэтому раствор главного компонента можно считать однокомпонентным.

Литература

- [1] Рубинов, А. Н., Т. И. Смольская, С. А. Михнов: ЖПС 13, 386 (1970).
- [2] Фаркаш Э., Л. Козма, Ф. Пинтер: Acta Phys. et Chem. Szeged 11, 423 (1973).
- [3] Drake, I. M., R. I. Morse: Opt. Commun. 13, 109 (1974).
- [4] Erikson, L. E.: J. Luminescence 5, 1 (1972).
- [5] Степанов Б. И.: ДАН СССР 112, 839 (1957).
- [6] Кечкемети И., Л. Козма, Я. Хевеши: Acta Phys. et Chem. Szeged 12, 3 (1966).
- [7] Кечкемети, И., Б. Рац, Ж. Бор, Л. Козма: Acta Phys. et Chem. Szeged 20, 14 (1975).

PHOTODECOMPOSITION OF LASER DYES

L. Kozma, É. Farkas, I. Ketskemény and M. Molnár

The paper presents the results of spectroscopic investigation of photochemical products of rhodamine dyes. The different components were separated by chromatography. Absorption and emission spectra were measured. The conditions of photochemical production of rhodamine derivatives and their influence on lasing properties of these dyes were studied on the base of experimental data.



ИССЛЕДОВАНИЕ ГЕНЕРАЦИИ ПОТУШЕННЫХ РАСТВОРОВ ФЛУОРЕСЦЕИНА

Л. КОЗМА, К. ЧЕРНАИ*, И. КЕЧКЕМЕТИ, Б. РАЦ и Ж. БОР

Институт экспериментальной физики университета им.
А. Йожефа, г. Сегед

(Поступило в редакцию 1 февраля 1976 г.)

В работе описывается изучение генерации потушенных растворов. Показано, что сильно потушенные растворы со сравнительно низким порогом генерируют, и с ростом концентрации тушителя выход люминесценции и к. п. д. генерации пропорционально уменьшаются относительно друг друга.

Изучение люминесценции потушенных растворов красителей [1] позволило выяснить природу основных процессов, происходящих в центрах люминесценции. Так как тушение люминесценции посторонними веществами уменьшает квантовый выход и длительность возбужденного состояния, можно ожидать, что особенности генерации потушенных растворов дают ценные дополнительные сведения о механизме генерации сложных молекул. Первые исследования в этой области показали, что при сильной лазерной накачке выступают наведенные потери, обусловленные $S_1^* \rightarrow S_n^*$ переходами [2]. В работе [3] показано, что тушение верхнего лазерного уровня S_1^* в значительной мере уменьшает наведенные потери. К сожалению, при этих исследованиях не изучался процесс генерационной способности потушенных растворов. Очевидно, что тушение вызывает два противоположно влияющих процесса: уменьшение η , которое ухудшает генерацию, и уменьшение наведенных потерь, которое улучшает её. В ряде работ показано (см., например, [4]), что некоторые тушители уменьшают и вредные потери $T-T$ переходов. В нашем эксперименте генерация произошла в наносекундном режиме, поэтому населенность триплетного уровня не играет роли.

Цель настоящей работы — описать изучение генерации потушенных растворов флуоресцеина. В качестве тушителя использовался KJ , концентрация которого менялась в пределах 0—1 моль/л. Растворителем служила смесь этилового спирта (85%) и воды (15%) или вода, концентрация флуоресцеина (производства фирмы Merck) была равна $2 \cdot 10^{-3}$ моль/л. Спектры поглощения и флуоресценции, а также квантовый выход определяли на спектрофотометре [5]. Генерация растворов изучалась с накачкой азотным лазером [6] в поперечном варианте. Максимальная мощность накачки — 100 квт с длительностью 5 нсек,

* Кафедра физики и химии Педагогического института, г. Суботица

а $\lambda = 337,1$ нм. Активный раствор находился в кювете с активной длиной 1 см, на торцах которой происходила генерация. Энергия накачки и генерация измерялась термостолбами в относительных единицах. Изменение энергии накачки осуществлялось применением стеклянных пластинок в качестве фильтров.

Зависимость относительного квантового выхода люминесценции η и относительного к. п. д. генерации от

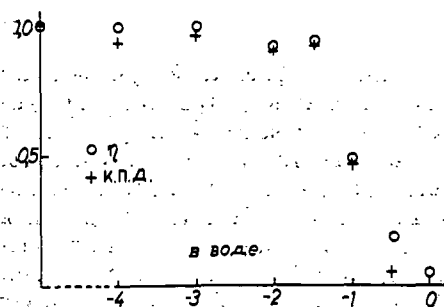
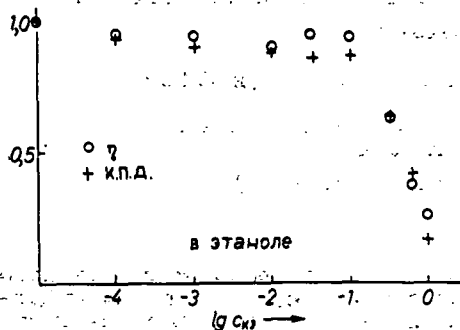


Рис. 1

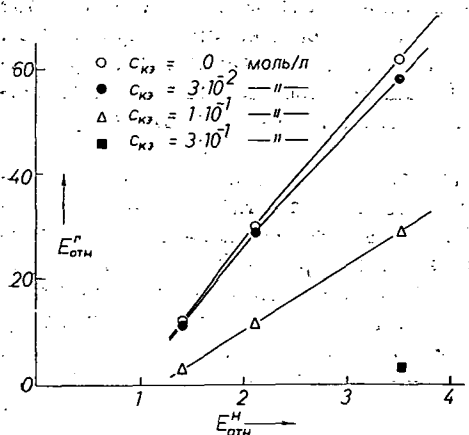


Рис. 2

концентрации тушителя показаны на рис. 1. Видно, что выход люминесценции флуоресцеина в этаноле уменьшается в 5 раз, а в воде — в 20 раз при концентрации тушителя 1 моль/л. Длительность возбужденного состояния уменьшается в такой же мере [1]. Можно было бы ожидать, что при таком сильном тушении генерации может вовсе и не быть. Эксперимент показывает, что выход генерации параллельно меняется с выходом люминесценции. Это хорошо видно из рис. 1 (выходы изображены в долях выхода непотушенного раствора), где и при больших концентрациях тушителя получен такой же относительный к. п. д. генерации, как и люминесценции.

Сравнительно большая генерационная способность потушенных растворов, вероятно, связана с тем, что тушение уменьшает наведенные потери [3] в канале $S_1^* \rightarrow S_n^*$, вследствие чего уменьшается порог и увеличивается энергия генерации. Рис. 2 показывает зависимость энергии генерации от энергии накачки водного раствора при четырех концентрациях тушителя. Энергия накачки измерена в относительных единицах. Видно, что энергия генерации почти линейно зависит от энергии накачки, и крутизна кривых уменьшается с падением выхода люминесценции. Значения порога непотушенного раствора и при концентрации тушителя $3 \cdot 10^{-2}$ моль/л одинаковые, а при $c = 1 \cdot 10^{-1}$ моль/л, когда выход люминесценции падает на 50%, порог возрастает приблизительно на 20%. Увеличение концентрации тушителя

на $3 \cdot 10^{-1}$ моль/л уменьшает выход люминесценции на 18%, а порог увеличивается приблизительно в 3 раза, причем к. п. д. генерации падает на 5%.

Наши результаты показывают, что у потушенных растворов сохраняется генерационная способность, причем порог генерации увеличивается в незначительной мере, и энергия лазера падает, как и выход люминесценции. Эти особенности могут быть связаны с тем, что элементарные акты тушения второго рода происходят после элементарных актов возбуждения, поэтому накачка создает инверсионную населенность активных молекул практически независимо от концентрации тушителя. Во время разгорания люминесценции или генерации развивается и тушение, уменьшающее число спонтанных и вынужденных излучающих переходов, вследствие чего падает выход обоих излучений.

Для детального объяснения влияния тушения верхнего лазерного уровня на работу лазера проводятся дальнейшие исследования вопроса.

Литература

- [1] Галанин, М. Д.: Труды ФИАН СССР 5, 339 (1950); *Th. Förster: Fluoreszenz Organischer Verbindungen*, Vandenhoeck und Ruprecht, Göttingen, 1951.
- [2] Даско, А. Д., Л. Г. Пикулик, Л. Ф. Гладченко, В. А. Славенин: ЖПС 20, 649 (1974).
- [3] Гладченко, Л. Ф., А. Д., Даско, Л. Г. Пикулик: Материалы Всесоюзной конференции «Лазеры на основе сложных органических соединений» МИНСК, 1975, стр. 114.
- [4] Грузинский, В. В., С. Д. Давыдов: ЖПС 23, 1009 (1975).
- [5] *Ketskeméty, I., J. Dombi, R. Horvai, J. Hevesi, L. Kozma: Acta Phys. et Chem. Szeged 7, 17 (1961).*
- [6] *Кечкемети, И., Б. Рац, Ж. Бор., Л. Козма: Acta Techn. Hung. 80, 55 (1975).*

INVESTIGATION OF LASING OF QUENCHED FLUORESCHEIN SOLUTIONS

L. Kozma, K. Csernai, I. Ketskeméty, B. Rácz and Zs. Bor

The experimental investigation of quenched laser dye solutions is described. As shown, the strongly quenched solutions have a relatively low threshold, and increasing the concentration of quencher the quantum yield and laser efficiency decrease similarly.



PHOTOCONDUCTIVITY OF V_2O_5 -Si SANDWICH SYSTEM

By

Á. SÜLI, S. D. KURMASHEV*, L. MICHAILOVITS and I. HEVESI

Institute of Experimental Physics, Attila József University, Szeged

(Received January 5, 1976)

The photoconductivity of the V_2O_5 -Si system was studied in the wavelength range 380 nm to 1000 nm. The results of measurements led to the conclusion that the major part of the photocurrent observed near to the fundamental absorption edge of V_2O_5 can be attributed to the vanadium pentoxide layer. The relation between photocurrent and light intensity was found to be linear with good approximation. On the basis of the experimental results, a simplified band diagram of the system is suggested. Illuminating the system by white light of high intensity, 0.3 V photovoltage was observed.

Introduction

Though vanadium pentoxide is a widely studied semiconductor, to our knowledge only one paper concerning its photoconductivity has been published to this date. I. HEVESI *et. al.* [1] found very weak photoconductivity of V_2O_5 single crystals illuminated by white light and by the light of a He-Ne laser. Observation of this weak photoconductivity is difficult due to the high thermal sensitivity of V_2O_5 . The weakness of photoconductivity is supposed to be connected with the very high concentration of recombination centres in V_2O_5 crystals, which causes practically immediate recombination after generation of the carrier pairs produced by photons. We tried to reduce the effect of recombination by high electric fields on the V_2O_5 layer.

The present paper studies the photoconductivity of the V_2O_5 -Si system and wishes to prove the photoconduction of the V_2O_5 layer in the region of the fundamental absorption edge of V_2O_5 on the basis of experimental results.

Preparation of the samples

n-type silicon single crystal plates of 10 mm × 10 mm × 0.2 mm with 1.3 Ωcm resistivity were used to prepare the samples, the polished single crystals being of (111) orientation perpendicularly to the 10 mm × 10 mm plate. Ohmic contact was made on one of the silicon surfaces by phosphorus diffusion [2] and vacuum evaporation of gold; on the other surface a vanadium layer of 520 Å thickness was evapo-

*Physical Department of the State University, Odessa

rated in $5 \cdot 10^{-6}$ torr vacuum. The thickness of the layer was determined by a Thin Film Thickness and Deposition Rate Monitor type MSV-1841 made by the Hungarian Research Institute for Precision Engineering.

The silicon plates covered with vanadium layer were held in an oxygen stream of atmospheric pressure in an oven of 400°C temperature for a week. For obtaining electric contact, a gold streak of \sqcup shape, about 1 mm wide and of 3μ thickness



Fig. 1a. Front side of the samples: *a* free silicon surface; *b* free vanadium pentoxide surface; *c* gold electrode of 3μ thickness; *d* semipermeable gold film of about 500 \AA thickness.

Fig. 1b. Side-view of the structure: *a* semipermeable gold film; *b* gold electrode; *c* V_2O_5 layer; *d* Si plate; *e* Si layer with diffused in phosphorus; *f* gold back contact.

was evaporated onto the yellow vanadium pentoxide layer formed during the oxidation process. Then a gold film of 500 \AA thickness was evaporated to the interior of the \sqcup -shaped streak (Fig. 1a, 1b).

In order to perform optical measurements, vanadium pentoxide layers were prepared also on thin quartz plates with the method described.

Experimental

The $I-V$ characteristics of the samples were found to be assymetrical [3]; on illumination under reverse bias remarkable photocurrents could be observed.

The experimental set-up used to measure the photocurrent can be seen in Fig. 2. Before performing the measurements, the dependence on wavelength of the energy of light coming from the monochromator was determined by a Zeiss thermocouple type VTh 8 MM, the knowledge of the energy permitting to relate the photocurrent measured to the same photon number.

In the measurements, the dark current of the samples was compensated and only the photocurrent was determined.

Fig. 3 shows the results obtained with the samples No. 1 and 2, by illuminating a 0.5 mm wide portion of the free V_2O_5 surface in the immediate vicinity of the gold streak at 4 V reverse bias. The abscissa gives the wavelengths in nm, the ordinate the photocurrents for the same photon number in arbitrary units.

Fig. 4 gives the results obtained by illuminating the samples through the thin gold film, under the same conditions as in Fig. 3. For comparison, the above measurements were made also with a silicon solar cell using the same electrode arrangement and the same conditions of measurements with the difference, that the reverse bias

of the solar cell was 0.9 V. Fig. 5 shows the results obtained by illuminating a 0.5 mm wide portion of the free surface of the solar cell beside the electrode. While the relative photocurrent of the silicon p - n junction shows only one maximum at 900 nm, in Fig. 3 two maxima are seen in the curve of samples No. 1 and 2, at about 760 nm and 550 nm, and at about 800 nm and 560 nm, respectively. These maxima can be

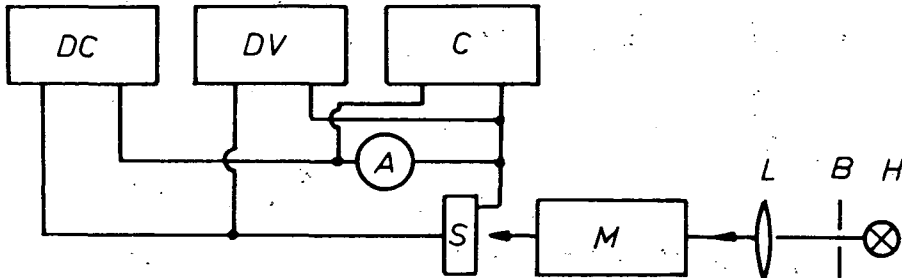


Fig. 2. Experimental set-up: DC current source; DV digital voltmeter; C compensator; A amperemeter; S sample; L lens; B diaphragm; H 150 W halogen lamp

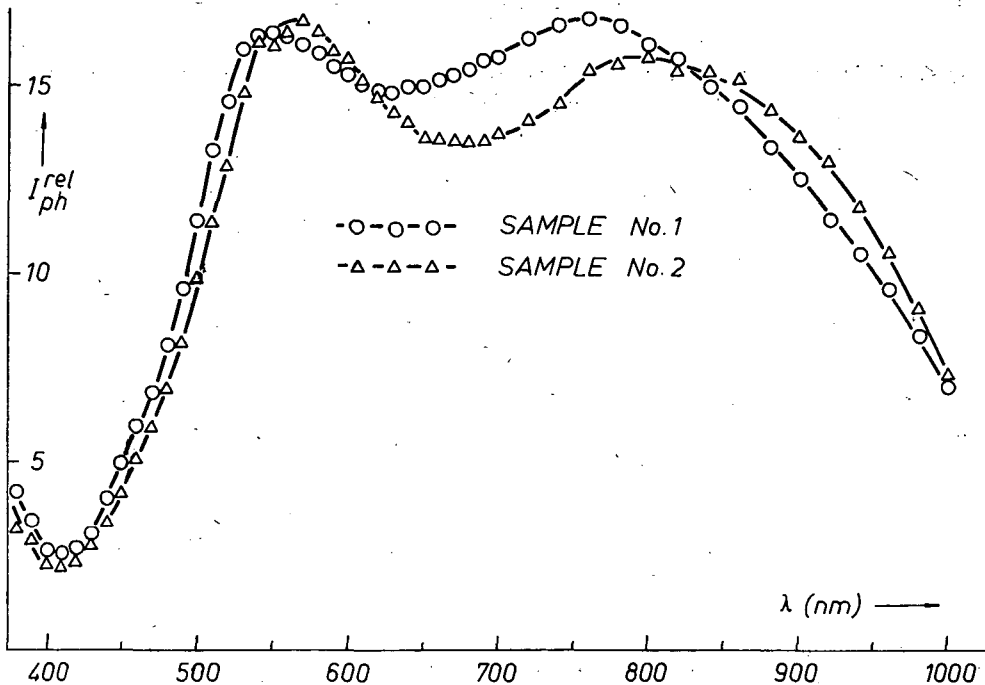


Fig. 3. Relative photocurrent vs. wavelength curves obtained at 4 V reverse bias by illuminating the free V_2O_5 surface in the immediate vicinity of the gold electrode

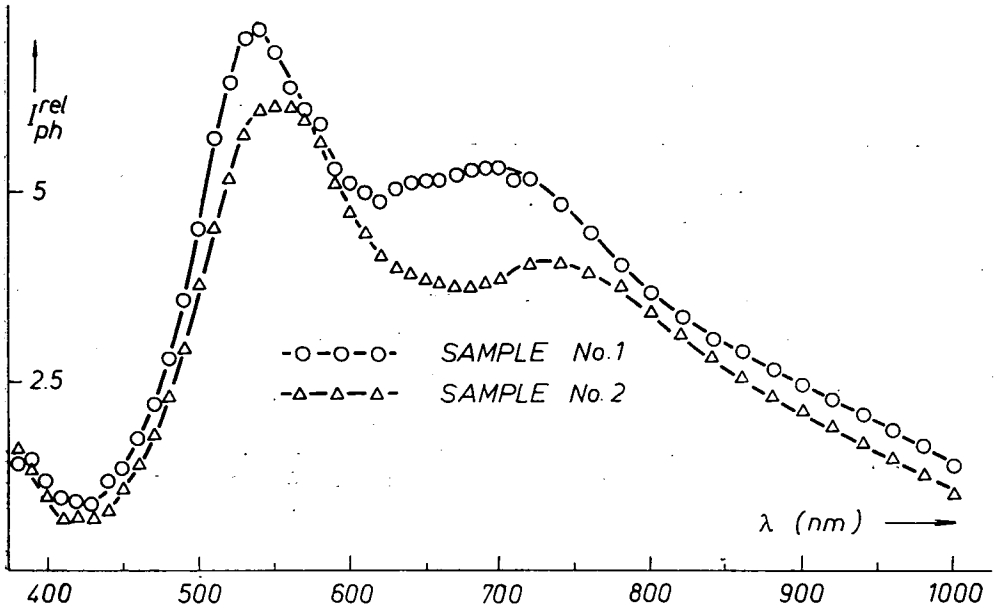


Fig. 4. Relative photocurrent vs. wavelength curves obtained at 4 V reverse bias by illuminating the samples through the gold film

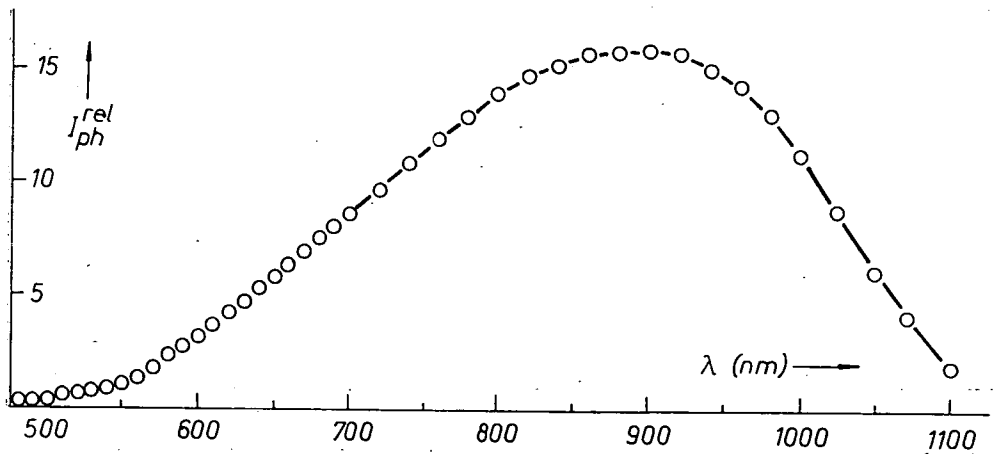


Fig. 5. Relative photocurrent vs. wavelength curve of a silicon solar cell

observed in Fig. 4 at about 700 nm and 540 nm, and at about 740 nm and 550 nm, respectively.

The dependence of the photocurrent on the reverse bias was measured on sample No. 1 with illumination by light of 1000 nm and 700 nm wavelengths. In Fig. 6 $\ln \frac{I_s + I_{ph}}{I_s}$ is plotted as a function of the reverse bias; I_{ph} means the photocurrent

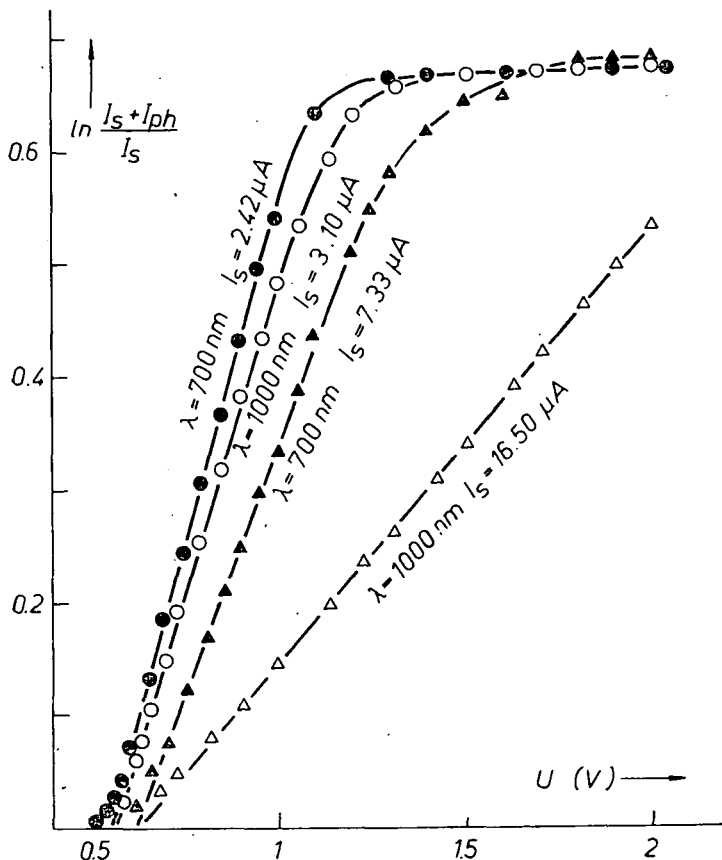


Fig. 6. Photocurrent vs. reverse bias curves. Open and full triangles: results obtained by illuminating the free V_2O_5 surface, open and full circles: those resulting from illumination through the gold film. I_{ph} : photocurrent, I_s saturation value of photocurrent

and I_s its saturation value. The results obtained by illuminating the free V_2O_5 surface are marked by open and full triangles, those obtained by illuminating through the gold film by open and full circles, respectively. Each curve of Fig. 6 shows a linear increase, the extrapolation of which gives intersections with the abscissa corresponding to 0.56 V and 0.62 V, respectively.

The relation between light intensity and photocurrent was measured by decreasing the light intensity by a calibrated grey wedge. The results of illuminating sample No. 1 at 4 V reverse bias with light of 550 nm wavelength are shown in Fig. 7. The results obtained by illuminating the free V_2O_5 surface are marked by

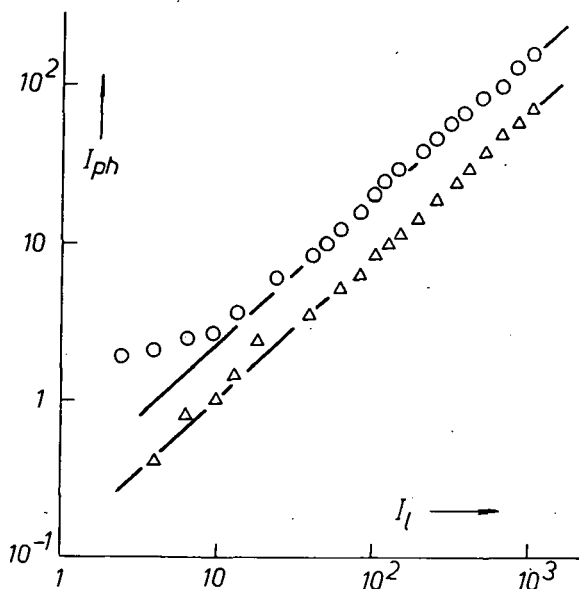


Fig. 7. Photocurrent vs. light intensity curves at 500 nm wavelength plotted in arbitrary units. Circles denote results of illumination of the V_2O_5 surface, triangles those of illumination through the gold film

circles, those of illumination through the gold film by triangles, respectively. The abscissas give the light intensities, the ordinates the photocurrents, both in arbitrary units.

The dependence on wavelength of the transmission of the gold film was determined by comparing the transmission of the mica mask used for the evaporation of the gold film with a mica plate of the same quality and thickness, using a spectrophotometer Optica Milano CF4DR. The transmission curve of the gold film shown in Fig. 8 was calculated from the transmission data of the mask covered with gold film and of the mica plate.

The transmission spectrum of the V_2O_5 layer of the samples was determined as described above using a V_2O_5 layer on a quartz plate, the layer being of the same thickness as that the V_2O_5 on the sample, and a quartz plate of the same thickness and quality than the quartz plate covered with V_2O_5 . The results are shown in Fig. 9.

Illuminating the samples with white light of high intensity, a photovoltage of 0.3 V was obtained; the silicon side of the sample became negatively charged.

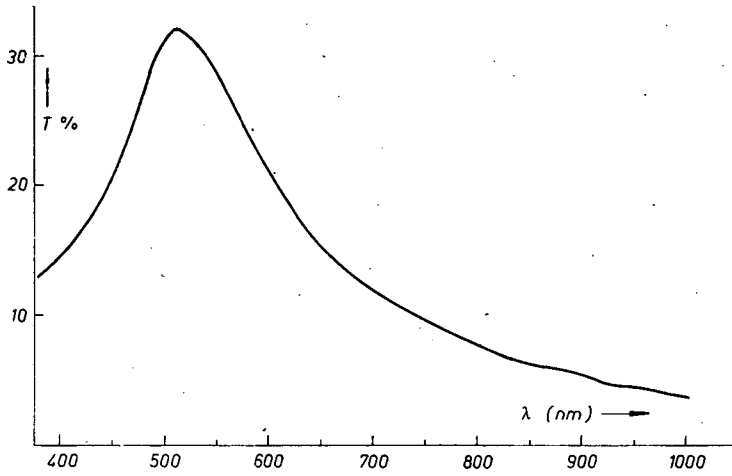


Fig. 8. Transmission curve of the gold film covering the V_2O_5 layer

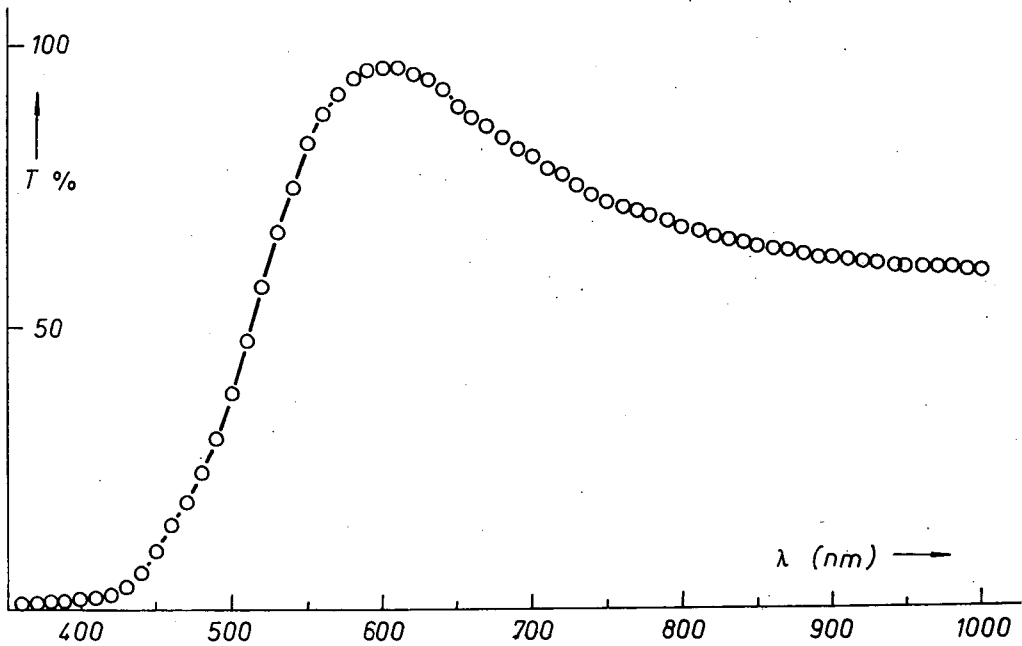


Fig. 9. Transmission curve of the V_2O_5 layer of the samples. Calculated thickness of the layer: ~ 0.16 — 0.18μ

Conclusions

Taking into account the transmission curve of the gold film shown in Fig. 8, the deviation in the shape of the curves seen in Figs. 3 and 4, namely the shift of the maxima at longer wavelengths towards shorter ones and the increase in relative amplitude of the maxima at shorter wavelengths in Fig. 4, can be explained.

The thickness of the V_2O_5 layer on silicon plates was calculated to be $0.16\ \mu\text{--}0.18\ \mu$, using the results of KENNEDY *et al.* [4] for the density of amorphous V_2O_5 .

Comparing the transmission curve of the V_2O_5 layer shown in Fig. 9 with that obtained by SINCLAIR [5] for a sputtered V_2O_5 layer of $0.8\ \mu$ thickness, the agreement seems to be satisfactory, taking into account the difference in thickness. However, our curve appears shifted towards shorter wavelengths by about 70–80 nm compared with SINCLAIR's results.

From the photocurrent *vs.* reverse bias curves, presented in Fig. 6, the existence of a potential barrier between silicon and vanadium pentoxide can be deduced.

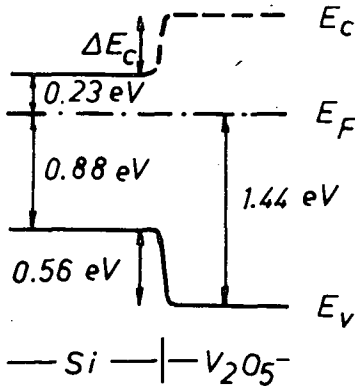


Fig. 10. Energy band diagram of the V_2O_5 -Si system in first approximation

Its height was found to be 0.56 eV from the intersections of the linear portions with the horizontal axis of the curves marked by open and full circles, respectively. The intersection of the two other curves is found at 0.62 V; however, the former value seems to be more probable, because the latter was determined by illuminating the free surface of the V_2O_5 layer, and in this case the voltage drop on the parts of free V_2O_5 surface not covered by the electrode may be noticeable, as shown also by the intersection of the curves at higher voltage.

Taking into account the data concerning the position of the Fermi level and the band gap width of silicon of $1.3\ \Omega\text{cm}$ resistivity [6], the energy band diagram of the V_2O_5 -Si system is given in first approximation¹ in Fig. 10. From the measured value of photovoltage it can be

concluded that the value of ΔE_c is only slightly higher than 0.3 eV, so the band gap attributed to amorphous vanadium pentoxide is about 2 eV, lower than the 2.4 eV obtained for crystalline V_2O_5 .

The photocurrent observed may be caused by carriers generated in the silicon and in the vanadium pentoxide layer alike. In order to separate both photoeffects, the relative photocurrents I_{ph}^{rel} pertaining to given wavelengths were divided by the transmission T of the V_2O_5 layer for the same wavelengths. The values obtained are shown in Fig. 11. Let us suppose that, at a given wavelength, N_0 photons arrive on the surface of the sample, and N photons on the V_2O_5 -Si interface: then $N = N_0 T$,

$$I_{ph}^{rel} = c \frac{I_{ph}}{N_0}, \text{ where } c \text{ is constant and } I_{ph} \text{ is the photocurrent measured; } \frac{I_{ph}^{rel}}{T} = c \frac{I_{ph}}{N},$$

¹ A more detailed band diagram to be described in [3].

If the reflexion on the interface is taken to be negligible, and the photocurrent, supposed for the moment to be caused only by photons absorbed in the silicon, then $\frac{I_{ph}^{rel}}{T}$ is proportional to the quantum yield. It seems reasonable to interpret the apparently marked increase of the quantum yield at wavelengths shorter than 500 nm as caused by the circumstance that in this wavelength range carriers are generated by photons also in the V_2O_5 layer.

With respect to the above, the relative photocurrent *vs.* wavelength curve shown in Fig. 3 can be interpreted as follows: at wavelengths longer than 500 nm

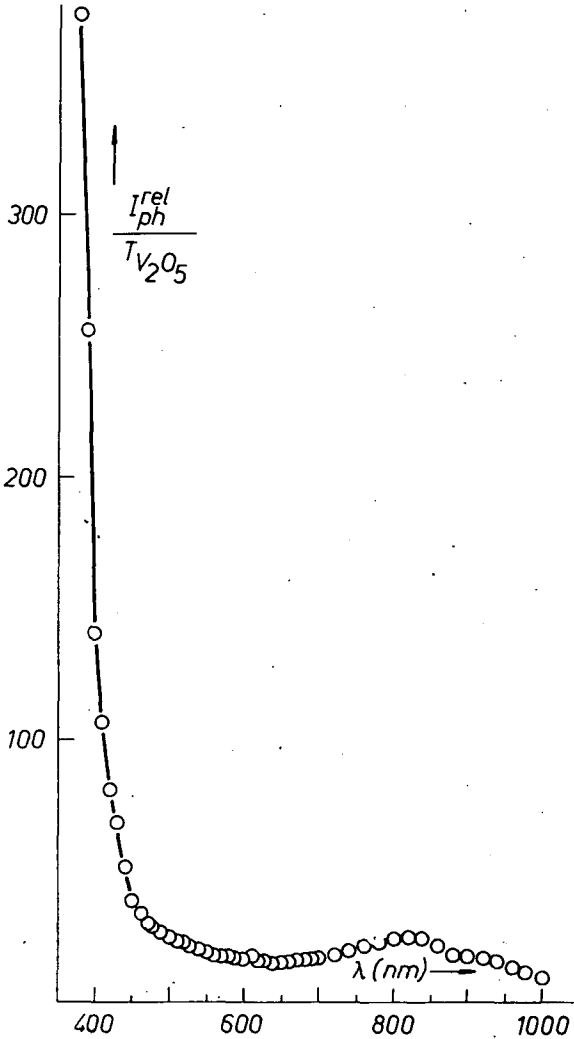


Fig. 11. The relative photocurrent divided by the transmission of the V_2O_5 layer

the photocurrent is mainly due to the silicon, the photoconductivity of vanadium pentoxide being important only at wavelengths shorter than 500 nm. The striking difference in the curves of Fig. 3 and Fig. 5 can be probably caused by the circumstance that the V_2O_5 layer acts as an antireflexive layer on the silicon, and thus the photocurrent of the silicon begins to decrease only at wavelengths shorter than

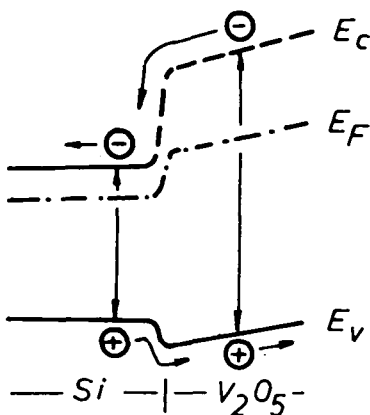


Fig. 12. Simplified mechanism of photoconductivity of the V_2O_5 -Si system

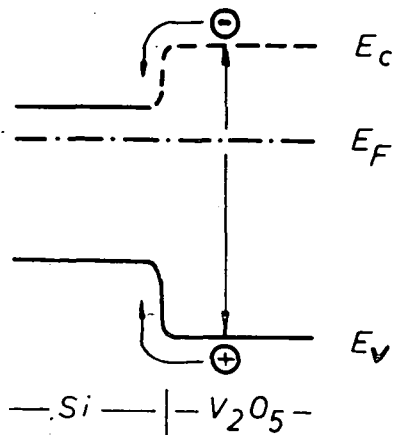


Fig. 13. The mechanism of photovoltage generation in first approximation

500 nm. The supposition of an antireflexive layer seems to be supported by the fact that in the wavelength region longer than 500 nm the value 1.8 was obtained for the refractive index of the V_2O_5 layer on the basis of literature data concerning the refractive index of crystalline V_2O_5 [8] and density values of amorphous V_2O_5 [4]; the refractive index of Si is surely higher than 3.42 in this wavelength range [6]. The decrease of the relative photocurrents towards shorter wavelength in the range 540 nm — 420 nm can be supposed to be due to the marked increase of the reflexion and absorption of the V_2O_5 layer (see Fig. 3 and 9); here the comparatively lower photocurrent from the V_2O_5 appears instead of the higher photocurrent of the silicon. At wavelengths shorter than 400 nm the increase in photocurrent may be attributed only to the V_2O_5 layer.

A simplified mechanism of the photoconductivity is shown in Fig. 12. From the electron-hole pairs generated by the light in the silicon, only the holes can pass the potential barrier lowered by the applied voltage, while from the V_2O_5 only the electrons are able to reach the silicon.

The mechanism of photovoltage generation is shown in first approximation in Fig. 13. Part of the holes and electrons generated in the V_2O_5 by the light diffuse into the silicon. The ratio of the electrons and holes reaching the silicon is approxi-

mately $\sqrt{\frac{D_n \tau_n}{D_p \tau_p}}$, where D_n and D_p are the diffusion coefficients, τ_n and τ_p the lifetimes in V_2O_5 of the electrons and holes, respectively. Vanadium pentoxide being a n -type semiconductor, the relations $D_n > D_p$; $\tau_n > \tau_p$ are valid. Thus the silicon must be charged negatively, as observed.

References

- [1] *Hevesi, I., J. Lang, G. G. Chemeresyuk*: Acta Phys. et Chem. Szeged **19**, 25 (1973).
- [2] *Süli, A., L. Michailovits, F. Liszt*: Acta Phys. et Chem. Szeged **20**, 333 (1974).
- [3] *Mačkus, P., A. Süli, M. I. Török, I. Hevesi*: Thin Solid Films **00**, 0000 (1976).
- [4] *Kennedy, T. N., R. Hakim, J. D. Mackenzie*: Mat. Res. Bull. **2**, 193 (1967).
- [5] *Sinclair, W. R.*: Electrochem. Soc. J. **118**, 341 (1971).
- [6] *Wolf, H. F.*: Silicon Semiconductor Data, Pergamon Press, London, 1969.
- [7] *Bodó, Z., I. Hevesi*: Phys. stat. sol. **20**, 145 (1967).
- [8] *Kenny, N., C. R. Kannewurf, D. H. Whitmore*: J. Phys. et Chem. Sol. **27**, 1237 (1966).

ФОТОПРОВОДИМОСТЬ V_2O_5 -Si СЭНДВИЧЕВЫХ СТРУКТУР

А. Шюли, С. Д. Курмашев, Л. Михайлович и И. Гевеши

Исследована фотопроводимость V_2O_5 -Si системы в области длин волн от 380 до 1000 нм. На основании полученных результатов мы пришли к выводу, что, в области края собственного погашения V_2O_5 , найденная фотопроводимость в основном обусловлена слоем V_2O_5 . Зависимость между интенсивностью света и фототоком с хорошим приближением является линейной. На основании полученных экспериментальных данных составлена упрощенная диаграмма полос системы. При освещении белым светом большой интенсивности было найдено фотонапряжение в системе равное 0,3 вольту.



**THE ROLE OF EXCITED STATES IN THE PHOTOLYSIS
OF *n*-BUTYRALDEHYDE, I.
Triplet State Quenching by Piperylene**

By

M. TÖLGYESI, T. BÉRCES and Á. NACSA

Reaction Kinetics Research Group of the Hungarian Academy of Sciences, Szeged

(Received 10 February, 1976)

Experimental techniques suitable for the study of the role played by excited states in the photolysis of *n*-butyraldehyde are described. Preliminary experimental results obtained with piperylene quencher in the vapor phase and isooctane are given, and the contributions of the excited singlet and triplet states in the four major primary photochemical processes of *n*-butyraldehyde photolysis at 313 nm were estimated.

Introduction

A detailed study of the vapor phase photolysis of *n*-butyraldehyde was made by BLACET and CALVERT [1, 2] which elucidated most of the major photochemical primary and secondary processes. Although recent work carried out in our laboratory [3] showed the nature of primary reactions and the mechanism of secondary processes to be more complex than originally assumed by BLACET and CALVERT nevertheless the basic mechanistic features of the photolysis seem to be fairly well established. However, much less is known of the role played by the excited singlet and triplet states in the photolysis of *n*-butyraldehyde. Most of the investigations in this field dealt with excited state precursors of only one or two primary photochemical processes—often only with those involved in the NORRISH type II elimination—and the conclusions were of qualitative nature.

Vapor phase experiments have definitely proved that both NORRISH type I decomposition into *n*-propyl and formyl radicals and type II ethylene elimination may occur from the triplet state.

On the basis of the very low yield of ethylene obtained in the mercury-sensitized decomposition of *n*-butyraldehyde as compared to the direct photolysis, BORRELL and NORRISH suggested [4] that only excited singlet molecules can undergo type II elimination. However, in a later paper NORRISH and WAYNE showed [5] the failure of BORRELL and NORRISH to detect the type II products in the sensitized reaction to be caused by the consumption of the ethylene in secondary reactions during extended photolysis.

BORKOWSKI and AUSLOOS [6] investigated the vapor phase fluorescence and its relationship to the photolysis of *n*-butyraldehyde. They could show that the fluorescence emitted by butyraldehyde was not affected by the addition of biacetyl,

however, a strong emission — ascribed to triplet excited biacetyl formed in a triplet energy transfer process — was observed. At 334 nm, biacetyl reduced the relative rate of C_2H_4 formation by nearly a factor of ten, but did not appreciably affect the yield of propane. On the basis of these observations it was concluded that an excited triplet aldehyde molecule is involved in the type II elimination and the type I decomposition occurs from a singlet electronic state and/or from a triplet electronic state excited to a high vibrational level.

The investigations of REBBERT and AUSLOOS [7] at 313 nm wavelength showed that both type I and type II decomposition of *n*-butyraldehyde can be photosensitized by acetone. On the basis of luminescence measurements it was suggested that an acetone molecule can transfer its triplet-state energy to form a triplet excited aldehyde molecule. Consequently, the results on the sensitized decomposition of *n*-butyraldehyde may be taken as evidence for the occurrence of type I and type II reactions from the triplet state of the aldehyde.

The effect of *cis*-butene-2 and biacetyl on the vapor phase photolysis of *n*-butyraldehyde at 313 nm has been investigated by CUNDALL and DAVIES [8]. Since both dissociation and ethylene elimination was quenched at 321 K by biacetyl and by *cis*-butene-2 (and simultaneous isomerization of the latter compound occurred) it was concluded that type I and type II processes occur through a triplet state. (However, the possibility of contribution to the type I reaction from the singlet state was not excluded.) On the basis of observed relative quenching efficiency of biacetyl and *cis*-butene-2, it was suggested that type I and type II reactions occur from upper and lower vibrational levels of the triplet state, which are however similar (not far) in energy.

Information available on the role of the excited states in solution is less detailed than in the vapor phase. The photolysis of *n*-butyraldehyde in solution was studied by COYLE [9]. Relative quantum yields for type II product and for cyclobutanol formation in benzene were reported. Piperylene was used to quench reactions occurring from the triplet state. It was found that part of the photochemical reaction was quenched efficiently and part was relatively unaffected. Hence, it was concluded that reaction occurs to an appreciable extent from both the $n\pi^*$ triplet and the $\pi\pi^*$ singlet states, respectively. From the slopes of STERN—VOLMER plots, a triplet-state lifetime of $3.5 \cdot 10^{-8}$ s was obtained.

Recently LEBOURGEOIS *et al.* [10] published a paper on the photochemical behaviour of *n*-butyraldehyde in solution. Conclusions were drawn from measurements of absorption, fluorescence and aldehyde consumption; product analysis was not attempted. Naphthalene quenching experiments were made to show that the triplet state is responsible for the major part of the photochemical reactions. The quantum yield for reactions occurring from the singlet excited state was estimated to be less than 0.14. It was suggested that at *n*-butyraldehyde concentrations less than 10^{-1} mol · dm⁻³ the singlet-state molecules react in unimolecular reactions, while at higher concentrations the reaction of an excited singlet and a ground state aldehyde molecule dominates. The triplet state was assumed to be consumed in a bimolecular reaction — in an interaction between a triplet excited and a ground state butyraldehyde molecule — yielding a pair of butyryl and hydroxybutyl radicals which recombine to form an acetoin homologue. LEBOURGEOIS *et al.* estimate the lifetime of the excited singlet state to be $6 \cdot 10^{-10}$ s at low aldehyde concentrations. The triplet-state lifetime was shown to decrease with increasing aldehyde concentra-

tion in the range of 10^{-2} to 10^{-1} mol·dm⁻³; the lifetime values reported were around 10^{-8} s.

Survey of the information available in literature on the nature of the excited-state precursors of the various primary photochemical products of *n*-butyraldehyde shows that further quantitative data are required in particular for the relative singlet and triplet contributions to the individual primary processes, and for the energies and lifetimes of the excited states from which these reactions occur. A systematic study of these questions, both in the vapor phase and in solution, has been initiated in our laboratory. In this paper we present the preliminary results obtained with *cis*-piperylene (*cis*-pentadiene-1,3), generally known as an efficient quencher of the triplet states of carbonyl compounds.

Experimental

Materials

The *n*-butyraldehyde obtained from FLUKA AG was purified by precipitation with sodium hydrogen sulfite. The recovered aldehyde (generated in nitrogen atmosphere) was dried over anhydrous magnesium sulfate and further purified by repeated distillation *in vacuum*, only the middle fractions being retained. The purified sample contained about 0.5 percent isobutyraldehyde as determined by gas liquid chromatography; the amount of other impurities was around the detection limit of the flame ionization detector. The aldehyde was stored in dark *in vacuum*, in a flask closed with a greaseless polyethylene valve.

The *cis*-piperylene (FLUKA AG) was 99.6 percent pure, containing 0.4 percent *trans* isomer. Purification consisted of repeated bulb-to-bulb distillation *in vacuum*. The sample was stored in dark in a vessel equipped with a YOUNG valve (teflon sealing).

The isooctane used as solvent was obtained from FLUKA AG. Purification was carried out by distillation on a high performance column (theoretical plate number over 10). Only a middle fraction, shown to contain saturated C₈ and some C₇ hydrocarbons, was used.

Isopentane used as an internal standard was obtained from KOCH and LIGHT. The purification procedure was identical with that described for isooctane.

Apparatus and methods

The method used in the experiments may be divided in four working processes:

- (i) Preparation of the sample to be irradiated;
- (ii) Irradiation and light intensity measurement;
- (iii) Preparation of the sample for analysis;
- (iv) Analysis.

The first three working processes were somewhat different in case of the vapor phase investigations and in the experiments made in solution and require detailed description, while the method of analysis applied in the vapor phase and solution experiments was the same.

Preparation of the aldehyde vapor samples to be irradiated

The sample was prepared by direct evaporation of the components into the evacuated reaction vessel (irradiation cuvette). Pressures were measured with a quartz spiral-manometer (BODENSTEIN type) which was used as a null-instrument. The sample was left to stand 30 minutes to attain complete mixing of the components before irradiation.

Vapor phase irradiation and intensity measurement

The vapor phase experiments were carried out in a cylindrical quartz cell of 4.5 cm internal diameter and 8.0 cm length, equipped on both ends with sealed ultrasil planparallel windows. The cell was attached to a vacuum apparatus through a greaseless polyethylene valve. Temperature was kept constant by means of a thermostating jacket through which silicon oil from a thermostat was circulated.

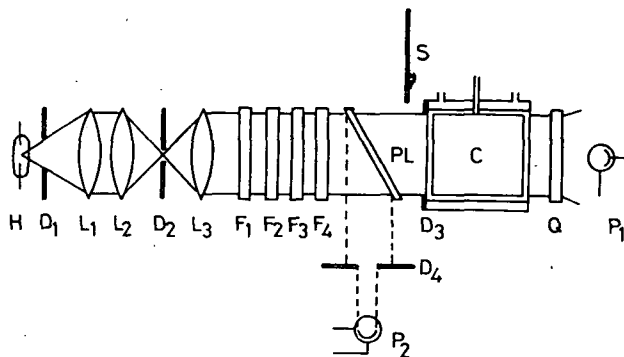


Fig. 1. Diagram of the irradiation line
(For the designations see the text.)

The irradiation line, installed on an optical bench, is shown in Fig. 1. The light source H was an OSRAM HBO—500 high pressure mercury arc mounted in a metal house. The ultrasil quartz lenses L_1 , L_2 and L_3 as well as the diaphragms D_1 and D_2 served to obtain a nearly parallel but slightly convergent beam. A third diaphragm D_3 cut the cross-section of the beam to the size which ensured that the light filled the irradiation cell C almost completely. Irradiation could be started or interrupted by moving the shutter S .

A band in the 313 nm region was isolated using a combination of four filters, F_1 — F_4 , which are described in Table I. The light emerging from the filter combination showed a width of 3 nm at the half height of the band.

The light intensities were measured by means of a PRESSLER DGL 490a vacuum photocell P_1 which was placed behind the reaction cell C . The photocell was connected to a 100V high-stability DC power supply unit and the signal, after amplification, could be either read or recorded. In order to reduce the light intensity

Table I

Filter combination used to isolate a band in the 313 nm region

Designation of the filter	Optical depth in mm	Description of the filter
F ₁	25	64 g NiSO ₄ ·6 H ₂ O + 10 g CoSO ₄ ·6 H ₂ O + + 100 cm ³ H ₂ O
F ₂	25	5·10 ⁻⁴ mol·dm ⁻³ K ₂ CrO ₄
F ₃	10	0.0245 mol·dm ⁻³ KHC ₈ H ₄ O ₄
F ₄	4	UG 11 (SCHOTT, Jena)

to the level required by the photocell, a fluorescent screen *Q* was placed between *C* and *P*₁. This was similar to PARKER's quantum counter [11], and consisted of a cell of 10 mm optical depth containing a solution of 1.1·10⁻³ mol·dm⁻³ fluorescein, 0.5 *N* sodium carbonate and 0.05 *N* sodium bicarbonate. The whole quantum counter system was calibrated by means of a ferrioxalate actinometer. The calibration was shown to be linear in the light intensity range used by us for irradiation (2·10⁻¹¹ to 3·10⁻⁹ einstein·cm⁻²·s⁻¹). In the calculation of the quantum yields, measured intensities were corrected for the reflexion on the optical surfaces.

Much attention was paid to use stable light intensity during irradiation. Therefore a power supply unit was developed for the mercury arc which could be used in (i) voltage stabilized-, (ii) current stabilized-, (iii) light intensity stabilized-, and (iv) externally controlled working mode. In quantitative photochemical investigations, the light intensity stabilized mode was used, and a controlling system kept the light intensity of the mercury arc constant at a pre-set value.

The controlling system consisted of the mercury arc *H*, the power supply unit and a photocell *P*₂ (type DGL 490a, Deutsche Glimmlampengesellschaft PRESSLER, Leipzig). A fraction of the exciting radiation was reflected by a planparallel quartz plate *PL* onto the cathode of the photocell *P*₂. An error signal, the difference between the photocell current and the pre-set current proportional to the required light intensity, was used to control the power supply unit of the mercury arc.

With this controlling system the long range drift of the intensity of the exciting light was kept within ±2 percent. The short range stability was better than the accuracy of the readings, corresponding to about ±0.2 percent of the intensity.

Preparation of the irradiated vapor phase samples for analysis

After irradiation, the reaction cell was attached to a vacuum line, the gas mixture was led through a trap cooled to liquid air temperature, and the non-condensable products were collected by a TOEPLER pump and their volume was measured in a gas burette. The products condensable at liquid air temperature were dissolved in isooctane containing isopentane and cyclohexanone as internal standards which was introduced previous to the whole procedure into a small tube attached to the bottom of the trap. Finally, the small tube containing the solution of the products was sealed off. Both the gas and the solution sample was analysed by gas chromatography.

Preparation of the solution samples to be irradiated

The isooctane solvent containing isopentane as internal standard was carefully degassed. Then solutions of *n*-butyraldehyde and of piperylene, respectively, were prepared in two separate vacuum lines by freezing known amounts of these compounds on the top of given volumes of the solvent. These solutions as well the solvent were used to prepare a set of samples in which the concentration of the aldehyde and that of the internal standard was constant but the concentration of piperylene varied. The cylindrical Uviol cuvettes (1.2 cm internal diameter) containing the solution samples were sealed off, detached from the vacuum line and subjected to irradiation.

Irradiation of the solution samples

A series of solution samples with varying piperylene concentration were irradiated simultaneously. Two methods, termed method *A* and method *B* were used.

In method *A*, the optical line was similar to that used in the vapor phase irradiations (see Fig. 1.) except for the design of the reaction cell and the thermostating jacket. A cuvette holder drum accommodating 12 cuvettes was rotating at the end of the optical line. Thus, all the samples absorbed the same number of light quanta. The cuvette holder drum was enclosed in a cylindrical vessel which could serve as an air or liquid thermostat. There was a quartz window on the vessel where the light beam entered.

In method *B*, a rotating mercury arc (a 125W PHILIPS medium pressure arc connected to a current stabilized DC power supply unit) was surrounded by 8 sample cuvettes. The Uviol cuvettes were mounted vertically on a fixed base parallel to and in equal distances from the central mercury arc. The arc was surrounded by a spherical filter jacket (optical depth = 2.5 cm), made of Uviol glass, through which a filter solution circulated. The filter solution which isolated a band in the 313 nm region was prepared by dissolving 32 g $\text{NiSO}_4 \cdot 6\text{H}_2\text{O}$ + 10g $\text{CoSO}_4 \cdot 6\text{H}_2\text{O}$ + 0.5g $\text{KHC}_8\text{H}_4\text{O}_4$ in 100 cm³ water. Because of the decomposition of the potassium hydrogen phthalate on irradiation, the filter solution had to be replaced in each experiment. The spectral distribution of the exciting light in this set-up may be characterized by 1.5 nm width at the half height of the band.

Preparation for analysis of the irradiated solution samples

In experiments where analysis of the CO product was not made, no special preparation of the sample was required. The cuvette was opened, the second internal standard (cyclohexanone) was added and the sample was ready for analysis.

In the rest of the experiments the cuvette equipped with a break seal was attached to a vacuum line, the break seal was opened and the whole content was distilled into a trap kept at liquid air temperature. The non-condensable products were collected by a TOEPLER pump and their volume was measured in a gas burette. The condensable products were sealed into a small tube attached to the bottom of the trap. Both gas and liquid samples were analysed by gas chromatography.

Analysis

Product analysis was carried out on a HEWLETT—PACKARD type 5751G and a CARLO—ERBA Linea DACI gas chromatograph. Nitrogen carrier gas was used and flame ionization detection was generally applied, except for the hydrogen measurements (thermal conductivity detector). Peak areas were measured (using a HEWLETT—PACKARD type 3370B digital integrator) against that of an internal standard (either isopentane or cyclohexanone) or against the peak area of a product the amount of which in the sample was already known from another analysis. Altogether four columns were required for the detailed quantitative analysis of the composition of the irradiated samples:

- (i) 2.5 m Molecular Sieve 5A, stainless steel tube of 6 mm i.d.;
- (ii) 1.8 m Alumina, stainless steel tube of 6 mm i.d.;
- (iii) 3.0 m Porapak QS deactivated with 0.5 percent Apiezon L, stainless steel tube of 2.5 mm i.d.;
- (iv) 30 m SCOT column with Carbowax 20M stationary phase, 0.25 mm i.d.

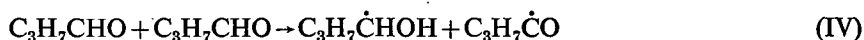
The non-condensable gas fraction was analysed for hydrogen on the Molecular Sieve column at 343 K, and for methane on the Alumina column at 373 K. The amount of CO was obtained from the volume of the gas fraction measured in the gas burette by taking into account the H₂ and CH₄ content.

The liquid fraction (condensable at liquid air temperature) was analysed for ethane, ethylene, propane and propylene on the Alumina column at 373 K; ethylene, propane, piperylene, *n*-butyraldehyde and *n*-hexane were measured against isopentane internal standard on the Porapak QS column at 443 K. Finally, *n*-butanol, cyclobutanol, 4-heptanol and 4-heptanone were analysed on the SCOT column at 383 K using cyclohexanone as internal standard.

Results and discussion

In the investigations described in this paper, the role of the excited singlet and triplet states of the aldehyde molecule in the major primary photochemical processes of *n*-butyraldehyde photolysis was studied by observing the effect of piperylene on the quantum yields of certain products characteristic for the primary processes dealt with.

A detailed study of the photolysis of *n*-butyraldehyde is in progress in our laboratory [3], and the results obtained so far show that seven more or less important primary processes occur at 313 nm both in the vapor phase and in isooctane solution. The major ones are



Two of these (*i.e.* the NORRISH type II decomposition and the rearrangement step II') yield stable products. On the other hand the NORRISH type I decomposition into *n*-propyl and formyl radicals, and the reaction of an excited state and a ground state aldehyde molecule forming hydroxybutyl and *n*-butyryl radicals are followed by secondary processes.

If a primary process occurs from two excited states and one of them (*i.e.* a triplet state) is quenched and the other (*i.e.* an excited singlet state) is unaffected by a quencher, then the contributions of the quenched and unquenched states can be given by

$$\eta^T = (\Phi^0 - \Phi^\infty) / \Phi^0 \quad (1)$$

and

$$\eta^S = \Phi^\infty / \Phi^0 \quad (2)$$

where Φ^0 and Φ^∞ designate the quantum yields of a primary product obtained in the absence of the quencher and at a quencher concentration high enough to deactivate completely the quenched state, respectively. For reactions II and II' the primary products can be measured directly in the irradiated sample, thus η^T and η^S are obtained in a straightforward manner. However, this is not the case for reactions I and IV where only the products formed in secondary free radical reactions can be measured. Nevertheless, if certain conditions are fulfilled, some secondary products might be found, the quenching characteristics of which supply information on the role played by various excited state precursors.

The choice of the characteristic product quantum yields to be used in equ. (1) and (2) in order to calculate η^T and η^S , respectively, for reactions I and IV, requires careful consideration of the kinetics and the stoichiometry of the secondary free radical processes. Important points on which special emphasis should be laid are the following:

- (i) If reaction chains are involved in the formation of the secondary products, then quenchers are expected to alter considerably the chain length and the stoichiometry of the reaction, therefore simple correlation does usually not exist between product quenching and the contribution of the various excited states to the particular primary process.
- (ii) Assuming that chains do not occur or chain length is very short, nevertheless the stoichiometry of the reaction changes on addition of a quencher if the radical formed in the primary process is consumed in competitive elementary steps among which some are first and others are second order with respect to the free radical. In such cases information on the role played by the various excited state precursors can be obtained from quenching plots where the weighted sum of the quantum yields of all (or all significant) products formed in the reactions of the primary free radical are plotted against the quencher concentration.
- (iii) In the simplest case where the quencher does not alter the reaction stoichiometry, any product may be chosen as the characteristic one. Thus, the quantum yields of any product may be used to obtain η^T and η^S by means of equ. (1) and (2), respectively.

(iv) In the case considered above it has been tacitly assumed that only physical quenching (triplet energy transfer) occurs. However, if the quencher reacts with the free radicals, then chemical quenching of the reactive intermediates is superimposed upon the physical quenching of the excited state precursor, causing an overestimation of the role played by the quenchable excited state.

A study of secondary photochemical processes in the gas and liquid phase photolysis of *n*-butyraldehyde at 313 nm, carried out in our laboratory (see [3] and subsequent papers), revealed that the mechanism is complex. Chains occur in the vapor phase photolysis, however the chain length is short (less than 1.3) at room temperature. The information (see [3] and subsequent papers) available on the mechanism of the free radical processes following reactions I and IV demand that η^T and η^S be obtained from quenching plots where the weighted sum of the quantum yields of all significant products formed in the reactions of the appropriate primary radical are taken into account (compare with paragraph ii above).

Table II and III give the product quantum yields measured by us in the vapor

Table II

Product quantum yields obtained in the gas phase without added piperylene at 313 nm wavelength and room temperature. $[C_3H_7CHO]_0 = 2.7 \cdot 10^{-3} \text{ mol} \cdot \text{dm}^{-3}$; $I_0 = 6.5 \cdot 10^{-10} \text{ einstein} \cdot \text{cm}^{-2} \cdot \text{s}^{-1}$

C_2H_4	CH_3CHO	Cyclo- butanol	CO	C_3H_8	C_6H_{14}	C_3H_6	4-Hepta- none	4-Hepta- nol	<i>n</i> -Bu- tanol
0.17	0.18	0.032	0.43	0.29	0.093	0.019	0.004	0.008	0.010

phase and in isooctane, respectively. The two sets of quantum yields shown in Table III were obtained by method A and B at considerably different intensities. Products of very little importance (see [3]) are not included in the tables. The results clearly show that the same products are formed in the vapor phase and in isooctane.

Table III

Product quantum yields obtained in isooctane without added piperylene at 313 nm wavelength and room temperature. $[C_3H_7CHO]_0 = 1 \cdot 10^{-2} \text{ mol} \cdot \text{dm}^{-3}$; ${}^a I_0 = 2.8 \cdot 10^{-10} \text{ einstein} \cdot \text{cm}^{-2} \cdot \text{s}^{-1}$ (Method A); ${}^b I_0 = 5.0 \cdot 10^{-9} \text{ einstein} \cdot \text{cm}^{-2} \cdot \text{s}^{-1}$ (Method B)

	C_2H_4	CH_3CHO	Cyclo- butanol	CO	C_3H_8	C_6H_{14}	C_3H_6	4-Hepta- none	4-Hepta- nol	<i>n</i> -Bu- tanol
ϕ^0 ^{a)}	0.13	0.14	0.034		0.29	0.010	0.006	0.012	0.027	0.059
ϕ^0 ^{b)}	0.12	0.12	0.043	0.17	0.19	0.011	0.010	0.011	0.029	0.085

Ethylene and acetaldehyde are the products of the NORRISH type II decomposition of *n*-butyraldehyde, and the presence of cyclobutanol among the products both in the vapor phase and in isooctane indicates the occurrence of reaction II'. The C_2H_4 or CH_3CHO and the cyclobutanol are primary products characteristic for primary reactions II and II', respectively.

Butyraldehyde decomposition according to reaction I gives formyl and *n*-propyl radicals. The subsequent reactions of the formyl radicals yield carbon monoxide as the sole significant product both in the vapor phase and in isooctane, thus the type I decomposition may be characterized by the measurement of CO formation. Reactions of the *n*-propyl radicals give various reaction products. It may be shown (see [3] and subsequent papers) that the predominant part of the propyl radicals is recovered in the form of C_3H_8 , C_6H_{14} and C_3H_6 . A minor part of the propyl radicals is consumed in the vapor phase in reactions leading to the formation of hepta-4-one and hepta-4-ol. (It is to be noted, however, that in solution the latter compounds are formed by other routes.) Since 4-heptanone and 4-heptanol are minor products of negligible importance from our point of view, the characteristic type I product quantum yield can be expressed as the weighted sum $\Phi_{C_3H_8} + 2\Phi_{C_6H_{14}} + \Phi_{C_3H_6}$. (A factor of 2 appears before the *n*-hexane quantum yield because two C_3H_7 radicals are consumed in the formation of a C_6H_{14} molecule.)

Secondary processes of the hydroxybutyl radical formed in reaction IV give 4-heptanol and *n*-butanol. Other products formed in hydroxybutyl radical reactions were detected [3] but are of little importance under the conditions of our investigations. Thus one may suggest the sum $\Phi_{4\text{-heptanol}} + \Phi_{n\text{-butanol}}$ as the quantum yield characteristic for reaction IV.

The quenching plots for the type II products obtained in the vapor phase and in solution are shown in Fig. 2 and 3, respectively. The yields of C_2H_4 and CH_3CHO

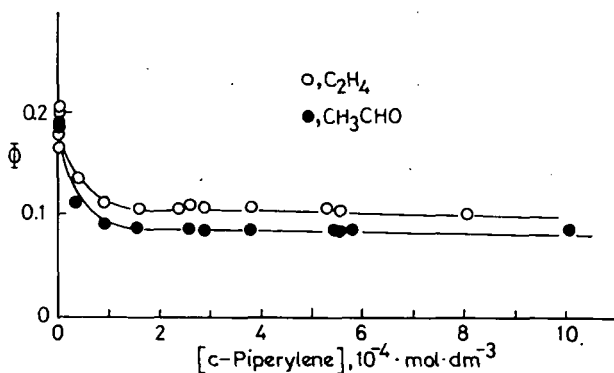


Fig. 2. Quenching plots of ethylene and acetaldehyde in the vapor phase. $T=298 \text{ K}$, $[C_3H_7CHO]=2.7 \cdot 10^{-3} \text{ mol} \cdot \text{dm}^{-3}$, $\lambda=313 \text{ nm}$, $I_0=6.5 \cdot 10^{-10} \text{ einstein} \cdot \text{cm}^{-2} \cdot \text{s}^{-1}$

agree in solution both in the absence and in the presence of the quencher. However, there is a minor disagreement (exceeding the error limits) apparent in the vapor phase, for which satisfactory explanation has not been found so far. The quantum yields decrease with increasing quencher concentration and seem to attain a limiting value at around 10^{-4} and $10^{-3} \text{ mol} \cdot \text{dm}^{-3}$ piperylene concentrations in the vapor phase and in isooctane, respectively. If the residual reaction is assumed to occur from the singlet excited state and the quencherable part from the triplet state, then one obtains with equ. (1) and (2) for the triplet and singlet state contributions,

respectively, to the type II decomposition: $\eta^T=0.45$ and $\eta^S=0.55$ (vapor phase), $\eta^T=0.75$ and $\eta^S=0.25$ (solution).

The results on the quenching of the cyclobutanol formation by piperylene in the vapor phase and in solution are shown in Fig. 4. and 5., respectively. Again the quen-

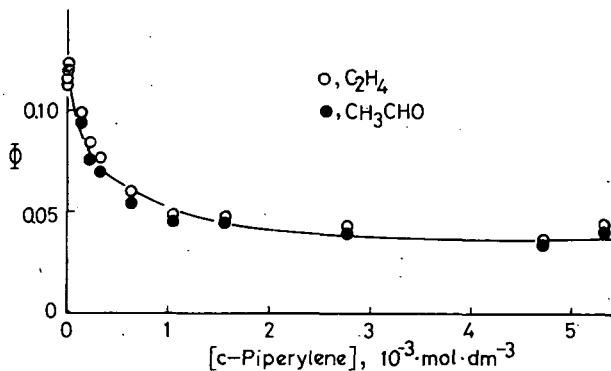


Fig. 3. Quenching plots of ethylene and acetaldehyde in isooctane. $T=298 \text{ K}$, $[\text{C}_3\text{H}_7\text{CHO}]_0=1 \cdot 10^{-2} \text{ mol} \cdot \text{dm}^{-3}$, $\lambda=313 \text{ nm}$, $I_0=5.0 \cdot 10^{-9} \text{ einstein} \cdot \text{cm}^{-2} \cdot \text{s}^{-1}$

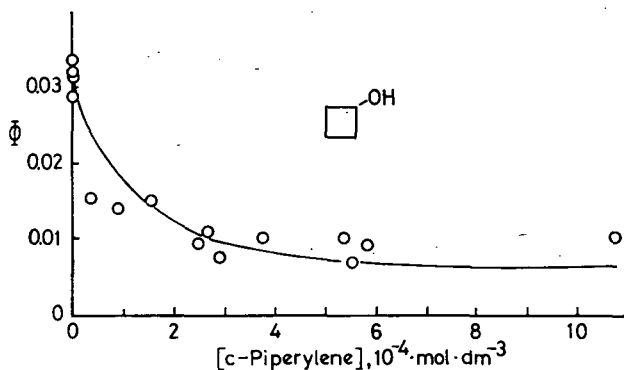


Fig. 4. Quenching of cyclobutanol formation in the vapor phase. $T=298 \text{ K}$, $[\text{C}_3\text{H}_7\text{CHO}]_0=2.7 \cdot 10^{-3} \text{ mol} \cdot \text{dm}^{-3}$; $\lambda=313 \text{ nm}$, $I_0=6.5 \cdot 10^{-10} \text{ einstein} \cdot \text{cm}^{-2} \cdot \text{s}^{-1}$

ching curves seem to level off above 10^{-4} and $10^{-3} \text{ mol} \cdot \text{dm}^{-3}$ in the vapor phase and in isooctane, respectively. Assuming that, at high quencher concentrations, cyclobutanol formation originates from the excited singlet state, one obtains for the contribution of the two excited state precursors $\eta^T=0.80$ and $\eta^S=0.20$ in the vapor phase, and $\eta^T=0.80$ and $\eta^S=0.20$ in isooctane.

Quenching of carbon monoxide, propane, *n*-hexane and propylene formation by piperylene in the vapor phase and in solution is shown in Fig. 6 and 7, respectively.

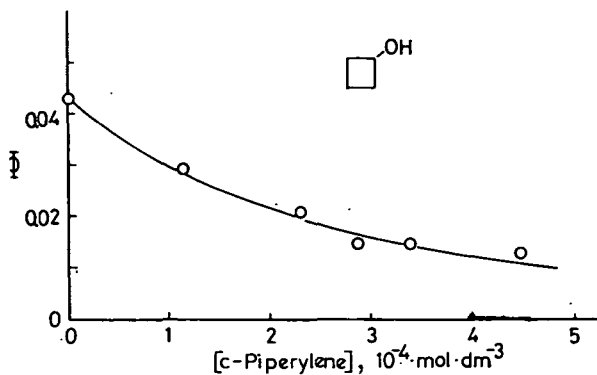


Fig. 5. Quenching of cyclobutanol formation in isoctane. $T=298\text{ K}$, $[C_3H_7CHO]_0=1\cdot 10^{-2}\text{ mol}\cdot\text{dm}^{-3}$, $\lambda=313\text{ nm}$, $I_0=5.0\cdot 10^{-9}\text{ einstein}\cdot\text{cm}^{-2}\cdot\text{s}^{-1}$

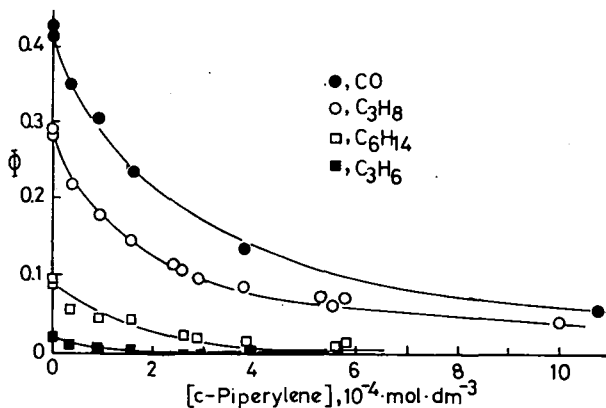


Fig. 6. Quenching of CO, propane, *n*-hexane and propylene formation in the vapor phase. $T=298\text{ K}$, $[C_3H_7CHO]_0=2.7\cdot 10^{-3}\text{ mol}\cdot\text{dm}^{-3}$, $\lambda=313\text{ nm}$, $I_0=6.5\cdot 10^{-10}\text{ einstein}\cdot\text{cm}^{-2}\cdot\text{s}^{-1}$

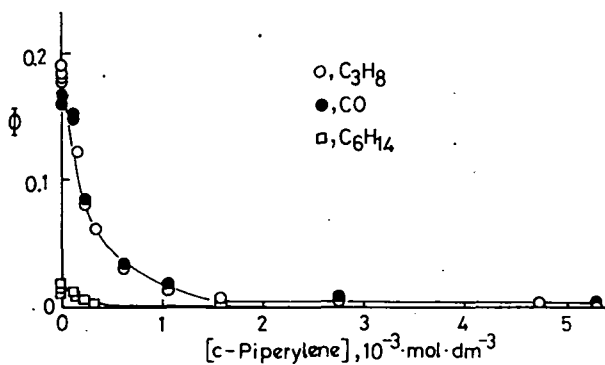


Fig. 7. Quenching of CO, propane and *n*-hexane formation in isoctane. $T=298\text{ K}$, $[C_3H_7CHO]_0=1\cdot 10^{-2}\text{ mol}\cdot\text{dm}^{-3}$, $\lambda=313\text{ nm}$, $I_0=5.0\cdot 10^{-9}\text{ einstein}\cdot\text{cm}^{-2}\cdot\text{s}^{-1}$

It may be seen from the figures that the formation of the products related to the type I decomposition is influenced to a great extent by piperylene, indicating the significant role played by the triplet state in the NORRISH type I decomposition. This is true especially for the reaction occurring in isooctane. The change in stoichiometry with increasing piperylene concentration is also apparent from the figures. (Note that the quantum yield of *n*-hexane formation decreases more rapidly than that of propane.)

In Fig. 8 and 9 the relative quenching plots of characteristic type I product quantum yields are shown for the vapor phase and for isooctane solution, respectively. It is important to note that the relative quenching curves based on the sum $C_3H_8 + 2C_6H_{14} + C_3H_6$ agree within the limits of experimental error with those obtained from CO measurements. This supports our choice made for expressing the characteristic product quantum yield. The quenching curves suggest that $\eta^T > 0.80$ and

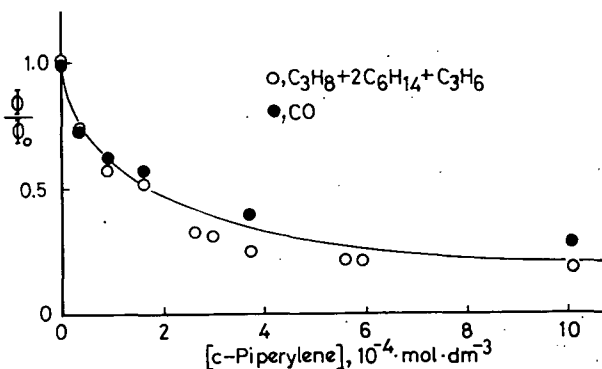


Fig. 8. Relative quenching plot of the characteristic type I product quantum yields ϕ_{CO} and $(\phi_{C_3H_8} + 2\phi_{C_6H_{14}} + \phi_{C_3H_6})$, in the vapor phase

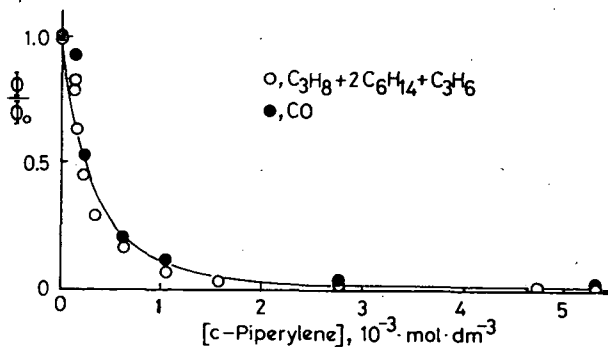


Fig. 9. Relative quenching plot of the characteristic type I product quantum yields, ϕ_{CO} and $(\phi_{C_3H_8} + 2\phi_{C_6H_{14}} + \phi_{C_3H_6})$, in isooctane

$\eta^S < 0.20$ in the vapor phase, while $\eta^T > 0.95$ and $\eta^S < 0.05$ in isooctane. However, for reasons which we are going to describe below, these results should be accepted with some reserve.

The results on the quenching of 4-heptanol and *n*-butanol formation in the vapor phase and in isooctane are given in Fig. 10 and 11, respectively. The corresponding

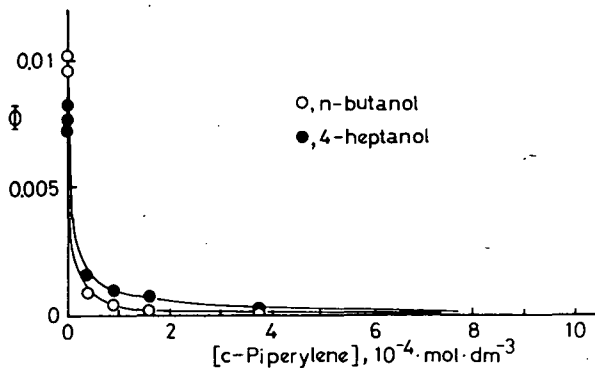


Fig. 10. Quenching of 4-heptanol and *n*-butanol formation by piperylene in the vapor phase. $T = 298 \text{ K}$, $[C_3H_7CHO]_0 = 2.7 \cdot 10^{-3} \text{ mol} \cdot \text{dm}^{-3}$, $\lambda = 313 \text{ nm}$, $I_0 = 6.5 \cdot 10^{-10} \text{ einstein} \cdot \text{cm}^{-2} \cdot \text{s}^{-1}$

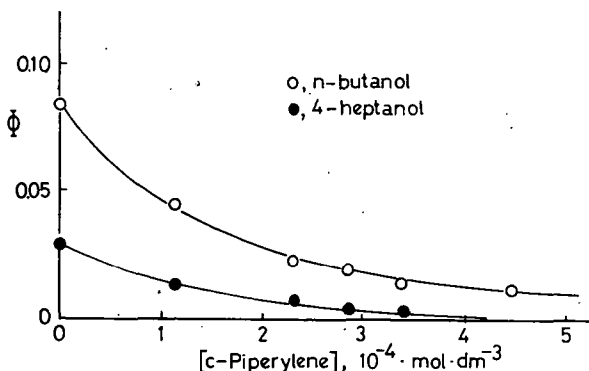


Fig. 11. Quenching of 4-heptanol and *n*-butanol formation by piperylene in isooctane. $T = 298 \text{ K}$, $[C_3H_7CHO] = 1 \cdot 10^{-2} \text{ mol} \cdot \text{dm}^{-3}$, $\lambda = 313 \text{ nm}$, $I_0 = 5 \cdot 10^{-9} \text{ einstein} \cdot \text{cm}^{-2} \cdot \text{s}^{-1}$

relative quenching plots of the characteristic product quantum yields (the sum of the quantum yields of 4-heptanol and *n*-butanol formation) are shown in Fig. 10 and 11. From these one may conclude that, under the conditions of our investigation, reaction IV occurs from the triplet state; *i.e.* $\eta^T \sim 1.0$ and $\eta^S \sim 0$ both in the vapor phase and in isooctane.

The excited singlet and triplet state contributions to primary reactions I, II, II' and IV in *n*-butyraldehyde photolysis, obtained from piperylene quenching experiments, are summarized in Table IV. The results show the excited state precursor involved in reaction I and IV to be the triplet aldehyde molecule, while reactions II and II' occur from both the excited singlet and the triplet states. The role of the triplet state is more important in isoctane than in the vapor phase.

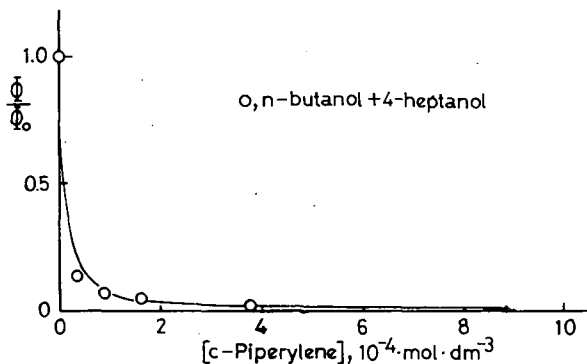


Fig. 12. Relative quenching plot of the characteristic product quantum yield for reaction IV in the vapor phase

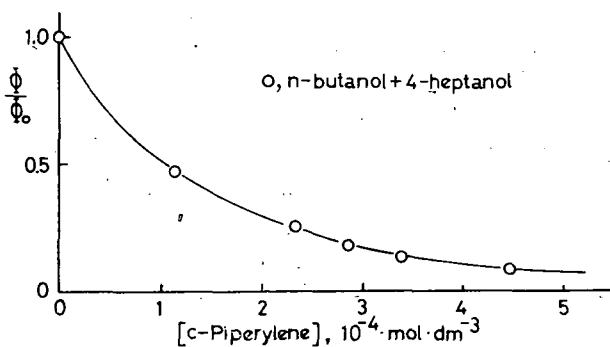


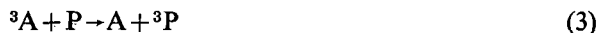
Fig. 13. Relative quenching plot of the characteristic product quantum yield for reaction IV in isoctane

The singlet state energy of *n*-butyraldehyde has been estimated by LEBOURGEOIS *et al.* [10], on the basis of the fluorescence and absorption spectra, to be about $86 \text{ kcal} \cdot \text{mol}^{-1}$. The *n*-butyraldehyde quenches the triplet state of acetone [7] (for which a triplet energy of $80 \text{ kcal} \cdot \text{mol}^{-1}$ has been estimated [12]), on the other hand *cis*-butene-2 (with a triplet energy of about $78.8 \text{ kcal} \cdot \text{mol}^{-1}$ [13]) is an inefficient quencher of the triplet *n*-butyraldehyde [14]. From these data we estimated the lowest level of the triplet state of *n*-butyraldehyde to be about $78 \text{ kcal} \cdot \text{mol}^{-1}$ above the ground state.

Table IV
The role of the excited singlet and triplet states in primary reactions
I, II, II' and IV of n-butyraldehyde photolysis

	Reaction I	Reaction II	Reaction II'	Reaction IV
Vapor phase				
η^S	< 0.20	0.55	0.20	~0
η^T	> 0.80	0.45	0.80	~1.0
Solution				
η^S	< 0.05	0.25	0.20	~0
η^T	> 0.95	0.75	0.80	~1.0

The *cis*-piperylene has a low triplet state energy (which is about 56.9 kcal · mol⁻¹ above the ground state [15]), thus very efficient triplet energy transfer is expected to occur from *n*-butyraldehyde to the conjugated olefin:



where A and ³A stand for the ground state and triplet state of the aldehyde, while P and ³P designate the ground state and triplet state of piperylene, respectively. In accordance with this supposition we found that low concentrations of piperylene (10⁻⁴ mol · dm⁻³ in the vapor phase and 10⁻³ mol · dm⁻³ in solution) quenched the decomposition of *n*-butyraldehyde. The quenching effect of piperylene is caused by energy transfer, which is indicated by the simultaneous occurrence of the *cis-trans* isomerization of the olefin. Thus, there is no doubt that efficient triplet energy transfer took place under the conditions used in our experiments, however, it has not been examined in this paper whether some singlet energy transfer also occurred at the highest piperylene concentrations. Experiments planned at even higher quencher concentrations — which are in progress in our laboratory — shall throw light on this question.

Only physical quenching caused by piperylene has been considered so far. However, free radicals formed in the primary processes might react with the conjugated olefin causing chemical quenching which could remain unrecognized. The observation [14] that the quantum yield of piperylene *cis-trans* isomerization was found to be similar but somewhat less than the value expected from the extent of decrease of product quantum yields seems to indicate that some trapping of the free radicals occurred. If this is so, the role of the triplet state in reaction I (and perhaps in reaction IV) could be somewhat less and that of the excited singlet state a little more important than indicated by the figures given in Table IV. Further experiments with triplet quenchers not reacting with free radicals are in progress and the results will be reported in another paper.

* * *

The authors express their thanks to Dr. S. FÖRGETEG for his assistance in the experimental work.

References

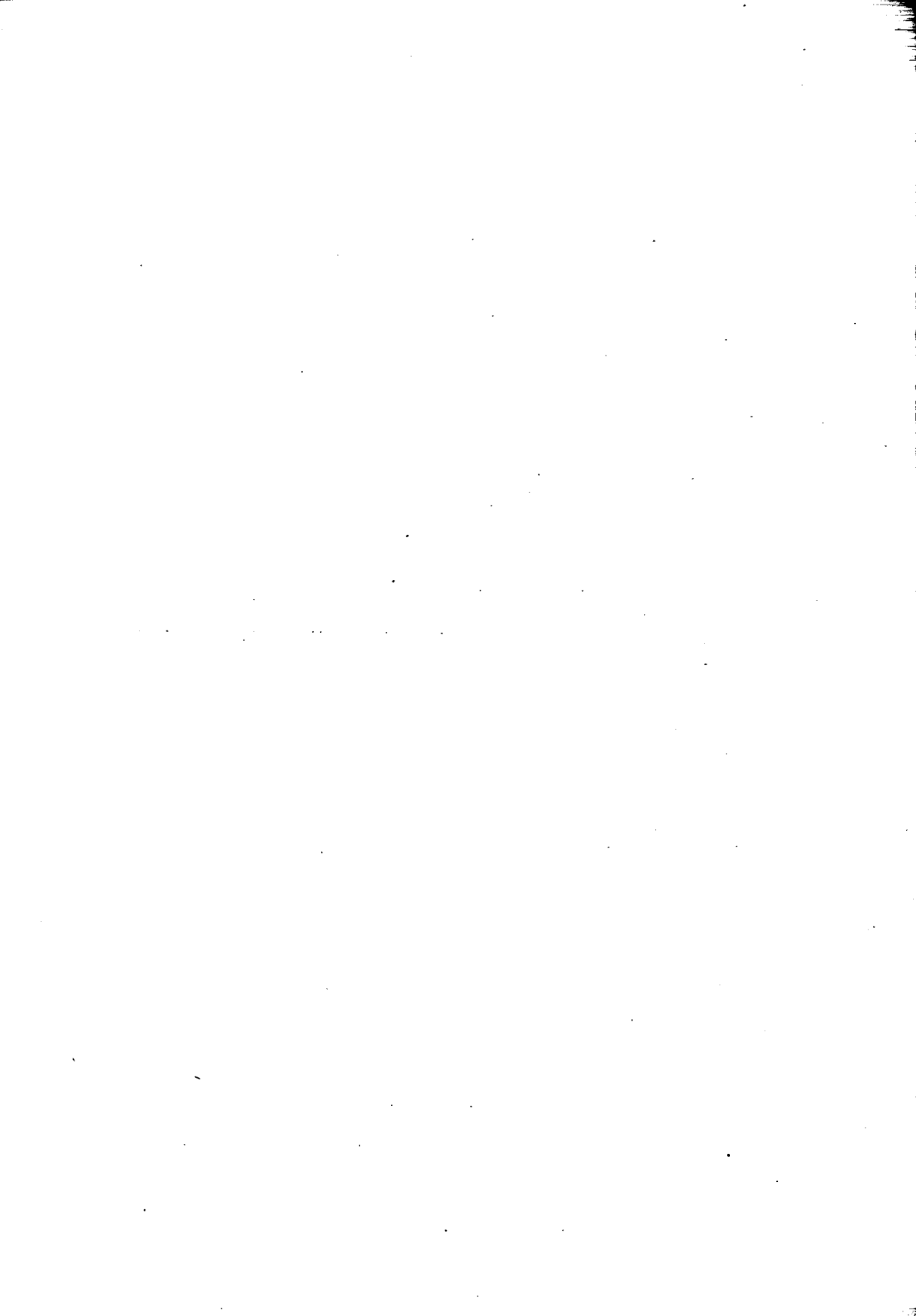
- [1] *Blacet, F. E., J. G. Calvert*: J. Amer. Chem. Soc. **73**, 661 (1951).
- [2] *Blacet, F. E., J. G. Calvert*: J. Amer. Chem. Soc. **73**, 667 (1951).
- [3] *Förgeteg, S., T. Bérces, S. Dóbbé*: Acta Chim. Acad. Sci. Hung., to be published.
- [4] *Borrel, P., R. G. W. Norrish*: Proc. Roy. Soc. A **262**, 19 (1961).
- [5] *Norrish, R. G. W., R. P. Wayne*: Proc. Roy. Soc. A **284**, 1 (1965).
- [6] *Borkowski, R. P., P. Ausloos*: J. Amer. Chem. Soc. **84**, 4044 (1962).
- [7] *Rebber, R. E., P. Ausloos*: J. Amer. Chem. Soc. **86**, 4803 (1964).
- [8] *Cundall, R. B., A. S. Davies*: Trans. Faraday Soc. **62**, 2444 (1966).
- [9] *Coyle, J. D.*: J. Chem. Soc. (B) **2254** (1971).
- [10] *Lebourgeois, P., R. Arnaud, J. Lemaire*: J. Chim. phys. **71**, 481 (1974).
- [11] *Parker, C. A.*: Photoluminescence of Solutions, Elsevier Publ. Co., Amsterdam, 1968, p. 204.
- [12] *Borkman, R. F., D. R. Kearns*: J. Chem. Phys. **44**, 945 (1966).
- [13] *Archer, A. S., R. B. Cundall, G. B. Evans, T. F. Palmer*: Proc. Roy. Soc. A **233**, 385 (1973).
- [14] *Tölgyesi, M., T. Bérces*: unpublished results.
- [15] *Lamola, A. A., G. S. Hammond*: J. Chem. Phys. **43**, 2129 (1965).

РОЛЬ ВОЗБУЖДЕННЫХ СОСТОЯНИЙ В ФОТОЛИЗЕ *n*-МАСЛЯНОГО АЛЬДЕГИДА, I.

Тушение триплетного состояния пипериленом

М. Тельдеши, Т. Берцеш и А. Нача

Описан экспериментальный метод пригодный для изучения роли возбужденных состояний в фотолизе *n*-масляного альдегида. Даны предварительные экспериментальные результаты полученные с применением в качестве тушителя пиперилена в газовой фазе и в растворе (растворитель изооктан) и оценены доли синглетного и триплетного состояний в четырех главных первичных фотохимических процессах фотолиза *n*-масляного альдегида при длине волны 313 нм.



KINETICS AND MECHANISM OF THE THERMAL DECOMPOSITION OF METAL CHLORITES, CHLORATES, AND PERCHLORATES

By

F. SOLYMOSI

Reaction Kinetics Research Group of the Hungarian Academy of Sciences, Szeged

(Received February 10, 1976)

Studies related to the thermal decomposition of different metal chlorites, chlorates and perchlorates are reviewed and a critical survey on various interpretations of the thermal behaviour of these salts is given.

Introduction

Halogen oxyacids and their salts occupy an important place in the system of inorganic chemistry. During the past twenty years there has been particularly great interest in this family of compounds, as demonstrated by the several hundred publications on their physical and chemical properties, and primarily on their thermal stabilities. The main cause of this great interest is that many of these compounds are widely used in practice as source of oxygen. They comprise one of the most important constituents of solid propellants, and are also employed in various pyrotechnic and explosive mixtures.

The primary aims of the present work are to review the considerable experimental and theoretical material, to emphasize on the more important results, and to discuss these at a high level.

Thermal stability of alkali chlorites

According to early observations, sodium chlorite is easily explosible on shock; when heated, chlorate and chloride is formed, accompanied by a slight amount of oxygen evolution (see [1, 2]). TAYLOR *et al.* [3] stated that sodium chlorite is highly resistant to long period of storing at room temperature: after 10 years of storage its weight loss was negligible and, as can be seen from Table I, its composition has not much altered either.

At higher temperatures (150° C) decomposition was not observed after 30 minutes, above 200° C, however, a considerable amount of chlorate formation was noted. It has also been observed that sodium chlorite explode only if the surface of the metal performing the striking contained grease.

The thermal stability of chlorites has been studied in detail only recently applying derivatographic methods as well as kinetic measurements [1].

Table I
The composition of solid NaClO₂ after different storing periods at 25° C [3]

Compound	Composition in weight %			
	Starting material	after 4 months	after 22 months	after 130 months
NaClO ₂	84.90	87.00	87.59	86.63
NaCl	2.40	2.28	2.05	2.77
NaClO	0.00	0.00	0.11	0.00
NaClO ₃	2.96	1.76	1.35	1.97
Na ₂ CO ₃	13.52	10.12	7.47	9.17
	103.78	101.16	98.57	100.54

The derivatograms of sodium chlorite are plotted in Fig. 1.a. There are three exothermic peaks on the DTA curve, at 191, 273° and 557° C. An endothermic change appeared at 260° C. From the first two exothermic peaks only the second was connected with a very slight but reproducible weight loss (about 1%). The decomposition of the substance started at 440–450° C. On increasing the heating rate (from 3° C/min. to 18° C/min.) the exothermic peaks and also the onset of the loss of weight were shifted towards higher temperature.

Interrupting the measurements after the second exothermic process at 280° and 320° C and cooling down the sample, the substance did not exhibit in a repeated experiment the exothermic peaks previously observed (Fig. 1.b).

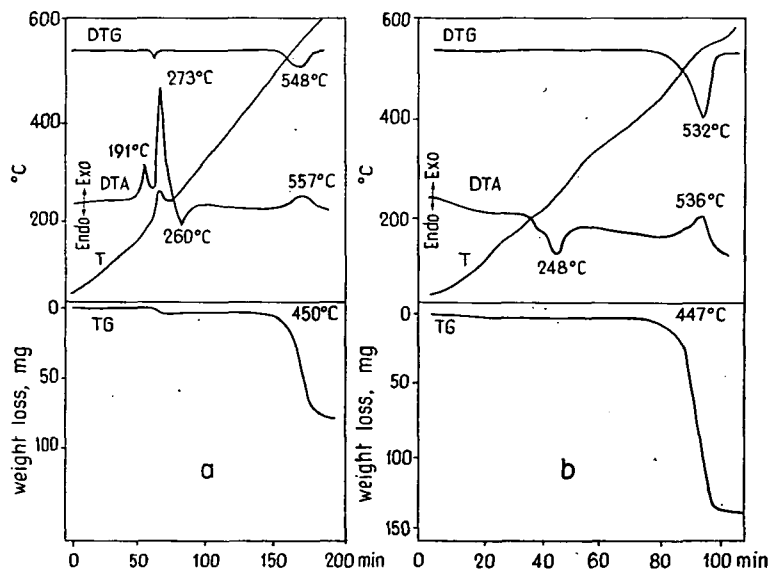


Fig. 1. Derivatogram of NaClO₂ (a). Derivatogram after the interruption at 280° C (b). Weight of substance: 210 mg; heating rate: 6° C/min. [1]

The solid residue obtained at the interruption did not contain any sodium chlorite: its composition was: 73.7% NaClO_3 and 24.3% NaCl . These results show that under the experimental conditions applied sodium chlorite is transformed into sodium chlorate and sodium chloride according to the equation



The exothermic character of the reaction is in accordance with the reaction heat calculated from the heats of formation of the substances (Table II). The endo-

Table II
Heat of reaction of different transformations of chlorites

Compound	Heat of formation kcal/mole	ΔH_1 /mole	ΔH_2 /mole	ΔH_3 /mole	ΔH_4 /mole
LiClO_2	-84.88	+13.98	+5.01	-12.82	+27.36
NaClO_2	-72.65	-13.08	-17.24	-25.58	+45.90
KClO_2	-78.90	-14.60	-18.15	-25.27	+71.40
RbClO_2	-74.50	-17.50	-21.13	-28.41	+70.1
CsClO_2	-74.46	-19.54	-22.04	-29.04	+73.02
$\text{Ba}(\text{ClO}_2)_2$	-158.2	-23.5	-31.45	-47.36	+25.2
AgClO_2	0.0	-5.73	-13.9	-30.36	+3.26
$\text{Pb}(\text{ClO}_2)_2$	—	—	—	—	—

$$\Delta H_1: \text{for } \text{MeClO}_2 + \frac{1}{2} \text{O}_2 = \text{MeClO}_3$$

$$\Delta H_2: \text{for } \text{MeClO}_2 = \frac{2}{3} \text{MeClO}_3 + \frac{1}{3} \text{MeCl}$$

$$\Delta H_3: \text{for } \text{MeClO}_2 = \text{MeCl} + \text{O}_2$$

$$\Delta H_4: \text{for } 2 \text{MeClO}_2 = \text{Me}_2\text{O} + \text{Cl}_2 + \frac{1}{2} \text{O}_2$$

thermic change experienced at 260° C as well as the decomposition which started above 448° C were due to melting and decomposition of the sodium chlorate. The latter process is characterized on the DTA curves by an exothermic peak. If the interruption was carried out at 160° C, *i.e.* before the appearance of the first exothermic peak, only 5% NaClO_3 was found in the sample.

The derivatogram of sodium chlorite was taken in the presence of sodium chlorate and sodium chloride, respectively (mole ratio 1:1). It appeared that the products of the disproportionation reaction did not essentially influence the characteristics of sodium chlorite transformation.

The derivatographic study of the other alkali metal chlorites is hampered to a considerable extent by the fact that these compounds are appreciably more hygroscopic than sodium chlorite. Their thermal behaviour is similar to that of sodium chlorite [2]. The sharp exotherm peak indicating the disproportionation reaction is accompanied by only an extremely small weight loss (1—2%) on the TG curve (Fig. 2).

The data concerning the thermal transformation of the compounds are listed in Table III.

Table III

Exothermic peaks on DTA curves belonging to the disproportionation of chlorites [1, 2, 4]

Compound	LiClO ₂	NaClO ₂	KClO ₂	RbClO ₂	CsClO ₂	Ba(ClO ₂) ₂	Pb(ClO ₂) ₂	AgClO ₂
°C	210	191	185	155	120	220	123.5	95

Comparison of the thermal behaviour of the alkali metal chlorites shows that the beginning of the exothermic peak belonging to the disproportionation of the chlorites



decreases from lithium to cesium. On the other hand, the temperature of the weight decrease corresponding to the decomposition of the chlorate at higher temperature increases from lithium to cesium.

The kinetics of the disproportionation of alkali chlorites, under isothermal

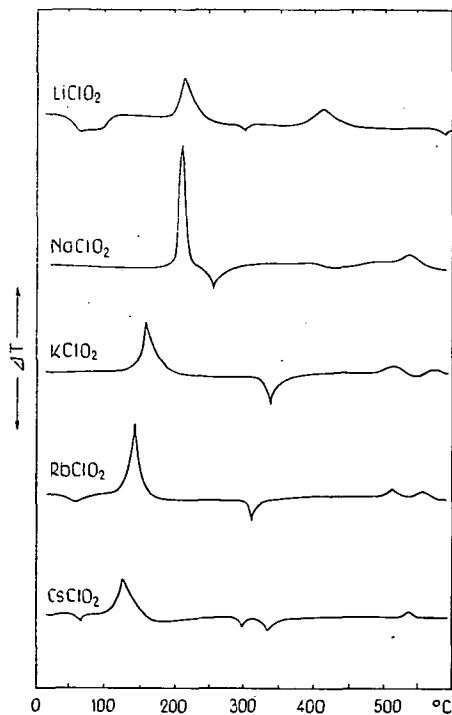


Fig. 2. DTA curves of alkali chlorites in air. Heating rate 3°/min. [2]. Weight of substance: 50 mg

condition, has been studied in the temperature range between 52 to 180° C. [1, 2]. The reaction starts without induction period and its rate increases with increasing temperature. The reaction is adequately described by the first order equation up to 50–70% and 30–40% conversion at higher and lower temperatures, respectively.

The temperature of the disproportionation reaction decreased from lithium (152–180° C) to cesium (52–98° C). The activation energies were found to vary between 15–28 kcal/mole. Many attempts have been made to decompose sodium chlorite under isothermal conditions. However, the substance only disproportionated into chlorate and chloride even at higher temperatures, (300–400° C) without any gas evolution. The slow gas evolution experienced above 400° C is the result of the decomposition of sodium chlorate formed in the disproportionation. The same behaviour was found for the other alkali chlorites.

Thermal stability of barium, silver and lead chlorites

Among the other metal chlorites, detailed studies were carried out only on barium, lead and silver chlorites [1, 4].

The thermal behaviour, the TG and DTA curves of these compounds essentially differed from that of the alkali chlorites. Parallel to the large heat evolution, extremely fast decomposition appeared on the TG curve at the following temperatures (Figs. 3 and 4):

barium chlorite 190° C,
 silver chlorite 120° C,
 lead chlorite 103° C.

On applying 1°/min heating rate, the behaviour of chlorites altered, namely they were converted almost at the above temperatures into chlorates and chloride accompanied by an exothermic heat change without any decomposition.

The direction of conversion of barium chlorite was influenced by addition of foreign substances (barium chloride, barium chlorate, aluminium oxide, nickel oxide.) In such cases, decomposition of the compound did not occur even when 6°/min. heating rate was used. All these findings indicate that the direction of conversion of barium, silver, and lead chlorite — contrary to that of the sodium chlorite — is extremely sensitive to the temperature and to experimental conditions.

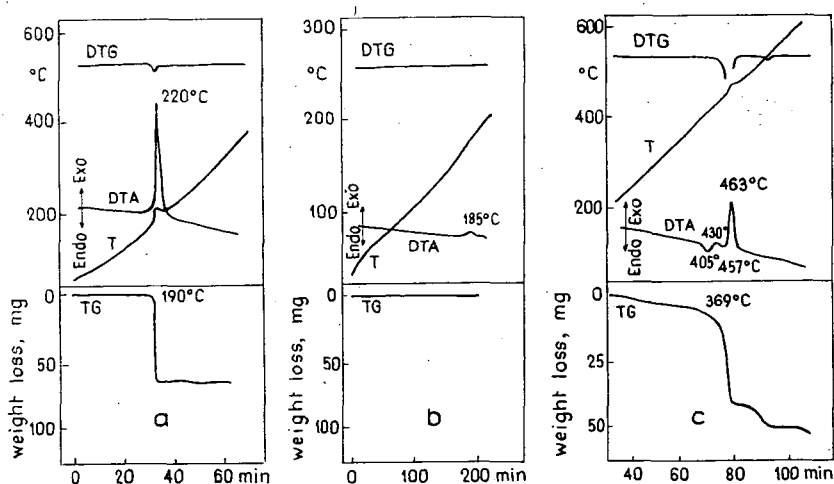


Fig. 3. Derivatogram of $\text{Ba}(\text{ClO}_2)_2$ [1]. Weight of substance: 160 mg; heating rate: (a) 6°/min.; (b) 1°/min.; (c) continuation of the former measurement with 6°/min.

The disproportionation of barium, lead and silver chlorites has been studied kinetically at lower temperatures, and the activation energies were found to be 23, 26 and 39 kcal/mole. The slow decomposition of barium and lead chlorites could not be studied either, as at the moment of beginning of gas evolution the decomposition

immediately turned into explosion. The activation energies calculated from the temperature dependence of the induction period before the explosion were found to be 38.8; and 28 kcal/mole (Fig. 5). The explosion proved to be of thermal origin; at the moment of explosion the temperature rise was between 40 and 80° C.

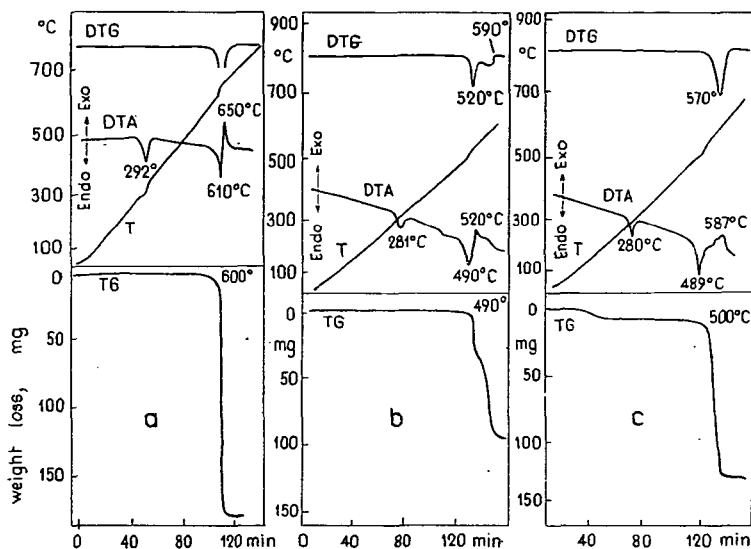


Fig. 4. Derivatogram of $\text{Pb}(\text{ClO}_3)_2$ [1]. Weight of substance: 100 mg; heating rate: (a) 6°/min.; (b) 1°/min.; (c) continuation at a heating rate of 6°/min. of the measurement interrupted at 150° C

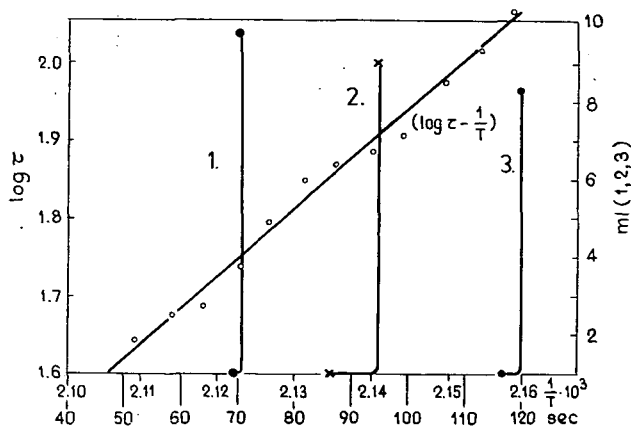


Fig. 5. Explosion of $\text{Ba}(\text{ClO}_3)_2$ at different temperatures and the Arrhenius diagram of the induction periods [1]; τ = induction period before the explosion, ml = the amount of gases formed during the explosion. (1), at 196° C; (2), at 192° C; (3), at 190° C

Among the chlorites investigated, silver chlorite was the only compound the slow decomposition of which was observed. In vacuum the reaction occurred according to equation



The decomposition was of autocatalytic character; the acceleration period followed the equation

$$\log p = k \cdot t + c.$$

The activation energy was found to be 48.2 kcal/mole. In the period following the rate maximum the monomolecular decay equation described the decomposition. The activation energy was 24.8 kcal/mole.

Table IV
Kinetic data for the reactions of chlorites

Compound	Temperature range °C	Methods	Activation energy kcal/mole	Frequency factor min ⁻¹	Kinetic equation
<i>Disproportionation</i>					
LiClO ₂	152—180	chemical analysis in air	24.2	6.28 · 10 ⁸	first order
NaClO ₂	140—160	chemical analysis in air	54.2	1.85 · 10 ²⁵	first order
KClO ₂	100—140	chemical analysis in air	28.3	—	first order
RbClO ₂	90—120	chemical analysis in air	20.0	2.86 · 10 ⁸	first order
CsClO ₂	52—98	chemical analysis in air	15.2	1.11 · 10 ⁸	first order
Ba(ClO ₂) ₂	130—170	chemical analysis in air	23.5	3.88 · 10 ⁹	first order
Pb(ClO ₂) ₂	75.5—95	chemical analysis in air	39.4	1.62 · 10 ²¹	first order
<i>Decomposition</i>					
AgClO ₂	85—105	chemical analysis in air	26.0	1.74 · 10 ¹⁶	first order
<i>Explosion</i>					
AgClO ₂	108—125	in air ml of gases	53.0	—	induction period
Ba(ClO ₂) ₂	190—210	in air ml of gases	38.8	—	induction period
Pb(ClO ₂) ₂	112—115	in air ml of gases	28.0	—	induction period

Data concerning the thermal behaviour of other metal chlorites are very scarce in literature. Calcium and strontium chlorites decompose upon contact with a hot wire, and they explode upon percussion [5]. Zinc and cadmium chlorites containing two moles of crystal water did not explode upon percussion; in vacuum however, they, changed into basic salt accompanied by loss of water and chlorine evolution [5]. Mercurous chlorite decomposes upon heating and percussion to mercurous chloride. Mercuric chlorite explodes upon percussion while chloride is being formed. In greater quantity, it easily explodes at room temperature immediately after its preparation [6]. The light yellow thallium chlorite becomes brownish in 15–20 min after preparation. It decomposes completely at 30° C after 13–15 hours accompanied by a very slight gas evolution. It explodes violently accompanied by sound at 45° C into chlorine, oxygen and a little chlorine dioxide [7]. Nickel chlorite containing two moles of crystal water explodes at a temperature as low as that of the water bath. Upon percussion it explodes similarly as copper chlorite [8, 9]. Kinetic data for the reactions of chlorites are collected in Table IV. Data concerning the physical properties and bonding of the metal chlorites are given in Table V.

Table V
Some physical constants of chlorites

Compounds	Density	Ionization potential of cations eV	F*	Refractive index n_D^{25}	K Dielectric constant at 350 Kc/s	Absorption edge Å	Optical activation energy E_0 (eV)	Thermal activation energy E_T (eV)	K_0/K	Ionic character of bond %
LiClO ₂		5.390	2.915		9.213	2875	4.31			67.4
NaClO ₂		5.138	2.407	1.547	6.535	2660	4.66	1.70	0.366	68.5
KClO ₂		4.339	1.661	1.529	4.073	2760	4.49		0.5739	73.0
RbClO ₂		4.176	1.423		4.687	2925	4.23			73.8
CsClO ₂		3.833	1.303		7.267	3366	3.68			75.1
Ba(ClO ₂) ₂	3.60	10.00	—	1.645	4.215	2900	4.28	2.75	0.642	44.95
AgClO ₂	4.30	7.56	3.394	2.1	5.282	4050	3.06	2.55	0.835	35.8
Pb(ClO ₂) ₂	5.10	15.03	3.876	2.1	5.417	4000	3.10	2.52	0.814	16.99

$$F^* = \frac{Z^* \cdot e}{r^2} = \text{effective electric field strength of cation}$$

r = radius of cation

Z^* = effective nuclear charge number, $Z^* \cdot e = (Z - S)e$

Z = nuclear charge, S = screening number

$K_0 = n^2$

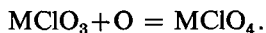
* The effective electric field strength of barium cannot be calculated due to the lack of data for the determination of its screening number.

Mechanism of disproportionation and decomposition of chlorites

Although the disproportionation of chlorine oxy salts has been known for a long time, however, detailed measurements were carried out only with the alkali chlorates, but even these not from the kinetic point of view. The possible reason for this is that, besides disproportionation, the decomposition of chlorates also

occurs. To evaluate the mechanism of the disproportionation of chlorites, it is advisable to take into account the different views concerning the disproportionation of chlorates. According to GLASNER and WEIDENFELD [10] the atomic oxygen formed during the decomposition of potassium chlorate reacts with the chloride *i.e.* with the solid product of the chlorate decomposition, yielding potassium perchlorate.

BOSCH and ATEN's [11] isotopic investigations, however, did not prove this conception. According to the calculations of MARKOVITZ, BORYTA and STEWART [12, 13] it is thermodynamically possible that the perchlorate is produced by oxidation of the chlorate with molecular oxygen. However, DODÉ and BASSET's [14] former experiments, in case of sodium chlorate did not give perchlorate even under 1200 atm. oxygen pressure at 475° C. The result was the same when MARKOVITZ kept the mixture of lithium chlorate and lithium chloride under 100 atm. pressure of oxygen at 150° C for several days. Therefore, they described the formation of perchlorate by assuming a reaction between atomic oxygen and chlorate:



As can be seen in Table II, the oxidation of chlorites by molecular oxygen is thermodynamically also possible. Kinetically, however, it was not observed in any case of chlorites. It may be assumed here, too, that the oxidation proceeds with the assistance of the atomic oxygen formed during the decomposition of chlorite. In this case we should take as the first step the reaction



which is followed by the processes



(S=solid surface for the recombination of oxygen atoms.) However the fact that, at a lower temperature, the disproportionation of chlorites occurs without gas formation and, moreover sodium chlorite does not decompose at all, raises some doubt about the internal oxidation mechanism.

The failure of the oxygen atoms to recombine can be accepted only if $W_4 \ll W_3$. Since the rates of both reactions depend on the rate of formation of oxygen atoms, a further condition of the absence of oxygen formation is that

$$W_1 \ll W_3.$$

Although these reaction rate relations cannot be excluded, it would be expected that at high temperature, when W_1 and W_2 have very high values (and thus the oxygen atoms form rapidly), the recombination reaction proceeds with measurable rate, too. In the case of sodium chlorite the oxygen evolution was less than 1% even at 400° C, when the disproportionation reaction occurred instantaneously. If we accept the formation of, and oxidation by, atomic oxygen when sodium chlorite is heated up to an elevated temperature, but still below the disproportionation

nation temperature of sodium chlorate, the oxygen atom should oxidize not only the remaining chlorite, but — to a smaller extent — the formed chlorate, too. From pure sodium chlorite, however, sodium perchlorate did not form even at

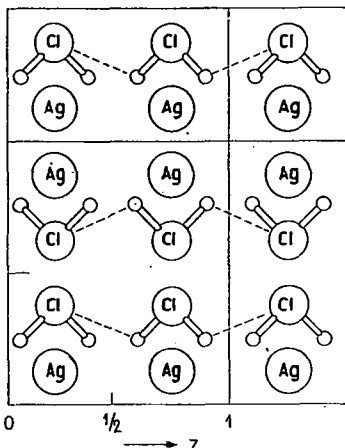


Fig. 6. The structure of AgClO_2 viewed along the a axis. The dashed lines indicate the planes of new Cl—O bonds formed during the disproportionation

greater thermodynamic stability of chlorate, rearranged to form chlorate and chloride. This process is illustrated in Fig. 6.

Whichever mechanism is accepted, the step to be activated in the disproportionation of chlorites obviously is the rupture of the original Cl—O bond. According to the internal oxidation mechanism the activation energy of the reaction should be consistent with the value of the dissociation energy of the chlorine—oxygen bond. The calculated value of the latter is 64.295 kcal/mole [15]. In the decomposition of chlorates and perchlorates, where this step proved to be the rate determining reaction, nearly the same activation energies were obtained (see later). In the present case the activation energies of the reaction were significantly lower. In our opinion the values of activation energy are in better agreement with a rearrangement process taking place between the chlorite ions. In this case, owing to the formation of the new Cl—O bond, evidently a smaller value of energy is needed for the breaking of the original Cl—O linkage. In the most favourable case (if the fractional decomposition $\alpha=1$) the value of activation energy will be equivalent to the differences between the dissociation energies of the chlorine—oxygen bonds in the two compounds, *i.e.*

$$E = D_{\text{dissociating}} - \beta D_{\text{forming}} \quad (\beta = \text{constant})$$

As a primary step in the explosion of chlorites, two reactions, the electron transfer process and the rupture of Cl—O bond can be taken into account. In the case of barium chlorite, however the reaction products as well as the activation energy calculated from the temperature dependence of induction periods contradict to this mechanism.

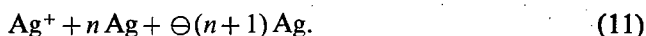
As the explosion of chlorites is preceded by an extremely slight decomposition, it was assumed that the disproportionation of chlorites during the induction period and the heat developed due to this reaction play a significant part in the occurrence of the explosion of chlorites [1]. The chemical analysis of the solid products obtained at the interruption of the heating immediately before the explosion proved the validity of this idea, as in barium chlorite 3—5%, and in lead chlorite about 2.5—5.5% chlorate was found. Accordingly, on heating the chlorites rapidly to a high temperature, the formation of chlorate sets in immediately, however, on the effect of the reaction heat, the rate of the disruption of further Cl—O bonds will increase to such an extent that there will be no possibility for the formation of new Cl—O bonds, *i.e.* for the stabilization of chlorite in form of chlorate. As the reaction



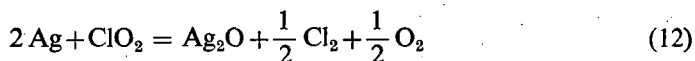
is much more exothermic (Table II) than the disproportionation reaction, this may result in further acceleration of the reaction. This conception is proved by the thermal behaviour of barium chlorite and lead chlorite at a slow heating rate (1° C/min.). In these case explosion did not occur because the dissipation of the heat of the disproportionation reaction was secured, so chlorite completely transformed into chlorate. The chlorites failed to explode in the presence of inert substances even using a heating rate of 6° C/min. which can be explained in the same way, namely by assuming the absorption of the heat produced by the disproportionation.

Alkali chlorites, contrary to other chlorites, did not explode, what is more they did not decompose even upon the effect of the great amount of reaction heat released instantaneously when the substance had been heated at an extremely high rate. This behaviour, is, in all probability, due to the greater thermal stability of alkali chlorates compared to that of other chlorates.

In the case of silver chlorite, which is more covalent in character, it was assumed that the electron transfer reaction plays a dominant role both in the decomposition and explosion [4]



The decomposition products (ClO_2 and Ag) as well as the calculated and measured activation energies seem to support this mechanism. In the explosion of silver chlorite the reaction occurring between the silver and chlorine dioxide formed:



must also be taken into consideration.

Thermal stability of alkali chlorates

Considerably more data are available on the thermal behaviour of chlorates than on that of chlorites. It has been observed as early as at the turn of the century that upon the effect of heat, chlorates partly disproportionated and partly decomposed. Foreign substances, especially oxides, were found to influence the direction and rate of conversion to a considerable extent.

A characteristic feature of alkali chlorates is the great temperature difference between their melting point and the initial temperature of their decomposition. A few degrees above their melting points the compounds — with the exception of cesium chlorate — underwent a decomposition of less than 1% within 2 days. Consequently, the melting points given for alkali chlorates can be considered as „congruent”.

A number of workers have studied the thermal behaviour of alkali chlorates by means of differential thermal analysis, as well as by thermogravimetric, differential thermogravimetric and by combined derivatographic methods [16—20]. The most detailed investigations, extended to all of the alkaline chlorates, were carried out under the same experimental conditions by MARKOVITZ, BORYTA and STEWART [12].

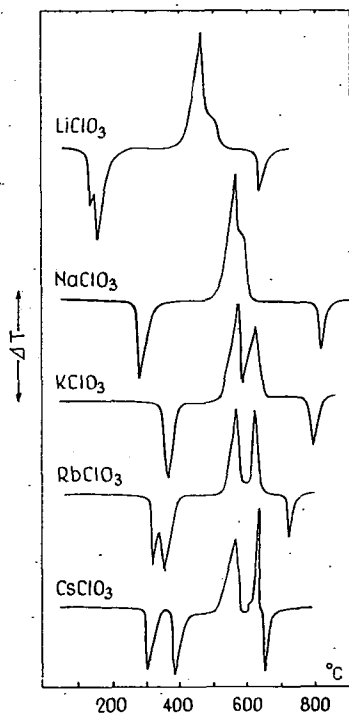


Fig. 7. DTA curves of pure alkali metal chlorates [12]. Heating rate: 4° C/min; weight of substances: 1 g

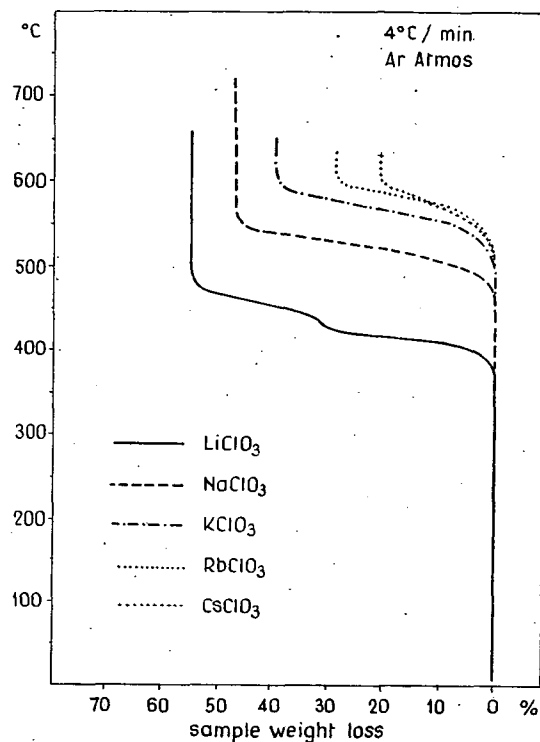


Fig. 8. Thermogram for pure alkali metal chlorates [12]. Heating rate: 4° C/min. Argon atmosphere

DTA and thermogravimetric curves obtained by these authors are given, in Fig. 7 and 8, where the first endotherm peaks correspond to the crystallographic transition as well as to melting of the substance. In the case of potassium, rubidium and cesium chlorates, two exothermic peaks can be well distinguished, while in that of lithium and sodium chlorates the exothermic peaks are obviously the results of several consecutive processes. The compositions of the samples before the appearance of the first exothermic peak are shown in Table VI. From the results of the chemical

Table VI

Composition of alkali chlorates heated to peak temperatures of first exotherms on DTA curves. Heating rate: 4°/min. [12]

Compound	Residue composition, %			Percentage decomposition		Peak temperature °C
	MClO ₃	MCl	MClO ₄	to MCl	to MClO ₄	
LiClO ₃	0.9	68.2	30.3	57.8	40.2	425
NaClO ₃	2.6	47.3	50.1	30.5	66.9	542
KClO ₃	0.9	33.9	65.2	12.1	87.0	566
PbClO ₃	1.6	32.9	65.5	11.0	87.4	563
CsClO ₃	1.3	34.0	64.7	12.4	86.3	560

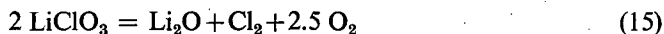
analysis it is apparent that the first exothermic peak is also the result of two simultaneously occurring reactions



The second exothermic peak represents the decomposition of perchlorate formed during the disproportionation of chlorates. On heating lithium and sodium chlorates, the decomposition of perchlorate formed in the disproportionation commenced as soon as the first exothermic peak began to take shape.

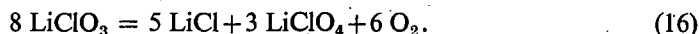
The values of percentage weight-loss indicate that chlorine is formed practically only in the decomposition of lithium chlorate.

The extent of the reaction



is only about 4% of the decomposition. An extremely low chlorine formation was observed in the decomposition of sodium chlorate, too.

More detailed thermogravimetric measurements revealed that an appreciable decomposition of lithium chlorate has commenced at 370° C [13]. A notable decrease in the rate of decomposition occurred at 430° C. The percentage weight-loss up to this point was 27.7% which corresponds to the reaction



Above 430° C the decomposition of lithium perchlorate formed in the above reaction takes place at a considerably higher rate than that of pure lithium perchlorate; this may be attributed to the catalytic effect of the lithium chloride present. The

results of the measurement made at 339° C under isothermal conditions indicated that the disproportionation and decomposition of lithium chlorate practically occurs at identical rate.

Addition of lithium chloride (50 mole %) to lithium chlorate catalyzed both the decomposition and the disproportionation reaction. A significant weight-loss was observable at a temperature as low as 343° C.

The decomposition of sodium chlorate has been studied from the kinetical point of view in the temperature range between 450—480° C [18]. There is a time lag of only few minutes before the reaction. As the pressure of the oxygen evolved during the decomposition increases linearly up to $\alpha=0.5$ with time, the rate constants of the decomposition were determined from the slope of the α - t curves. From the temperature dependence of the rate constants obtained in this way a value of 68 kcal/mole was calculated for the activation energy.

After the gas evolution had ceased, undecomposed chlorate could not be detected in the solid residue. Besides sodium chloride, however, the solid residue contained a considerable amount, (about 40 w%) of perchlorate due to the disproportionation reaction. It was attempted to separate the decomposition and disproportionation by changing the reaction temperature, but without any success.

The formation of sodium perchlorate was studied at the same temperatures. At 390° C, where the decomposition of sodium chlorate is negligible, disproportionation is also extremely slow. After 5 hours only 2.5% of sodium perchlorate was formed. On increasing the temperature the perchlorate content increased, and above 450° C it ran parallel with the decomposition.

The decomposition of potassium chlorate has also been studied under isothermal condition, mainly to find out more about the influence exerted by potassium chloride on the conversion of the compound. The opinions concerning this effect vary considerably. According to FARMER and FIRTH [21] potassium chloride did not alter the rate of formation of perchlorate, however, it accelerated oxygen evolution. The investigations of OTTO and FRY [22, 23], on the other hand, showed an opposite effect. GLASNER and WEIDENFELD [10] stated that the effect of potassium chloride depends on its pre-history. Potassium chloride, originating from the decomposition of potassium perchlorate, as well as commercial potassium chloride, treated at 600° C for 1 hour, accelerated the formation of potassium perchlorate, however, they hardly had any effect on the rate of oxygen evolution, whereas C.p. KCl dried at 110° C decreased the extent of formation of potassium perchlorate.

The activation energy of the decomposition of pure salt was calculated from the temperature dependence of the time elapsed until 20% oxygen evolution; it was found to be 54 kcal/mole [10]. Nearly identical activation energies were found from the temperature dependence of the quarter and half-times of the decomposition [24]. From the chemical analysis of the substances, pretreated at various temperatures, GLASNER and WEIDENFELD [10] came to the conclusion that perchlorate formation occurs not in a simultaneous but in a consecutive reaction.

Kinetic analysis of the decomposition of potassium chlorate has been attempted by TOBISAVA [25] without success. The failure was attributed to the complication of the rate—time curves due to irregularities of bubbling and splashing in the molten salt. According to the measurements of RUDLOFF and FREEMAN [26] the decomposition takes place in two well defined steps; one third of the theoretically calculated weight loss occurred in the first step. This part of the decomposition was described by sec-

ond order equation. The values of the activation energies of the decomposition of various chlorate-chloride mixtures were in the range between 62—66 kcal/mole. They observed that at lower temperatures, potassium chloride exerted an inhibiting effect on the decomposition of chlorate while at higher temperatures its catalytic effect became dominant. A small amount of potassium perchlorate had no effect on the decomposition however, when present in greater amounts, is shifted the commencement of the decomposition towards higher temperatures.

Thermal decomposition of other metal chlorates

Barium chlorate

A derivatogram of barium chlorate is shown in Fig. 9 [18]. The initial loss of weight starting at 146° C, and the endothermic peak at 170° C belonging to this process, are due to the loss of the one mole of crystal water. The endothermic peak indicating the melting of barium chlorate is to be found at 404° C. Simultaneously the decomposition of the substance occurs, which on increasing the temperature becomes extremely rapid, but later — in spite of the higher temperature — slows

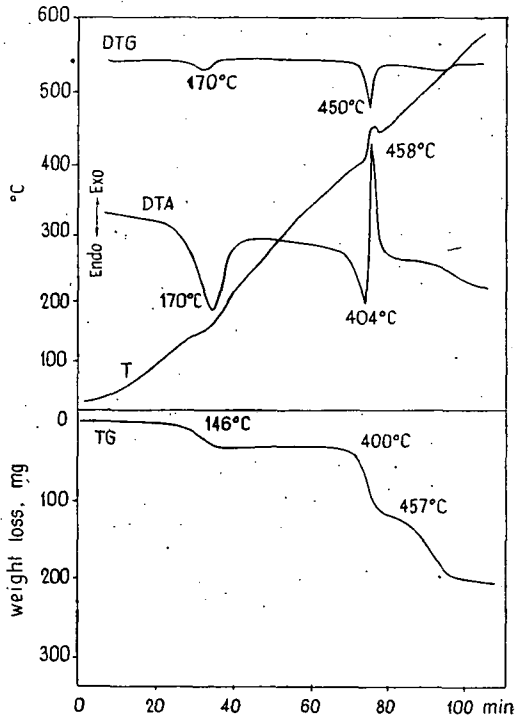
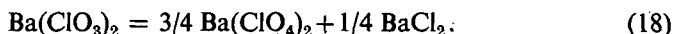


Fig. 9. Derivatogram of Ba(ClO₃)₂. Heating rate: 6° C/min [18].

down again. The decomposition of barium chlorate is an exothermic process. On the basis of the analysis of samples corresponding to various parts of the derivatogram, the decomposition and the disproportionation of the substance proceeds in molten state according to the following reactions;



The slow weight-loss observed on the TG curve at 457° C is the result of the decomposition of the perchlorate formed



The measurements made under isothermal conditions gave similar results [27, 18]. At temperatures below the melting point the rate of the decomposition is extremely slow. However, as the temperature was getting near to the melting point (around 396° C) the behaviour of the substance suddenly changed and the rate of its decomposition became very rapid.

In spite of the rapid decomposition of the substance disproportionation also takes place. After about 70—80% decomposition the rate of gas evolution considerably decreased. According to visual observations the cessation and the considerable decrease in the rate of gas evolution, respectively coincided with the solidification of the reacting system.

However, the solidification of the system alone does not seem to be a sufficient reason for the great rate decrease, since the solid substance decompose even at 380° C. It is more probable that the glass-like state of the substance also plays a part in the greater stability of the solidified melt; its surface and porosity markedly differ from those of the initial solid substance.

For the kinetic analysis of the pressure-time curves, the PROUT—TOMPKINS relation proved to be most suitable. Owing to the considerable scattering of the rate constants, the activation energy of the decomposition could not successfully be determined, thus as an approximate value of 75 kcal/mole was given.

Silver chlorate

On the DTA curve of silver chlorate endothermic peaks can be found at 164 and 252° C (Fig. 10). The exothermic heat change accompanying the decomposition of the compound occurs at 340° C. The first and the second endothermic peaks correspond to the loss of the adsorbed water and to the melting of the compounds, respectively [28]. The decomposition of silver chlorate commences well above its melting point and takes place according to the reaction



The amount of chlorine and chlorine dioxide was not more than 2—3 per cent of the gas evolved.

Kinetic investigations were made in the temperature range 316–339° C [4, 28]. The reaction took place according to the first order equation (up to $\alpha=0.9$); the value of activation energy was 57.1 kcal/mole. Simultaneously with the decomposition of chlorate, disproportionation of the compound also occurred to a small extent (8–10%). In contrast to earlier findings [29], the explosion of silver chlorate was not observed even at temperatures as high as 400–450° C.

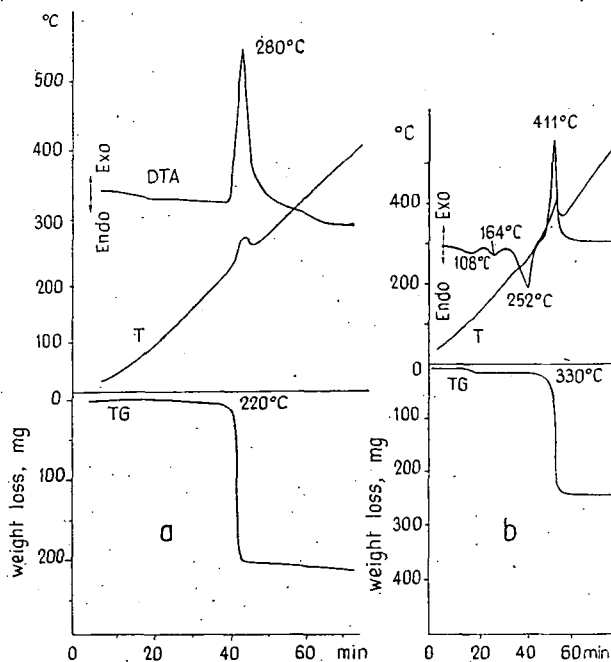
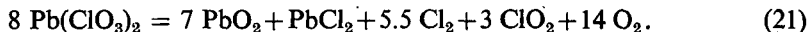


Fig. 10. Derivatogram of $\text{Pb}(\text{ClO}_3)_2$ (a) and AgClO_3 (b). Heating rate: 6° C/min. [18]

Lead chlorate

Thermogravimetric measurements indicate that lead chlorate begins to decompose at 220° C, and that the highly-exothermic decomposition is complete within a few seconds [18] (Fig. 10). The weight loss is 37.2%. Under isothermal conditions the reaction takes place completely at 194–216° C, with a weight loss of 35.2%. The solid residue was found to contain 84.39% PbO_2 and 14.9% PbCl_2 . Their molar ratio is 6.58. On the basis of the reaction products the decomposition of lead chlorate can be characterized by the following overall equation;



According to the equation, the weight loss is 34.8%, and the PbO_2 : PbCl_2 molar ratio is 7. The experimentally found Cl_2 : ClO_2 molar ratio likewise corresponds to the above reaction equation.

The pressure-time curve of the decomposition of lead chlorate is markedly different from that of other compounds (Fig. 11). The decomposition begins (after a heating period of a few minutes) without a time lag, and the following stages can be distinguished:

- (a) an initial fast decomposition of a deceleratory nature;
- (b) the subsequent slow reaction;
- (c) an extremely fast decomposition, in which about two thirds of the material decomposes;
- (d) a short, slow decay period.

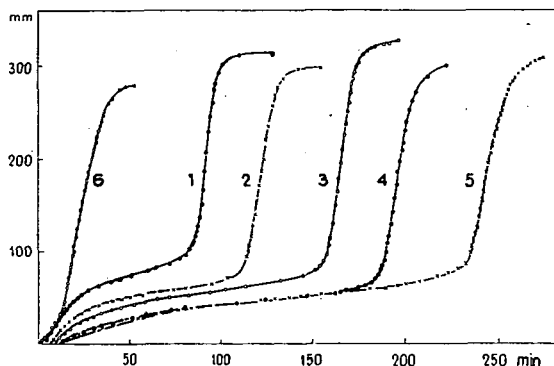


Fig. 11. Pressure vs. time curves of the decomposition of $\text{Pb}(\text{ClO}_3)_2$ [18]. (1) at 216°C ; (2) at 212°C ; (3) at 207°C ; (4) at 203°C ; (5) at 119.5°C ; (6) $\text{Pb}(\text{ClO}_3)_2$ + solid residue of decomposition, weight ratio 5:1, at 207°C

Decomposition curves of a similar nature resulted from the measurement of the pressure of oxygen, and of the change of weight of the sample. This showed that the sudden increase in pressure during the progress of the reaction is not a result of the decomposition of the chlorine dioxide already formed, but a characteristic property of the solid-phase decomposition of lead chlorate.

It is likely that the initial rapid decomposition is a surface reaction, which penetrates to some depth into interior of the crystal. The decomposition in the bulk actually occurs in the third very fast reaction, which is preceded by a long constant rate process. This can be regarded as an induction period of the former reaction. It was assumed that the decomposition in the third stage takes place at the interface between the salt and the products. This idea was supported by the effect of the reaction product (Fig. 11). In this case the slow constant rate process between the initial and the subsequent rapid reactions practically disappeared.

The first deceleration stage followed the monomolecular decay equation. The value of the activation energy was 51.2 kcal/mole. Analysis of the slowly accelerating decomposition following the first stage showed that the kinetics satisfied both the PROUT—TOMPkins and the AVRAMI—EROFYEV equations. The activation energy for this stage was 43.1 kcal/mole. The rate of decomposition of lead chlorate in the third stage was practically independent of temperature.

In contrast with the chlorates discussed above, experiments carried out at the decomposition temperature or below indicated that the lead chlorate did not disproportionate at all. At a higher temperature, 246° C, the substance (50 mg) exploded. The explosion was preceded by a well-measurable decomposition. The composition of the gas product was 84.5% O₂ and 15.2% Cl₂. The temperature-dependence of the induction periods of the explosion between 246 and 260° C gave an activation energy of 64.9 kcal/mole.

Thallium chlorate

The derivatograms of thallium chlorate show that the decomposition commences at 195° C and is accompanied by the evolution of much heat [18]. (Fig. 12). The second stage of the thermogram corresponds to the evaporation of TlCl, while in the third stage the decomposition of Tl₂O₃ occurs; both compounds are formed in the decomposition of TlClO₃.

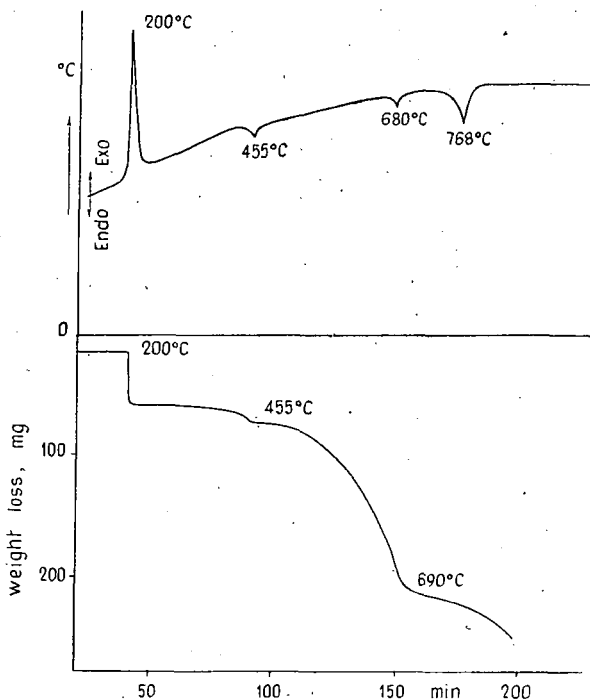
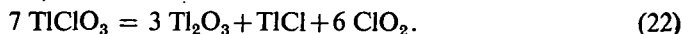


Fig. 12. Derivatogram of TlClO₃. Heating rate: 6° C/min [18]

Kinetic measurements were carried out at 150–170° C by measuring the decrease of weight of the sample. The gaseous products of the decomposition were completely frozen out by liquid air, showing that oxygen was not formed during the decomposition. The frozen-out gas was chlorine dioxide. In the course of the decomposition 21–26% of the material was converted to gaseous products. The

residual solid consisted of 85.63% Tl_2O_3 and 14.23% $TlCl$. The Tl_2O_3 : $TlCl$ molar ratio was 2.93. The solid material did not contain undecomposed thallium chlorate or thallium perchlorate.

Based on the above data, the overall equation for the decomposition of thallium chlorate is:



Accordingly the weight loss is 20.09%, and the Tl_2O_3 : $TlCl$ molar ratio is 3.

The PROUT—TOMPKINS equation proved suitable for the description of the decomposition in the range $\alpha=0.09$ — 0.9 . The decomposition was also described excellently by the AVRAMI—EROFEYEV relation in the range $\alpha=0.07$ — 0.95 . The temperature dependence of the rate constants gave an activation energy of

Table VII

Kinetic data for the decomposition of metal chlorates

Compound	Temperature range °C	Methods	Activation energy kcal/mole	Frequency factor (min^{-1}),	Kinetic equation	Validity $\alpha=$
NaClO_3	457—478	vacuum, O_2 pressure	68.6	$8.61 \cdot 10^{17}$	slope of p—t curves	0.0—0.55
	457—478	vacuum, O_2 pressure	70.9	$2.29 \cdot 10^{18}$	first-order	0.01—0.65
	457—478	vacuum, O_2 pressure	67.6	$5.77 \cdot 10^{17}$	first-order	0.65—0.95
KClO_3	460—500	in air O_2 ml	53.9	—	time for 10 ml O_2	—
	460—500	in air O_2 ml	52.5	—	Time elapsed until 20% of decomposition	—
	455—575	in air O_2 ml	54.0	—		
$\text{KClO}_3 + \text{KCl}$ 1:1	538—605	in air weight-loss	64.9	—	half-time $\tau_{1/2}$	
$\text{Ba}(\text{ClO}_3)_2$	380—405	vacuum O_2 pressure	75.0	—	Prout-Tompkins	
AgClO_3	316—339	vacuum, O_2 pressure	57.1	$1.0 \cdot 10^{19}$	first-order	0.2—0.7
$\text{Pb}(\text{ClO}_3)_2$	195—216	vacuum O_2 pressure	51.2 43.1	$1.81 \cdot 10^{21}$ $4.14 \cdot 10^{17}$	first-order Prout-Tompkins	—
	246—260 explosion	in air O_2 ml	64.9	—	induction period	
TiClO_3	150—171	vacuum weight-loss	34.5	$4.15 \cdot 10^{15}$	Prout-Tompkins	0.09—0.9
			36.6	$1.56 \cdot 10^{15}$	Avrami-Erofeyev $n=3$	0.07—0.95
			34.1	—	rate max.	

35.5 kcal/mole. When the thallium chlorate was mixed in advance with the solid residue, the decomposition began sooner and took place at a higher rate. If the gaseous products were removed continuously, or the experiments were carried out at atmospheric pressure, the course of the decomposition remained essentially unchanged. The solid reaction products showed a catalytic effect in this case, too.

Similarly to lead chlorate, on heating to a higher temperature thallium chlorate exploded. The explosion here was much milder than in the previous case. An explosion-like reaction first appeared at 196° C. The induction period was about 5 minutes. With the increase of the temperature the induction period decreased, but the violence of the explosion did not vary.

Table VII summarizes the kinetic data of the decomposition of chlorates.

Mechanisms of decomposition and disproportionation of the chlorates

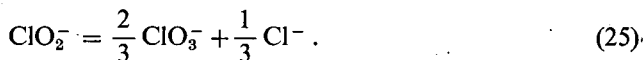
Because of the small number of kinetic studies and the possibility of parallel reactions, the evaluation of the mechanisms of the conversion of chlorates is fairly difficult. Although it has not proved possible so far to detect chlorite during the decompositions of the chlorates, it appears probable that the oxygen is not split off in a single step, but progressively, and that chlorite is formed as an intermediate:



In the following step the chlorite can react in one of two ways, either decomposing to chloride:



or disproportionating to chlorate and chloride:



Experiments with alkali metal chlorites, already described in detail above, showed that in the absence of catalysts only the latter reaction need to be taken into consideration, even at high temperature. At the temperature of decomposition of the chlorates, however, barium and silver chlorites no longer disproportionate, but decompose. Since both processes occur instantaneously at the temperature of decomposition of the chlorates, *the rate-determining step in the decomposition of the chlorates is at any event the first reaction, which means the rupture of the Cl—O bond.* The values of activation energy determined experimentally so far practically agree with the energy value necessary for breaking off the Cl—O bond. This explanation is supported by the values of the reaction heat calculated for reaction 23 (Table VIII) which, assuming the formation of atomic oxygen, agree well with the activation energy values determined for the decompositions of sodium, potassium and silver chlorates. It is very likely that this reaction mechanism also holds for the decompositions of the other metal chlorates giving chloride and oxygen.

In addition to the above decomposition mechanism, we may consider the possibility that the decompositions of chlorates proceed *via* an electron-transfer mechanism. In this case the rate-determining step should be the reaction



Table VIII
Equivalent heat of reaction for different transformations of chlorates

Compound	ΔH_1	ΔH_2	ΔH_3	ΔH_4	ΔH_5	ΔH_6
LiClO ₃	-27.70	-1.2	-23.2	—	-21.7	—
NaClO ₃	-12.5	+36.0	-8.1	+9.08 (+68.28)*	-8.5	+1.31
KClO ₃	-10.675	+50.3	-10.24	—	-10.1	—
RbClO ₃	-9.11	+54.35	-9.85	—	-10.1	—
CsClO ₃	-7.5	+58.05	-7.80	—	-7.9	—
Ba(ClO ₃) ₂	-11.93	+24.35	-7.14	+11.75 (+70.95)*	-5.55	+3.1
AgClO ₃	-24.57	+2.47	-7.67	+5.73 (+64.93)*	-2.02	+1.86

1. $\text{MeClO}_3 = \text{MeCl} + 1.5 \text{O}_2$
2. $\text{MeClO}_3 = \frac{1}{2} \text{Me}_2\text{O} + \text{gases}$
3. $\text{MeClO}_3 = \frac{3}{4} \text{MeClO}_4 + \frac{1}{4} \text{MeCl}$
4. $\text{MeClO}_3 = \text{MeClO}_2 + \frac{1}{2} \text{O}_2$ (or O)
5. $\text{MeClO}_3 + \frac{1}{2} \text{O}_2 = \text{MeClO}_4$
6. $\text{MeClO}_3 = \frac{1}{2} \text{MeClO}_4 + \frac{1}{2} \text{MeClO}_2$

* Assuming the formation of atomic oxygen in reaction 4.

i.e. the formation of the chlorate radical. In the case when the necessary data (absorption edge, dielectric constant and refractive index values) were known, the activation energy (E_T) required for the electron-transfer process has been calculated (Table IX). These activation energy values lie fairly close to those experimentally

Table IX
Some data for the structure and physical properties of chlorates

Compound	Crystal transition point °C	Melting point °C	Density	Refractive index	Dielectric constant at 350 kc/s K	K_0/K	Absorption edge Å	E_0 eV	E_T eV	Ionic character %
LiClO ₃	111	129	2.631							67.64
NaClO ₃		263	2.490	1.515	5.9	0.389				68.7
KClO ₃		357								73.0
RbClO ₃	323	342	3.184							
CsClO ₃	305	388	3.626							
Ba(ClO ₃) ₂		404	3.179	1.577	4.34	0.573				45.2
AgClO ₃		232	4.430	1.83	5.81	0.575	2550	4.86	2.79	36.0
Pb(ClO ₃) ₂		decomp.	5.047		11.78		2380	5.21		17.1
TlClO ₃		decomp.	4.047		7.78		2420	5.12		25.2

$$K_0 = n^3$$

K_0 = high frequency dielectric constant

K = low frequency dielectric constant

n = refractive index

E_0 = optical activation energy

E_T = thermal activation energy

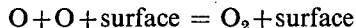
determined. However, in our view the electron-transfer mechanism does not play an essential role in the decomposition of chlorates, since chlorine and chlorine dioxide would be formed at any rate from the decomposition of the chlorate radicals, or from the interaction of the chlorate radical and the alkali metal. Chlorine however was formed only in negligibly small quantity in the course of the experiments. Nevertheless, it is not possible to exclude completely the electron-transfer mechanism in the cases of lead and thallium chlorates; though data for the calculations are lacking here.

In the treatment of the disproportionation of chlorites, a detailed account has already been given of the different views relating to the disproportionation of the oxyanions of chlorine. Although the experiments of BOSCH and ATEN [11] using potassium chloride containing labelled chlorine, excluded the formation of perchlorate in a reaction between the alkali metal chloride and atomic oxygen, a reaction of a similar type has recently been assumed between barium chloride and atomic oxygen [30]. However, taking into account the stabilities of the assumed intermediates $\text{Ba}(\text{OCl})_2$ and $\text{Ba}(\text{ClO})_2$ at the temperature of decomposition of barium chlorate, in our opinion this reaction path is very improbable. According to the thermodynamic data given in Table VIII, the oxidation of the chlorates, similarly to that of the chlorites, is thermodynamically possible with molecular oxygen, but kinetically the reaction does not occur, even at high oxygen pressures and high temperatures. As a result, the formation of perchlorate is due either to the reaction between chlorate and the atomic oxygen formed during the decomposition of chlorate:



or, similarly to the disproportionation of chlorites, to intermolecular rearrangement. To find decisive evidence for or against the mechanisms is very difficult. In any case it is probable that the disproportionation of chlorites and chlorates proceeds for similar reasons and in essentially the same way. Detailed kinetic measurements made in the case of the chlorites, and also certain other observations mentioned there, seem to contradict to the oxidation with atomic oxygen.

Similarly to the transformations of the chlorites, the disproportionations of both sodium and barium chlorate began prior to perceptible decomposition. With the oxidation mechanism this result can be explained only by the circumstance that the rate of oxidation of chlorate is much higher than the rate of recombination of oxygen atoms:

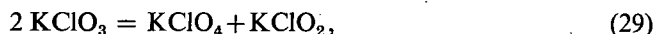


which cannot be ruled out because of the low concentration of oxygen atoms. In our view the intermolecular rearrangement is supported by the values of the reaction heats given in Table VIII. According to the oxidation mechanism, the rate-determining step in the perchlorate formation is in all probability the rupture of a $\text{Cl}-\text{O}$ bond of the chlorate ion (formation of atomic oxygen), *i.e.* the same reaction step as the rate-determining process of the decomposition. The reaction heat of the process has a fairly high value of 65—70 kcal/mole (see Table VIII), in good agreement with the values of the activation energy determined experimentally for the decompositions.

The simplest means of intermolecular rearrangement is an interaction between two chlorate ions, in the course of which one molecule of perchlorate and one molecule of chlorite are formed:



This chlorite rapidly disproportionates, with the formation of chlorate and chloride. Taking into account the considerations given in the discussion of the disproportionation of the chlorites, in the optimum case the activation energy of the disproportionation reaction will be equal to the difference of the two dissociation energies, that is the reaction heat, which can be seen from Table VIII to be endothermic by only a few kcal/mole. It is probable that in reality this optimum case does not hold, but on the above basis it seems very plausible that, in contrast with the oxidation of the chlorate, this reaction path is energetically substantially more favourable. A reaction mechanism agreeing many respects with that described earlier by us [18] was recently put forward by RUDLOFF and FREEMAN [26] for the disproportionation of potassium chlorate. It was assumed that the potassium perchlorate was formed by *direct oxygen transfer between two chlorate anions*. In accordance with the second-order kinetics, the potassium chlorate is first transformed in a slow reaction to potassium perchlorate and chlorite:



the potassium chlorite formed as an intermediate decomposing rapidly:



Their assumption that the potassium chlorite immediately decomposes to chloride and oxygen, however, is in contradiction with the thermal behaviour of alkali metal chlorites. As was pointed out earlier, the alkali metal chlorites do not decompose at even higher temperature, but disproportionate to chlorate. Accordingly the transformation of potassium chlorate into perchlorate and chlorite does not result in the formation of oxygen below the decomposition temperature of potassium perchlorate. The rate-decreasing effect of potassium chloride observed at lower temperature was explained by RUDLOFF and FREEMAN by the decrease of the probability of approach of the chlorate anions. The catalytic effect of the potassium chloride at higher temperatures was interpreted by the formation of polarizing centres in the melt. These polarizing centres may influence the electron shells of the oxygens of the chlorate and perchlorate anions.

The mechanisms of decomposition of chlorates which give rise predominantly to oxide formation is much more complex than that of alkali chlorates. An interesting fact in the decompositions of both salts investigated in more detail (lead and thallium chlorates) is that the metal ions were oxidized. This may occur in two ways: either by the molecular or atomic oxygen produced in the decomposition of the chlorate, or by means of internal oxidation within the crystal. The activation energy values are lower than the dissociation energy of the Cl—O bond, or in other words, than the energy necessary for the formation of atomic oxygen. This is in agreement with the fact that in both decompositions the chloride formation is about 6—7 times slower than that of the oxide formation. In our opinion, it is probable that Ti_2O_3 and PbO_2 are formed in intramolecular rearrangements, together with the production

of chlorine dioxide, which at the temperature of decomposition of lead chlorate partially decomposes on the solid residue to oxygen and chlorine.

In these cases perchlorate was not formed. This cannot be accounted for by decomposition of the compounds in the solid phase, since in the solid disproportionation of the chlorites does take place. It is much more probable that during an internal rearrangement the formation of the oxide of the metal of higher valency is associated with a substantially greater free energy decrease than that for the formation of the perchlorate. Due to the lack of the free enthalpies of formation of these chlorates and perchlorates, this assumption can not be confirmed for the time being. In addition it must be taken into consideration that in the decomposition of both chlorates metal oxide was formed. In the presence of the metal oxides, however, instead of the disproportionation of the chlorates the decomposition reaction predominates.

Although the investigations to date have been extended to relatively few substances, by considering the physical properties and bonding relations of the compounds and the characteristics of the cations (Table IX) it can be stated that the more ionic the compound, or the smaller the effective electric field strength (polarizing power) of the cations, the higher the temperature at which the compounds begin to decompose. There does not exist such a clear-cut relation for the disproportionation of the compounds. In the case of compounds of similar character, namely the alkali metal compounds, a reverse relation holds: the decrease of the ionic character, or the increase of the polarizing power of the cation, favours the formation of the oxyanions of chlorine with higher oxygen content. In the series, alkali metal — barium — silver — lead compounds, however, the finding for the decompositions also refers to the disproportionations.

Thermal stability of alkali metal perchlorates. Thermal analysis

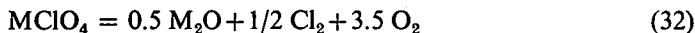
Although the thermal decomposition of the alkali metal perchlorates has already been studied before the turn of the century, and many observations were made which are still valid, nevertheless a significant advance in evaluating the thermal stabilities of these compounds was achieved only after the preparation of compounds of suitable purity and after the introduction of modern thermal analytical and kinetic methods. Thermogravimetric measurements and differential thermal analysis of solid perchlorates were carried out first by MARVIN and WOOLAVER [31], and then by GORDON and CAMPBELL [32]. These methods were later used by numerous authors, particularly in the study of the alkali metal compounds [17, 33—35]. A detailed thermal analytical investigation extended to each member of the group, under identical experimental conditions, was performed by MARKOVITZ *et al.* [36—40], and by SOLYOSI [35, 41]. The characteristics of their DTA curves [19] are shown in Fig. 13. With the exception of lithium perchlorate, the first endothermic peak in each of the DTA curves signifies the reversible transition from the rhombic to the cubic modification. The second endothermic peak is a result of the melting of the relevant substance and the exothermic peak belongs to the decomposition. In the case of lithium perchlorate, and, to a lesser extent, in the case of sodium perchlorate, too, the melting is well separated from the decomposition, whereas in the other cases the decomposition occurs immediately after the melting begins. The endothermic

peak at higher temperature results from the melting of the chloride formed in the decomposition of the perchlorate.

Thermogravimetric examinations (Fig. 14) indicate that the alkali metal perchlorates decompose in accordance with the basic equation



Oxide and chlorine formation:



was observed only in the decomposition of lithium perchlorate. Even here, however, the amount of chlorine evolved did not exceed 2% of the chlorine in the perchlorate.

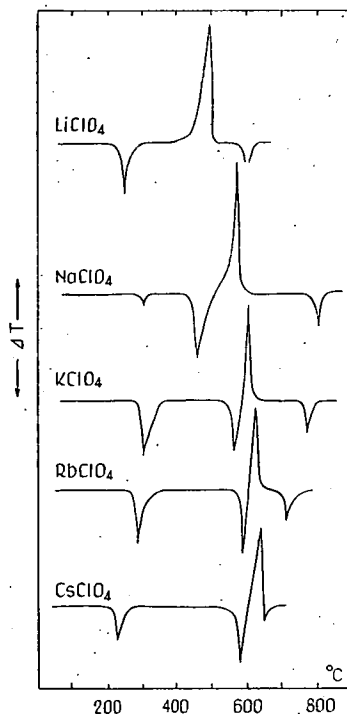


Fig. 13. DTA curves for alkali metal perchlorates. Heating rate: $4^\circ/\text{min}$. 1 g sample; Ar atmosphere [40]

The derivatographic method was used for a detailed study of the effects of the corresponding chlorides on the thermal behaviours of the alkali metal perchlorates [35]. With the exception of the lithium system, the chlorides markedly decreased the temperatures at which the alkali metal perchlorates melted and also the temperatures of the commencement of decomposition. Fig. 15 illustrates this effect in the case of $\text{RbClO}_4\text{—RbCl}$ system. The characteristic data concerning the effect of

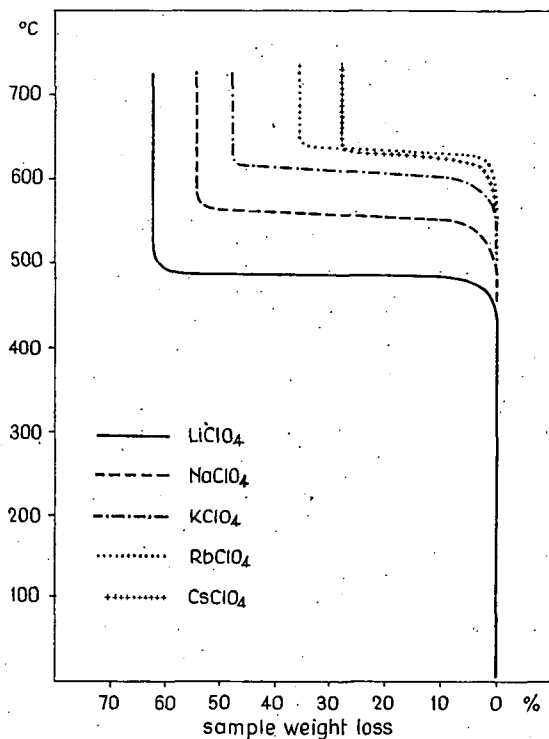


Fig. 14. TGA curves for pure alkali metal perchlorates. Heating rate: 4°/min; Ar atmosphere [40]

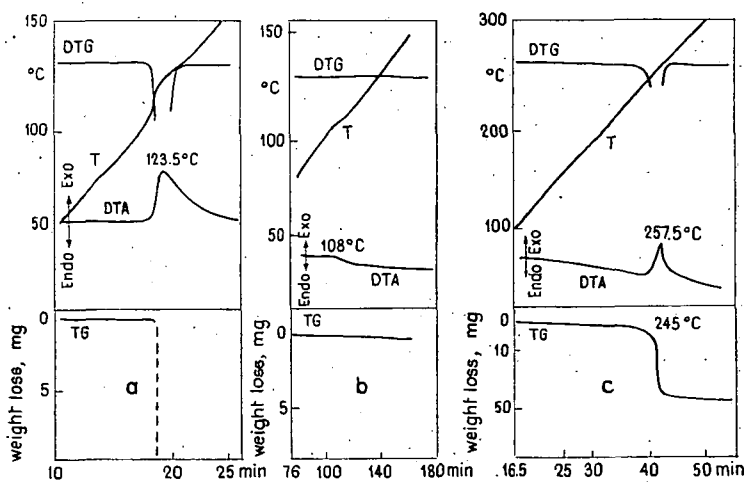


Fig. 15. Derivatograms of $RbClO_4$. Heating rate: 6°/min. (a) Pure $RbClO_4$; (b) $RbClO_4$: $RbCl$, 50:50; (c) $RbClO_4$: $RbCl$, 70:30 mole % [35]

Table X

*Thermal behaviour of alkali perchlorates in the presence of alkali chlorides.
Derivatographic investigation [35]*

$\text{LiClO}_4:\text{LiCl}$ mole %	Melting point °C	t °C*	$\text{NaClO}_4:$ NaCl mole %	Melting point °C	t °C*	$\text{KClO}_4:\text{KCl}$ mole %	Melting point °C	t °C*
100:0	247	450	100:0	471	507	100:0	570	550
90:10	243	420	90:10	428	500	90:10		
70:30	246	390	70:30	415	485	70:30	508	508
50:50	251	390	50:50	423	485	50:50	523	510

$\text{RbClO}_4:$ RbCl mole %	Melting point °C	t °C*	$\text{CsClO}_4:$ CsCl mole %	Melting point °C	t °C*
100:0	610	600	100:0	571	570
90:10			90:10	500	480
70:30	489	500	70:30	447	460
50:50	490	490	50:50	550	500

* Temperature of the onset of decomposition
Heating rate 6°/min.

alkali chlorides are collected in Table X. The addition of lithium chloride to lithium perchlorate hardly affected its melting point, but it exerted a large catalytic influence on the decomposition of the perchlorate.

More details concerning the nature of the decomposition of alkali perchlorates have been disclosed by kinetic investigations.

Kinetic studies

Lithium perchlorates

The kinetic study of the thermal decomposition of lithium perchlorate was first dealt with by MARKOVITZ and BORYTA [42]. The decomposition began only above 380° C and proceeded to the end in molten phase. The reaction is of auto-catalytic nature; the decomposition is preceded by a fairly long time lag. The above authors found the PROUT—TOMPKINS equation and the monomolecular decay equation to be suitable for the mathematical analysis of the decomposition curves. For the activation energies of the acceleration and breakdown stages as 52.2 and 62 kcal/mole, respectively, were obtained. The transition between the two rate laws was explained by the saturation of the perchlorate melt with lithium chloride.

Detailed measurements were carried out to detect possible intermediates in the decomposition. Lithium chlorate was found already at $\alpha=0.1$; its amount increased up to $\alpha=0.5$ (2%), but at higher values of α it decreased. Lithium chlorite could not be detected in any single case.

The phase-diagram of the LiClO_4 — LiCl system was studied in detail by means of differential thermal analysis and visual observations. It was concluded from the results obtained that the system is of simple eutectic type, and that the composition of the eutectic contains 91 mole % LiClO_4 .

Lithium chloride exerted a significant catalytic effect on the decomposition. In the presence of 5 mole % LiCl the decomposition began without a time lag, while 50 mole % LiCl changed the autocatalytic reaction to a deceleratory one. The addition of lithium chloride did not affect either the values of the rate constants or the activation energy of the decomposition. It was assumed, however, that the activation energy value mentioned above could be considered as that of the reaction affected by the lithium chloride formed in the decomposition. In agreement with this, from the temperature-dependence of the times elapsed up to a decomposition of only 0.5% the above authors obtained a higher activation energy value of 58.3 kcal/mole.

The catalytic effect of lithium chloride was supported by the results obtained using silver nitrate or silver perchlorate additives [43]. The decomposition of pure lithium perchlorate at 417.8° C was complete within a few hours. The presence of silver nitrate increased the stability of the compound to a considerable extent, and the time lag exceeded 30—35 hours. The phenomenon is clearly related to the insolubility of solid silver chloride in lithium perchlorate, and to the loss of the chloride catalyst. According to DTA investigations, however, at 455° C, the melting point of silver chloride, the decomposition of lithium perchlorate containing the silver ion becomes very rapid; this is presumably caused by the entry of the chloride ion into the solution during the melting of the silver chloride.

The decomposition of the compound was later studied by measuring the pressure of the O₂ evolved [35, 44]. Using the previous kinetic equations, a value of 52.6 kcal/mole was obtained for the activation energy of the acceleration stage, while the value for the decay stage, 41 kcal/mole, was significantly less than the value determined earlier.

Sodium perchlorate

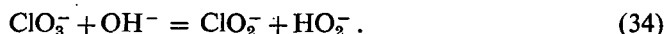
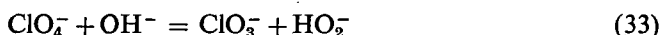
The decomposition of sodium perchlorate was studied kinetically first by BENARD and CABANE [45] in the range 330—428° C, that is below the melting point of the compound. Because of the extremely slow decomposition the reaction time exceeded several hundred hours, and even then the decomposition amounted to only a few percent. The authors determined the self-diffusion constant of the perchlorate ion, and also its temperature coefficient. Identical activation energies of 27—28 kcal/mole were obtained for the thermal decomposition and for the diffusion of the perchlorate ion.

The complete decomposition of sodium perchlorate proceeds with a measurable rate in the range 490—515° C [35, 44]. The reaction is of autocatalytic nature. The rate maximum is shifted towards a later stage of the decomposition by the increase of the reaction temperature. The decomposition is preceded by a time lag of a few minutes, which is practically independent of the temperature. The reaction proceeds completely in the direction of chloride formation. The α vs. t curves were well described by the PROUT—TOMPKINS relation. The activation energies of the acceleration and decay stages were found to be 57.3 and 57.0 kcal/mole, respectively. The first-order formula, too, was suitable for the mathematical analysis of the breakdown stage.

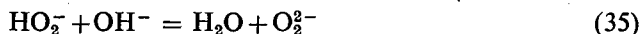
The decomposition began with maximum rate and the half-time of the reaction was decreased considerably by the preliminary addition of sodium chloride to the sodium perchlorate.

Very interesting results were obtained by the study of the decomposition of sodium perchlorate in a sodium hydroxide melt [46]. At 360—420° C the decomposition proceeded about 10^4 times faster than in the case of the pure perchlorate. In the first part of the reaction chlorate was formed, and this slowly decomposed to chloride and oxygen. The first reaction was about 12—18 times faster than the second process. The interesting observation was made that starting from sodium chlorate the disproportionation of the chlorate in a sodium hydroxide melt remained below 0.5%. It is questionable whether this is due to the lower temperature (which is not very probable), or to change in the decomposition mechanism.

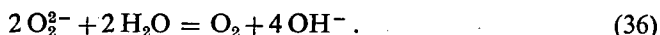
Both reactions can be described by first-order kinetics. The activation energy values for the two reactions were 47.3 and 53.2 kcal/mole, significantly lower than those determined for the decompositions of pure perchlorate and chlorate. The accelerating effect of hydroxide ion was interpreted by assuming of the reaction steps



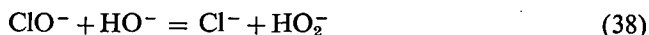
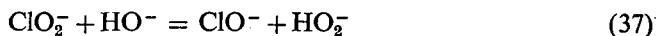
The HO_2^- formed reacts with OH^- :



and the peroxide formed is transformed as follows:



Accumulation of chlorite and hypochlorite was not observed, and this was explained by the rapid decomposition of the chlorite to chloride. This would mean that the direction of the transformation of sodium chlorite changes in a melt containing hydroxide ions, since measurements showed that NaClO_2 in the solid phase disproportionates without decomposition even at a higher temperature. This can be thought to proceed similarly as above:



The probable cause of the absence of disproportionation is the high affinity of oxyanions of chlorine for the hydroxide ion.

It emerged from a study of the effects of various additives that water, sodium peroxide, magnesium oxide and barium oxide exert only slight effects on the reactions.

Potassium perchlorate

The decomposition of potassium perchlorate was first investigated from a kinetic aspect by OTTO and FRY [47]. The reaction followed the first-order rate law. Chlorate was not observed as intermediate. According to HOFFMANN and MARIN [48], however, a partially decomposed perchlorate sample contained 14.55 weight% chlorate.

The first thorough studies were carried out by GLASNER *et al.* [49, 50] in vacuum and at atmospheric pressure. Although the compound melted during the decompo-

sition, the authors came to the conclusion that the reaction was independent of the physical state of the system and proceeded in accordance with the characteristics of a process of the type



It was further assumed that the molten phase can be regarded as quasicrystalline. The kinetic analysis of the reaction was performed with the modified PROUT—TOMPKINS equation. It was assumed that the decomposition of potassium perchlorate takes place according to two different basic processes [51]. The first, a fairly slow reaction, corresponds to the initiation of the decomposition, while the second, 500 times faster than the former, is the propagation of the decomposition by a chain-branching mechanism.

The applicability of the PROUT—TOMPKINS equation was later questioned by BIRCUMSHAW [52] who was the first to point out the extremely complex nature of the reaction. His main findings were as follows:

1. The solid-phase decomposition is accompanied at first by the formation of potassium chlorate and potassium chloride. The latter accelerates the reaction, and as a consequence of the accumulation of the potassium chlorate the system melts.
2. The melt-phase decomposition begins only on completion of the transition into the melt phase.
3. Accumulation of the potassium chloride leads to solidification of the melt and to slowing-down of the gas evolution.

HARVEY *et al.* [53] studied the decomposition of potassium perchlorate under the pressure of oxygen formed in static vacuum. It was observed that the decomposition rate depends on the concentration of the perchlorate and on the physical state of the reacting substance. This is shown in Fig. 16 where the data of four experiments at different temperatures are presented by plotting of $\log/P_f - P_t$ vs. time. P_f is the pressure of oxygen calculated for complete decomposition of the sample, P_t is the experimentally measured pressure at time t .

On the curves the points referring to the first phase change, to the end of melting and to the appearance of second solid phase calculated from phase diagram are also indicated. The decomposition can be described by two first-order equations before the appearance of the second solid phase; one of these equations refers to the initial slow decomposition in the solid phase, and the other to the subsequent rapid decomposition in the melt. (At the transition of the solid phase into the melt phase the reaction occurs in both phases.) The rate constant for the liquid-phase decomposition is about 50 times larger than that for the solid phase. The temperature-dependence of the rate constants was however, the same, and the value of the activation energy was 70 kcal/mole; it was concluded, therefore that the mechanism of the decomposition was the same in both phases. Potassium chlorate was found as intermediate only to the extent of 2—3%.

In the experiments of RODGERS and WASSINK [54] the activation energies of the reactions proceeding in the two phases differed by 18 kcal/mole. The most recent measurements of the author [35, 44], however, support the results of HARVEY *et al.*

They found that the rate and activation energy of the decomposition are practically independent of the pressure of the oxygen, and it was concluded that the oxygen does not participate in an equilibrium reaction [55]. However, as will be clear later, this refers only to molecular oxygen.

The investigations reported in the case of sodium perchlorate were extended by CABANE and BENARD [45] also to potassium perchlorate. The activation energies of the thermal decomposition and the self-diffusion of the perchlorate ion (30–32 kcal/mole) agreed well here, too.

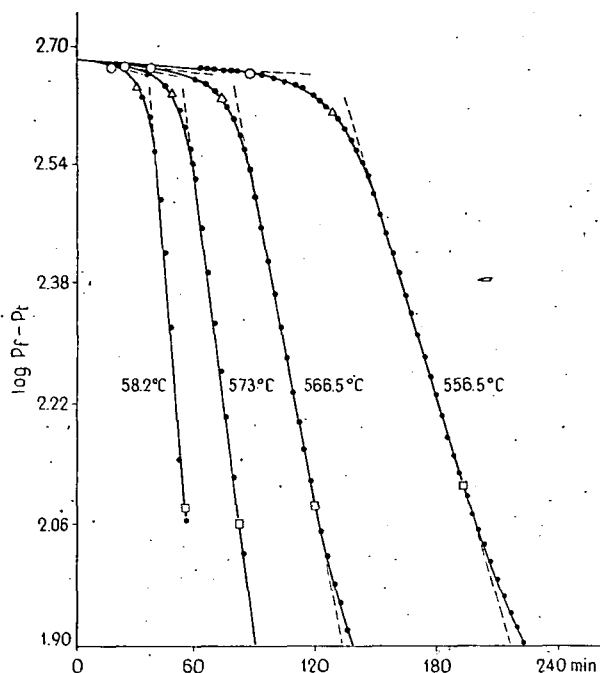


Fig. 16. Isothermal decomposition of KClO_4 at various temperatures: ● experimental points. Points calculated from phase diagram: ○ first phase change; △ end of melting; □ appearance of second solid phase [53]

The decomposition of potassium perchlorate in the solid phase was also studied by CORDES and SMITH [56]. The aim of their experiments was to investigate the solid-phase reaction under conditions where not even partial melting of the substance occurred. The extent of the decomposition in their experiments did not exceed 3.5%. The quantity of gases formed during the decomposition was measured with a Bendix "time of flight" mass-spectrometer, with the interesting result that on the initial heating of the substance to 400°C , not only oxygen but also CO_2 , ClO_2 and Cl_2 were formed. If the potassium perchlorate was pre-treated overnight at $400\text{--}430^\circ\text{C}$, then chlorine dioxide and chlorine were no longer found and the amount of carbon dioxide was minimal, too. (It must be mentioned that the formation of foreign gases was earlier also observed in the decomposition of sodium azide

during mass-spectrometric analysis [57].) The compound could not be freed from the carbon dioxide impurity, even if the sample was previously treated with perchloric acid. The solid residue consisted of chlorate and chloride, in a ratio corresponding to the amount of oxygen evolved. The amount of the chlorate was about ten times that of the chloride. By converting the peak-height for the oxygen to the number of moles of oxygen evolved per second, the specific rate k_s was obtained. This rate value remained constant even after a long time, if the substance had been pretreated at 400° C in vacuum. In the $\log k_s$ vs. $1/T$ graph no hysteresis was obtained on the increase or decrease of the temperature. Arrhenius functions for different samples from the same substance were parallel straight lines in the temperature range studied. About 30–40° C below the melting point of the pure substance, however, the reaction rate suddenly increased and points taken at these temperatures did not lie on the Arrhenius functions. It was concluded from the constancy of the reaction rate that the growth of nuclei does not play an essential part in the reaction, which can thus be regarded as a homogeneous solid-phase decomposition.

In our view, one of the reasons for the absence of changes in reaction rate, characteristic of the formation and growth of nuclei, may be the 12-hour pre-treatment of the substance at a temperature (400–450° C) commensurable with the reaction temperature (350–450° C); during this period the above processes may have already taken place to a greater or smaller extent.

As regards the effect of the solid reaction product, it was found by GLASNER and WEIDENFELD [49] that even a small amount (mole ratio 0.1) of potassium chloride decreases the induction period of the decomposition, while a larger amount (mole ratio 1) eliminates it completely. The reaction rate constants and the activation energy are practically unaffected by the chloride.

Rubidium perchlorate

A kinetic study of the total decomposition of rubidium perchlorate was carried out at 547–569° C [35, 44]. The reaction began at once, without a time lag, and led to the formation of rubidium chloride. The α vs. t curves were sigmoid type. The reaction initially proceeded in the solid phase, but, similarly as for potassium perchlorate, with progressing decomposition the substance melted.

The decomposition in this case could be described by two first-order equations, the first of which referred to the slow solid-phase decomposition, and the second to the faster molten-phase decomposition. The activation energies were 70.5 and 66.8 kcal/mole, respectively. The decomposition was described surprisingly well by the PROUT–TOMPKINS relation which gave one straight line for practically the entire decomposition. The value of the activation energy was 71.3 kcal/mole. Here too, the addition of rubidium chloride to the rubidium perchlorate changed the decomposition to one of deceleratory nature and also significantly increased the rate of the decomposition.

Using the method reported above, CORDES and SMITH [56] also studied the decomposition of rubidium perchlorate in the solid phase. The characteristics of the reaction agreed with those for the potassium perchlorate reaction. The measured reaction rate was practically the same, but the value of the activation energy was somewhat lower.

Table XI

Kinetic data of the decomposition of monovalent metal perchlorates

Compound	Temperature range °C	Method	Activation energy kcal/mole	Frequency factor (min ⁻¹)	Kinetic equation	Validity of equation
LiClO ₄	392—415	vacuum w-meas.	52.2	—	P—T	0.0—0.4
		vacuum w-meas.	62.0		first order	0.4—0.9
		vacuum w-meas.	58.3		time for decomp. of 0.5%	—
	411—431	vacuum p-meas.	52.6	6.58 · 10 ¹⁴	P—T	0.01—0.4
		vacuum p-meas.	41.0	8.83 · 10 ¹⁰	P—T	0.45—0.95
		vacuum p-meas.	43.9	5.12 · 10 ¹¹	first order	0.4—0.93
NaClO ₄	330—420	chem. anal.	28.0	—	initial rate	—
		vacuum p-meas.	57.3	2.7 · 10 ¹⁴	P—T	0.0—0.3
	490—515	p-meas.	57.1	1.57 · 10 ¹⁴	P—T	0.3—0.8
		p-meas.	59.2	4.89 · 10 ¹⁴	first order	0.55—0.95
		p-meas.	62.6	1.8 · 10 ¹⁵	CC	0.35—0.9
+ NaOH	360—420	in air,	47.3	3.57 · 10 ¹⁴	initial rate	ClO ₄ ⁻ decomp.
		chem. anal.	53.2	3.35 · 10 ¹⁵	initial rate	ClO ₃ ⁻ decomp.
KClO ₄	536—617	in air, O ₂ , ml	60.6	—	first order	—
	537—600	in air, O ₂ , ml	65.8	1.15 · 10 ¹⁶	P—T	—
	556—582	vacuum p-meas.	70.5	1.42 · 10 ¹⁵	first order	solid phase molten phase
		p-meas.	70.5	7.86 · 10 ¹⁶	first order	
	500—580	vacuum p-meas.	98.4	1.8 · 10 ²¹	first order	solid phase molten phase
		p-meas.	80.7	6.8 · 10 ¹⁷	first order	
	375—480	chem. anal.	30.0	—	initial rate	—
		vacuum p-meas.	69.0	1.16 · 10 ¹⁵	first order	
	549—575	p-meas.	71.5	1.05 · 10 ¹⁷	first order	0.0—0.15 (solid phase)
		p-meas.	75.4	5.45 · 10 ¹⁷	CC	0.3—0.9 (molten phase)
350—500	p-meas. mas. spectr.	50.2	3.78 · 10 ⁹	initial rate	0.28—0.85	
450—550	infra spectr.	44.3	—	second order	0.0—0.03	
RbClO ₄	547—569	vacuum p-meas.	71.3	1.03 · 10 ¹⁷	P—T	0.3—0.85
		p-meas.	70.4	8.19 · 10 ¹⁶	first order	0.01—0.28 (solid phase)

Table XI
(Continued)

Compound	Temperature range °C	Method	Activation energy kcal/mole	Frequency factor (min ⁻¹)	Kinetic equation	Validity of equation
RbClO ₄	350—500	p-meas.	66.8	4.28·10 ¹⁵	first order	0.4—0.92 (molten phase)
		p-meas.	72.3	4.02·10 ¹⁶	CC	0.2—0.95
		vacuum mass spectr.	46.0	6.0·10 ⁸	initial rate	0.0—0.03
CsClO ₄	528—558	vacuum			P—T	0.1—0.7 (solid phase)
		p-meas.	52.0	2.68·10 ¹²	first order	
	p-meas.	68.7	8.44·10 ¹⁵			
	385—475 350—500	p-meas.	57.0	2.12·10 ¹³	CC	0. —0.95
chem. anal. vacuum mass. spectr.		35.0 44.6	— 1.90·10 ⁸	initial rate	— 0.0—0.03	
AgClO ₄	414—445	vacuum	62.7		P—T	0.01—0.33 0.33—0.95
		p. meas.	52.4		P—T	
TlClO ₄	409—452	vacuum p. meas.	56.0		P—T	

W-meas. = weight measurement
P-meas. = pressure measurement
P—T = Prout—Tompkins equation
CC = „Contracting cube” formula

Cesium perchlorate

The temperature of decomposition of cesium perchlorate is lower than that of rubidium perchlorate, and in fact, even lower than that of potassium perchlorate. Kinetic measurements were made at 528—558 °C by following the pressure of oxygen in vacuum [35]. The course of the reaction is similar to that observed for potassium and rubidium perchlorates. The rate maximum occurred at about $\alpha=0.45$. Here too, the decomposition began in the solid phase, but as a result of the reaction product the substance melted below the melting point of the pure compound. The first-order equation gave a straight line for the initial solid-phase decomposition up to $\alpha=0.23$. The value of the activation energy was 68.7 kcal/mole. The description of the liquid-phase decomposition with the first-order equation was much less successful. The PROUT—TOMPKINS relation gave one straight line for the total decomposition. The value of the activation energy was 52 kcal/mole. The values of the activation energies calculated from the temperature-dependence of the times for the various stages of the decomposition were in the range 67—70 kcal/mole. Here too, preliminary addition of the reaction product, cesium chloride, accelerated the decomposition to a considerable extent.

A significantly lower value of activation energy was obtained by CABANE and BENARD [45], and also by CORDES and SMITH [56]. The former authors carried out

their investigation at 385–475° C, the latter at 350–450° C, where the extent of the decomposition was less than 3–4%. The activation energy value obtained by CABANE and BENARD agreed well with that determined for the self-diffusion of ClO_4^- in cesium perchlorate.

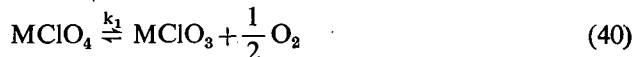
The kinetic data referring to the thermal decomposition of the alkali metal perchlorates are given in Table XI.

Mechanism of decomposition of the alkali metal perchlorates

It is clear from the results of the kinetic studies that the decomposition of the alkali metal perchlorates is fairly complex, and several consecutive and simultaneous processes must be taken into consideration. In establishing the characteristics and the mechanisms of the decomposition, a difference must be made between the experiments extending to the total decompositions of the compounds at higher temperatures, and the studies concerned primarily with the surface reactions of the crystals. The evaluation of the results of the first experimental series is particularly difficult due to the phase-change during the reaction, and to the melting of the substances well below the melting points of the pure materials. Lithium perchlorate is an exception, the decomposition taking place completely in the liquid phase.

A general feature of the decompositions of alkali perchlorates is their autocatalytic character. This is first of all the result of the melting of the compounds which is due to the effect of solid reaction products (chlorides). When the chlorides corresponding to the reaction products, were previously mixed to the perchlorate salts, the run of decompositions changed. The perchlorates melted at the very beginning of the decomposition, the autocatalytic character of the reaction disappeared and the decomposition started with a maximum rate. Accordingly, the catalytic effect of chlorides seems only apparent. The fact, however, that the decomposition of lithium perchlorate in the molten phase is also autocatalytic and the lithium chlorides exerted an accelerating effect on the decomposition, shows that the chloride might have some effect on the molten phase reaction in the former cases, too.

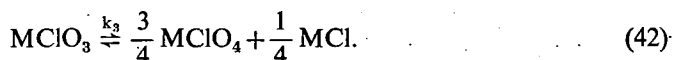
The values of activation energy of the decomposition of all alkali perchlorates were found to be in the range of 60–70 kcal/mole and practically the same for the solid and molten phase. This indicates that the chemical mechanism of the decomposition of perchlorates is essentially similar and the rate determining step, independently of the phases, is the same in every compound. The larger frequency factor obtained for decomposition in molten phase is probably the result of the larger mobility of the perchlorate ion. The decomposition of perchlorates can be thought as proceeding by the following steps. In the first step



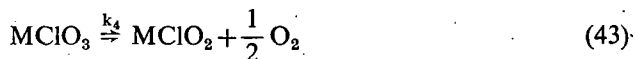
metal chlorate and oxygen are formed. The metal chlorate then decomposes partly into chloride and oxygen



and partly disproportionates into perchlorate and chloride



The occurrence of this latter reaction is indicated by experiments with chlorates. Although over 500° C the thermal decomposition of alkali chlorates is rapid, its disproportionation was observed even at this temperature. It is very likely that the decomposition of chlorate into chloride does not take place in one step but first chlorite is formed, which then decomposes into chloride



While the chlorate intermediate was found in decomposition of every alkali perchlorate, chlorite was not detected at all. The most plausible explanation for this seemed to be that at high temperature chlorites decompose extremely rapidly into chloride and oxygen. It was shown, however, that alkali chlorites did not decompose even in this temperature range into oxygen and chloride but instantaneously disproportionate into chlorate and chloride:



Regarding that alkali chlorates are less stable compounds than perchlorates ($k_2 > k_1$) and their amount never exceeds 2—3 per cent during the reaction, it can be rightly assumed that in the decomposition of all alkali perchlorates the reaction (40) is the rate-determining step. This step involves the rupture of the Cl—O bond. The dissociation energy of the Cl—O bond (64.295 kcal/mole [15]) is in good agreement with activation energies found experimentally.

A further proof for this mechanism can be obtained by calculating the endothermic heat of reaction of this step.

On the basis of the standard enthalpy of formation of perchlorates and chlorates, and supposing only a slight difference in their heat capacities, we obtain for ΔH° the value enlisted in the sixth column of Table XII. These values are much lower than the activation energies determined experimentally. Supposing, however, the formation of atomic oxygen ($\Delta H_f^\circ = 59.2$ kcal) the data shown in the last column are obtained. These values, with the exception of that for lithium perchlorate, agree very well with the activation energies measured.

Besides the rupture of the Cl—O bond, one can suppose the electron-transfer reaction between the anion and the cation as the rate determining step of the decomposition:

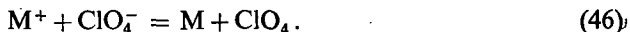


Table XII

Standard heat of formation for monovalent metal perchlorates and for their decomposition products

Compound	ΔH° MClO ₄	ΔH° MClO ₃	ΔH° MCl	ΔH° $\frac{1}{2}$ M ₂ O	$\Delta H^\circ_{\text{reac.}}$	$\Delta H^\circ_{\text{reac.}}$
LiClO ₄	-91.77	-70	-94.8	-71.3	21.77	80.9
NaClO ₄	-92.18	-85.7	-98.23	-51.46	6.5	65.7
KClO ₄	-103.6	-93.5	-104.17	-43.1	10.1	69.3
RbClO ₄	-103.87	-93.8	-105.1	-41.5	10.0	69.2
CsClO ₄	-105.86	-96.0	-106.4	-41.05	7.8	67.0
AgClO ₄	-7.75	-5.73			2.02	61.2

The sixth and seventh columns contain the heat of reaction of the processes $\text{MClO}_4 = \text{MClO}_3 + \frac{1}{2} \text{O}_2$ and $\text{MClO}_4 = \text{MClO}_3 + \text{O}$, respectively.

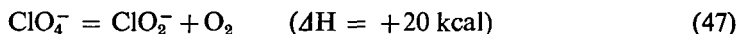
The electron-transfer reaction plays an important part in the decomposition of a number of ionic compounds as *e.g.* alkali azides. Of perchlorates, the decomposition of ammonium perchlorate between 200–300° C was supposed to take place according to this mechanism.

The thermal energy required for the transfer of an electron from the anion to the cation has been calculated from spectroscopic data in the case of potassium perchlorate [35]. The adsorption edge of alkali perchlorates is at about 6 eV [52], the low frequency dielectric constant (*K*) is 5.9 and the refractive index (*n*) is 1.4746. From these data the thermal activation energy was obtained to be 2.21 eV (51 kcal). Regarding that this value is much lower than the activation energy of the decomposition, we are of the opinion that the probability of an electron-transfer reaction can be excluded. The decomposition products (chloride and oxygen) are also against an electron-transfer reaction because in this case chlorine dioxide and chlorine must have been formed in the decomposition of the perchlorate radical or in the reaction between alkali metal and the perchlorate radical.

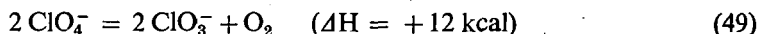
A separate discussion is required for the results of low temperature kinetic measurements when the decomposition occurred entirely on the surface layer of solid perchlorates and the conversion never exceeded 1–3%. The values of activation energies in one case [56] were between 40–50 kcal/mole and in another case [45] between 28–35 kcal/mole.

The values obtained by CABANE and BENARD [45] agreed with those measured in these compounds for the self-diffusion of the perchlorate ion; from this they concluded that the rate determining process of the thermal decomposition is the diffusion of the perchlorate ion.

Another explanation is offered by CORDES and SMITH [56] who considered two different modes of perchlorate decomposition; one of monomolecular type,



and one of bimolecular type,



The reaction heats of the above reaction steps, however, still differed from their experimentally determined activation energy values. If it is assumed that both starting steps lead to ${}^3\Sigma_gO_2$ and the multiplicity rules are valid for reactions occurring within a solid, the reported value of the reaction heat must be increased by at least 22 kcal/mole (${}^1\Delta_gO_2$) assuming singlet ClO_4^- and ClO_3^- . The reaction heat values thus calculated are then consistent with the measured activation energy value.

It was attempted to decide between the two primary steps on the basis of the value of the frequency factor. The expected pre-exponential factor of the monomolecular reaction step would be between 10^{11} and 10^{17} sec^{-1} , which is considerably higher than the experimentally determined value.

A bimolecular reaction could have such a low pre-exponential factor if the activated complex has restricted rotation while the reactants have free rotation. As activated complex, CORDES and SMITH suggested two adjacent ClO_4^- ions joined through a peroxide-like linkage, $(O_3Cl)-O-O-(ClO_3)$. In the calculation of the rate constants by the activated complex theory the following assumptions were made;

- the external rotation are restricted to harmonic oscillations in the complex,
- the ClO_4^- ion is freely rotating,
- the torsion mode for the dihedral angle $(ClO_3)-O-O-(ClO_3)$ is restricted by the lattice,
- the shortening of the Cl—Cl distance with respect to the value for the free ClO_4^- groups restricts the "pinwheel" rotations of the ClO_3 groups,
- the coulombic repulsion of the two charges affects only the activation energy and not the pre-exponential factor,
- the remaining internal vibrations are independent of the lattice forces,
- the transitional modes are represented by Einstein oscillators.

The force constant for the ClO_4^- ion was chosen to be the same as for KCl. The value obtained for the pre-exponential factor in the calculations, $1.2 \cdot 10^8$ sec^{-1} , was fairly close to the experimental value of 10^7 sec^{-1} and this was considered as a proof for the proposed mechanism. The change in Arrhenius factors with temperature was tentatively explained by the assumption that upon raising the temperature the lattice is able to open up to such an extent that the "pinwheel"-like motion of the ClO_3 groups is made possible, and, in addition, the other lattice constants also become weaker. The rate constant therefore increases, resulting in the increase of the value of the activation energy. This effect becomes even more pronounced when the substances melt.

Factors influencing the stability of alkali metal perchlorates

In spite of the fact that the temperature range of the decomposition of alkali metal perchlorates is relatively narrow, there are well defined differences between the temperatures of decomposition of these compounds. To characterize the stability of the substances, the temperature values have been calculated from the Arrhenius diagrams, where the rate constant of the decompositions (contracting cube formula) reaches the value of $5 \cdot 10^{-3}$. As it can be seen from Table XIII this characteristic temperature, increases from lithium to rubidium but it is lower for cesium.

As factors influencing the stability of perchlorates, the structural properties of the compounds, their physical constants and the character of the prevailing

Table XIII
Correlation between stability and bonding of metal perchlorates

Compound	Temp. of 2% decomp. °C [40]	T ₀ (°C)	F*	Ionic character of M—ClO ₄ bond %	Polarizing power of cations e/r	Polarisability of cations	Polarisability of oxygen ion in ClO ₄ ⁻
CsClO ₄	601	526	1.303	75.5	0.592	3.34	26.1
RbClO ₄	611	560	1.423	74.1	0.676	1.98	30.1
KClO ₄	583	547	1.661	73.2	0.752	1.33	25.4
NaClO ₄	522	508	2.407	68.9	1.053	0.41	25.3
LiClO ₄	470	410	2.915	67.8	1.667	0.03	20.3

T₀ is the temperature value where the rate constant of the decompositions calculated by the contracting cube formula, $1 - (1 - \alpha)^{1/3} = kt$, reaches the value of $5 \cdot 10^{-3}$.

$F^* = \frac{Z^*}{r^2}$; where F* = effective electric field strength of cations

Z* = effective nuclear charge

bonds have to be considered. Some of these properties are summarized in Table XIII. Evaluating the stability of perchlorates in the light of these data, it can be stated that *the more ionic a compound, the greater its stability*. The effective electric field strength of the cations affects the stability of perchlorates in a similar way. *The increase of the effective electric field strength of the cations results in a decrease of the temperature of the decomposition*. The only exception is cesium perchlorate, as its characteristic temperature is lower than that of the potassium salt. From among the physical properties of alkali metal perchlorates, the melting point of cesium perchlorate shows a similar behaviour. Considering the fact, that the melting of inorganic compounds results in an enhanced rate of decomposition, it could be rightly assumed that the lower stability of cesium perchlorate is the consequence of its lower melting point.

In our opinion, however, the origin of the strange behaviour both in melting and stability of cesium perchlorate is to be found in the large size of the cesium ion and, consequently, in its more marked polarizability. This is reflected in the polarity of the Cl—O bond which is less in the case of cesium perchlorate than in rubidium perchlorate.

References

- [1] Solymosi, F., T. Bãnsági: Acta Chim. Acad. Sci. Hung. **56**, 328 (1968).
- [2] Bãnsági, T., F. Solymosi: Proc. of the 5th International Conference on Thermal Analysis, Akadémiai Kiadó, Budapest, (1975) p. 505.
- [3] Taylor, M. C., J. F. White, C. P. Vincent, G. L. Cunningham: Ind. Chem. Eng. **32**, 900 (1940).
- [4] Solymosi, F.: Z. phys. Chem. N. F. **57**, 1 (1968).
- [5] Levi, G. R., E. Cippollone: Gazz. chim. ital. **53**, 203 (1923).
- [6] Levi, G. R.: Gazz. chim. ital. **53**, 246 (1923).
- [7] Solymosi, F., T. Bãnsági: Proc. of the 3th International Conference on Thermal Analysis, Birkhäuser Verlag, Basel, 1972, Vol. 2. p. 289.
- [8] Levi, G. R.: Gazz. chim. ital. **53**, 248 (1923).
- [9] Levi, G. R., E. Cippollone: Gazz. chim. ital. **53**, 240 (1923).
- [10] Glasner, A., L. Weidenfeld: J. Amer. Chem. Soc. **74**, 2464 (1952).
- [11] Bosch, A. V., A. H. W. Aten: J. Amer. Chem. Soc. **75**, 3835 (1953).
- [12] Markovitz, M. M., D. A. Boryta, H. Stewart: J. Phys. Chem. **68**, 2282 (1964).
- [13] Markovitz, M. M., D. A. Boryta, H. J. Stewart: J. Chem. Eng. Data **9**, 573 (1964).

- [14] *Dodé, M., J. Basset*: J. Bull. Soc. Chim. **2**, 344 (1935).
- [15] *Wagman, D. D., V. H. Evans, I. Halow, V. B. Parker, S. M. Bailey, R. H. Schum*: National Bureau of Standard NBS Tech. Note 270, 1965.
- [16] *Rocchiccioli, C.*: Compt. rend. **242**, 2922 (1956).
- [17] *Erdey, L., J. Simon, S. Gál*: Talanta **15**, 653 (1968).
- [18] *Solymosi, F., T. Bánsági*: Acta Chim. Acad. Sci. Hung. **56**, 337 (1968). Magyar Kémiai Folyóirat, **74**, 32 (1968).
- [19] *Simon, J., S. Gál, L. Erdey*: Acta Chim. Acad. Sci. Hung. **66**, 175 (1970).
- [20] *Yoshida, C., H. Osida*: Ind. Exp. Soc. Japan, **15**, 1 (1954).
- [21] *Farmer, W., J. B. Firth*: J. Chem. Soc. **125**, 82 (1924).
- [22] *Otto, C. E., H. S. Fry*: J. Amer. Chem. Soc. **45**, 1134 (1923).
- [23] *Otto, C. A., H. S. Fry*: J. Amer. Chem. Soc. **46**, 269 (1924).
- [24] *Solymosi, F., E. Krix*: Acta Chim. Acad. Sci. Hung. **34**, 241 (1962).
- [25] *Tobisawa, S.*: Bull. Chem. Soc. Japan, **34**, 89 (1961).
- [26] *Rudloff, W. K., R. S. Freeman*: J. Phys. Chem. **73**, 1209 (1969).
- [27] *Sodeau, W. H.*: J. Chem. Soc. **77**, 137 (1900).
- [28] *Solymosi, F.*: Magyar Kémiai Folyóirat **73**, 398 (1967).
- [29] *Sodeau, W. H.*: Proc. Chem. Soc. **16**, 209 (1900).
- [30] *Acheson, R. J., P. W. M. Jacobs*: Can. J. Chem. **47**, 3031 (1969).
- [31] *Marvin, G. G., L. B. Woolaver*: Anal. Chem. **17**, 474 (1945).
- [32] *Gordon, S., C. Campbell*: Anal. Chem. **27**, 1102 (1955).
- [33] *Erdey, L., F. Paulik, J. Paulik*: Mikrochim. Acta 699 (1966).
- [34] *Duval, C.*: Inorganic Thermogravimetric Analysis, Elsevier Publ. Co. Amsterdam 1953.
- [35] *Solymosi, F.*: Acta Chim. Acad. Sci. Hung. **57**, 11 (1968).
- [36] *Markovitz, M. M.*: J. Phys. Chem. **61**, 505 (1957); **62**, 827 (1958).
- [37] *Markovitz, M. M., R. F. Harris*: J. Phys. Chem. **63**, 1513 (1953).
- [38] *Markovitz, M. M., D. A. Boryta*: J. Phys. Chem. **64**, 1711 (1960).
- [39] *Markovitz, M. M., D. A. Boryta, R. F. Harris*: J. Phys. Chem. **65**, 261 (1961).
- [40] *Markovitz, M. M., D. A. Boryta*: J. Phys. Chem. **69**, 1114 (1965).
- [41] *Solymosi, F.*: Dissertation for degree of D. Sc. Szeged 1966.
- [42] *Markovitz, M. M., D. A. Boryta*: J. Phys. Chem. **65**, 1419 (1961).
- [43] *Markovitz, M. M., D. A. Boryta*: J. Phys. Chem. **66**, 358 (1962).
- [44] *Solymosi, F., Gy. Braun*: Acta Chim. Acad. Sci. Hung. **52**, 1 (1967).
- [45] *Cabane, J., J. Benard*: Bull. Soc. Chim. France **36** (1961).
- [46] *Seward, R. P., H. W. Otto*: J. Phys. Chem. **65**, 2078 (1961).
- [47] *Otto, H. W., K. Fry*: J. Amer. Chem. Soc. **45**, 1138 (1923).
- [48] *Hoffman, K. A., P. H. Marin*: Sitzber. preuss. Acad. Wiss. phys. math. Klasse 448 (1932).
- [49] *Glasner, A., L. Weidenfeld*: J. Amer. Chem. Soc. **74**, 2467 (1952).
- [50] *Glasner, A., A. E. Simchen*: Bull. Soc. Chim. France **18**, 233 (1951); **20**, 127 (1953).
- [51] *Simchen, A. E.*: J. Phys. Chem. **65**, 1093 (1961).
- [52] *Bircumshaw, L. L., R. T. Phillips*: J. Chem. Soc. 703 (1953).
- [53] *Harvey, A. E., M. T. Edmison, E. O. Jones, R. A. Seybert, K. A. Gatto*: J. Amer. Chem. Soc. **76**, 3270 (1954).
- [54] *Rodgers, T. A., C. J. Wassink*: Final Summary Report, University of Arkansas, 1958. Contract No. Da-23-072-ORD.
- [55] *Harvey, A. E., C. J. Wassink, T. A. Rodgers, K. H. Stern*: Annals of New York Acad. Sci. **79**, 971 (1960).
- [56] *Cordes, H. F., S. R. Smith*: J. Phys. Chem. **72**, 2189 (1968).
- [57] *Walker, R. F., F. Gane, F. P. Bowden*: Proc. Roy. Soc. **A294**, 417 (1966).
- [58] *Teltow, A.*: Z. phys. Chem. **B40**, 397 (1938).

КИНЕТИКА И МЕХАНИЗМ ТЕРМИЧЕСКОГО РАСПАДА ХЛОРИТОВ,
ХЛОРАТОВ И ПЕРХЛОРАТОВ МЕТАЛЛОВ
(ОБЗОР)

Ф. Шольмоши

Рассмотрены работы, занимающиеся вопросом термического распада хлоритов, хлоратов и перхлоратов разных металлов и дан критический обзор различных представлений о термических свойствах этих солей.



ИССЛЕДОВАНИЕ СТРУКТУРЫ И СВОЙСТВ МЫЛ, II. ИНФРАКРАСНЫЕ СПЕКТРЫ КАЛЬЦИЕВЫХ СОЛЕЙ АЛИФАТИЧЕСКИХ ОДНООСНОВНЫХ КИСЛОТ

И. А. АНДОР, З. КИШ,

Институт общей и физической химии университета им. Аттилы Йожефа, Сегед

и

Я. БАЛАЖ

Каферда коллоидной химии университета им. Аттилы Йожефа, Сегед

(Поступило в редакцию 20 марта 1976 г.)

Показана возможность получения кальциевых солей алифатических одноосновных кислот с четным числом углеродных атомов от капроновой до стеариновой кислоты, методом реакции на границе раздела фаз динамической эмульсии (РГФ). На основании термогравиметрических, рентгеноструктурных и ИК-спектроскопических данных установлены составы и наличие кристаллической структуры солей. Детально рассмотрены ИК-спектры кальциевых солей кислот, от уксусной до стеариновой, в твердой фазе в интервале частот от 3800 до 650 см^{-1} .

Несмотря на наличие в литературе ряда работ по ИК-спектрам различных солей [1, 2], еще очень мало попыток к описанию теоретически обоснованных корреляций. Это и неудивительно, так как имеющийся экспериментальный материал еще далеко не достаточен для составления теории колебательных спектров столь сложных молекул, как соли органических кислот. В особенности мало данных по ИК-спектрам солей многовалентных металлов по гомологическому ряду алифатических кислот [3].

Ранее в работе [4] нами был рассмотрен ИК-спектр лаурата кальция, полученного методом реакции на границе раздела фаз динамической эмульсии, в KBr -ной таблетке и была сделана попытка отнесения основных полос поглощения к соответствующим характеристическим колебаниям, на основании имеющихся литературных данных.

Задача данной работы заключалась в синтезе кальциевых солей алифатических одноосновных кислот с четным числом углеродных атомов, методом реакции на границе раздела фаз динамической эмульсии (РГФ), в определении основных характеристик полученных солей и в снятии их ИК-спектров в твердой фазе. Кроме этого мы ставили перед собой цель попытаться обнаружить основные закономерности проявляющиеся в смещении полос поглощения в ИК-спектрах кальциевых солей исследуемого ряда кислот.

Объекты и методы исследования

Алифатические одноосновные кислоты: капроновая (C_6), каприловая (C_8), каприновая (C_{10}), лауриновая (C_{12}), миристиновая (C_{14}), пальмитиновая (C_{16}), и стеариновая (C_{18}) использовались фирмы *Fluka* марки *puriss.* с содержанием основного продукта выше 99,5%-ов. Масляная (C_4) и уксусная (C_2) кислоты были фирмы *Loba-Chemie* также марки *puriss.* Ксилол, $Ca(OH)_2$ и другие реактивы использовались фирмы *Reanal* аналитической степени чистоты.

Синтез кальциевых солей гомологического ряда алифатических одноосновных кислот с чётным числом углеродных атомов ($CaAn_2$) производили следующим образом. Определенное количество $Ca(OH)_2$ суспендировали в дистиллированной воде. Соответствующую кислоту, в количестве превышающем эквивалентное на 10%-ов, растворяли в ксилоле. В реакционном сосуде, при сливании ксилола и воды (в соотношении фаз равном 0,8) с помощью гомогенизатора типа *Mixer Unipan-309*, получали динамическую нестабильную эмульсию. На границе раздела фаз эмульсии, при перемешивании со скоростью 4250 об/мин и температуре 25°C за 20 минут практически полностью происходило образование солей. Полноту протекания реакции проверяли потенциометрическим титрованием ксилольной фазы на содержание кислоты [5]. После тщательной многократной промывки продуктов обеими фазами, соли высушивали при комнатной температуре до постоянного веса. Об отсутствии остаточной кислоты в солях судили по ИК-спектрам по отсутствию полос при 2680, 1710 и 940 cm^{-1} .

Термогравиметрические и рентгеноструктурные измерения проводили как было описано ранее [4]. ИК-спектры были сняты на двухлучевом приборе типа *Unicam SP-1000* с дифракционной решеткой. Спектры образцов солей снимались в *KBr*-ных таблетках весом 0,2 г, при этом навески солей брали с расчётом $1 \cdot 10^{-5}$ молей соли на 0,8 г *KBr*. Волновые числа в максимумах поглощения указываются нами с точностью $\pm 5 cm^{-1}$.

В работе использованы символы видов характеристических колебаний предложенные в [6], которые были приведены нами в первом сообщении данной серии [4].

Экспериментальные данные и их обсуждение

Ранее нами [7] было проведено изучение реологических и коллоидных свойств эмульсионных систем, состоящих из кальциевых солей гомологического ряда алифатических кислот (C_6-C_{18}), ксилола и воды. При этом, естественно, рассматривались только свойства гетерогенной дисперсной системы в целом, после образования соответствующих солей методом РГФ. На наш взгляд, представляет интерес рассмотрение полноты протекания образования кальциевых солей жирных кислот в таких системах и определение некоторых свойств выделенных солей. Экспериментальные данные по выходу продуктов РГФ, по гидратному составу солей, а также принятые нами сокращения для их обозначения представлены в таблице I.

Из данных таблицы I видно, что методом РГФ из эмульсии ксилол — вода удалось выделить кальциевые соли кислот содержащих 6 и более углеродных

Таблица I
Выход продуктов РГФ и их гидратный состав

Кислота		Принятое сокращение названия соли	Избыток кислоты в ксилале, %	Выход продукта, %	Содержание H_2O , %	Состав $CaAl_2 \cdot xH_2O$
Тривиальное название	Число С					
Уксусная	2	$CaAc_2$	Не выделяется		9,2	$CaAc_2 \cdot 0,88 H_2O^*$
Масляная	4	$CaBt_2$	Не выделяется		7,8	$CaBt_2 \cdot 1,00 H_2O^*$
Капроновая	6	$CaKon_2$	8,0	~70	5,8	$CaKon_2 \cdot 0,94 H_2O$
Каприловая	8	$CaKil_2$	10,5	92	5,2	$CaKil_2 \cdot 0,91 H_2O$
Каприновая	10	$CaKin_2$	11,5	96	4,6	$CaKin_2 \cdot 1,04 H_2O$
Лауриновая	12	$CaLr_2$	12,0	97	3,8	$CaLr_2 \cdot 0,95 H_2O$
Миристиновая	14	$CaMir_2$	11,5	96	3,4	$CaMir_2 \cdot 0,94 H_2O$
Пальмитиновая	16	$CaPm_2$	11,5	95	3,0	$CaPm_2 \cdot 0,93 H_2O$
Стеариновая	18	$CaSt_2$	11,0	97	2,6	$CaSt_2 \cdot 0,93 H_2O$

*Соли получены способом замещения.

атомов в молекуле. Поскольку в реакции был введён 10%-ный избыток кислот, сведения о полноте протекания реакции можно получить при определении количества кислоты оставшейся в органической фазе после разделения фаз. В случае высших жирных кислот, начиная от каприновой, остаточное избыточное количество кислоты составляет 1,5—2%. Учитывая, что в солях не содержится кислоты, можно прийти к выводу, что РГФ происходит в достаточной мере полно.

Найденное весьма малое избыточное количество кислоты (0,5%) в случае образования каприлата кальция и недостаток кислоты в случае образования капроната, с принятием во внимание выхода этих продуктов, указывает на ухудшение условий прохождения образования солей методом РГФ для низших членов гомологического ряда. $CaBt_2$ и $CaAc_2$ совсем не выделялись, вследствие растворимости кислот и солей в водной фазе.

Необходимо отметить, что приведенные в таблице I данные выходов продуктов РГФ представляют собой только относительные величины, вследствие наблюдающихся систематических потерь, обусловленных применяемым прибором для диспергирования.

Данные термогравиметрического анализа солей и рассчитанный на основании этих данных гидратный состав солей представлены также в таблице I. Из данных таблицы видно, что составы всех полученных солей с хорошим приближением соответствуют моногидратам. Для получения $CaAc_2$ и $CaBt_2$ нами был избран метод замещения аниона в карбонате кальция соответствующим анионом кислоты [8], поскольку таким способом образовались также моногидраты.

Полученные методом РФГ кальциевые соли представляли собой бесцветные порошки, которые под микроскопом имели вид весьма мелких слипшихся кристалликов. При синтезе $CaLr_2$ [7], на основании дифракции рентгеновских лучей мы пришли к выводу, что данная соль образовалась с достаточно хорошо выраженной кристаллической структурой. Мы считали целесообразным провести рентгеноструктурный анализ для всех полученных нами образцов кальциевых солей, в том числе и для $CaAc_2$ и $CaBt_2$, полученных реакцией замещения. Во всех случаях были получены дифракционные спектры содержащие 10—12 достаточно интенсивных полос, что позволяет рассматривать все члены исследуемого гомологического ряда как кристаллические вещества.

ИК-спектры исследуемых солей в области длин волн от 2,7 до 5 мк показывают ожидаемые явления с некоторыми особенностями. Широкая диффузная полоса поглощения в области $3600\text{—}3200\text{ см}^{-1}$, соответствующая ν_{OH} колебаниям молекул воды, имеет максимум при 3400 см^{-1} . Ввиду того, что концентрации солей в таблетках должны были быть одинаковыми при принятой нами методике, следовало ожидать одинаковую интенсивность полос, принадлежащих колебаниям гидратной воды в солях, как это наблюдалось в действительности для карбоксилатных полос. Однако, несмотря на то, что точную количественную зависимость изменений интенсивности нельзя было установить, все же ярко выражено уменьшение интенсивности полосы при 3400 см^{-1} с увеличением длины углеродной цепи. Возможно, это явление может быть объяснено различной гигроскопичностью членов гомологического ряда.

По отсутствию в спектрах обычно острой полосы поглощения находящейся при 3644 см^{-1} , характерной для ν_{OH} связанных с катионом кальция гидроксидов [2], можно судить об отсутствии $Ca(OH)_2$ или основных солей, в количествах заслуживающих внимания, в исследуемых нами образцах.

Серия полос, соответствующая асимметричным и симметричным валентным колебаниям CN связей метильных и метиленовых групп, находящаяся при 2960, 2920, 2870 и 2850 см^{-1} , хорошо разрешена и наблюдается обычное изменение интенсивностей по гомологическому ряду солей [6].

Для солей карбоновых кислот наиболее интересна область спектра в интервале длин волн от 6 до 7,5 мк, где наблюдаются валентные колебания карбоксилатной группы. Детальный анализ спектра в этой области представляет особый интерес в виду того, что карбоксилатные колебания должны быть чувствительны как к природе катиона, так и аниона и весьма ценные сведения могут быть получены относительно структуры и характера связей в комплексах карбоновых кислот и их производных [9, 10]. Полученные нами ИК-спектры в этой области длин волн представлены на рисунке. Мы отмечали в предыдущем сообщении [4] расщепление полосы асимметричных валентных колебаний карбоксилата $\nu_{as}CO_2^-$ в спектре $CaLr \cdot H_2O$. В литературе не находим рассмотрения деталей этой полосы. Вполне возможно, что наблюдаемые нами полосы и достаточно явно выраженные плечи появляются только в спектрах кристаллических образцов гидратированных солей кальция.

Из рисунка видно, что в области проявления $\nu_{as}CO_2^-$ для $CaAc_2$ наблюдаются плечи при 1690 , 1640 и 1540 см^{-1} на полосе имеющей максимум при 1600 см^{-1} . При переходе к бутирату и капронату высокочастотная сторона полосы становится круче, исчезают плечи при 1690 и 1640 см^{-1} и плечо при

1620 см^{-1} выделяется более ярко. Максимум полосы поглощения смещается к 1595 и 1585 см^{-1} соответственно. Замечательно, что общая конфигурация серии полос в этой области становится постоянным и не претерпевает никаких изменений для всех дальнейших изученных членов гомологического ряда. Таким образом несомненно, что полученный в этой области вид спектра обусловлен колебаниями $\nu_{as} \text{CO}_2^-$ на которые влияют привода катиона, гидратный состав, резонантные взаимодействия с соседними карбоксилатными группами и, вероятно, даже кристаллическая структура исследуемого образца, в результате которых появляется сложный вид основной полосы поглощения.

Смещение наиболее интенсивного пика полосы $\nu_{as} \text{CO}_2^-$ в ряду $\text{CaAc}_2 > \text{CaBt}_2 > \text{CaKon}_2$ объясняем известным влиянием положительного индуктивного эффекта алкильных радикалов [11, 12]. Такое объяснение вполне приемлемо по аналогии с доказанным повышением частоты $\nu_{as} \text{CO}_2^-$ под влиянием заместителей с отрицательным индуктивным эффектом в ацетате натрия [13].

В отношении изменений четкости проявления отдельных полос поглощения, как видно из рисунка, аналогичную картину с предыдущим наблюдаем и в области 1475—1500 см^{-1} . В гомологическом ряду кальциевых солей, начиная от капроната, для высших членов ряда не обнаруживаются существенные изменения. Для бутирата и ацетата наблюдается перекрывание полос при 1475 ($\beta_s \text{CH}_2$) и 1460 см^{-1} ($\delta_{as} \text{CH}_3$), а также полос при 1440 ($\beta_s \alpha\text{-CH}_2$), и 1425 см^{-1} ($\nu_s \text{CO}_2^-$), поэтому нельзя судить о том, происходит ли смещение полосы симметричных валентных колебаний карбоксилата для первых членов ряда.

Область спектра в интервале от 1400 до 1150 см^{-1} привлекала внимание многих исследователей, в особенности после работ Брауна и Шеппарда [14], показавших наличие эквидистантной характерной серии полос в этой области для разных соединений содержащих алифатические цепи. Джонс [15] показал, что в этой, так называемой «области прогресси полос», в спектрах твердых веществ, содержащих алкильную цепь с примыкающей концевой полярной группой, число полос равно половине числа углеродных атомов цепи. Автор работы [16] уточнил, что число полос в прогрессии определяется только длин-

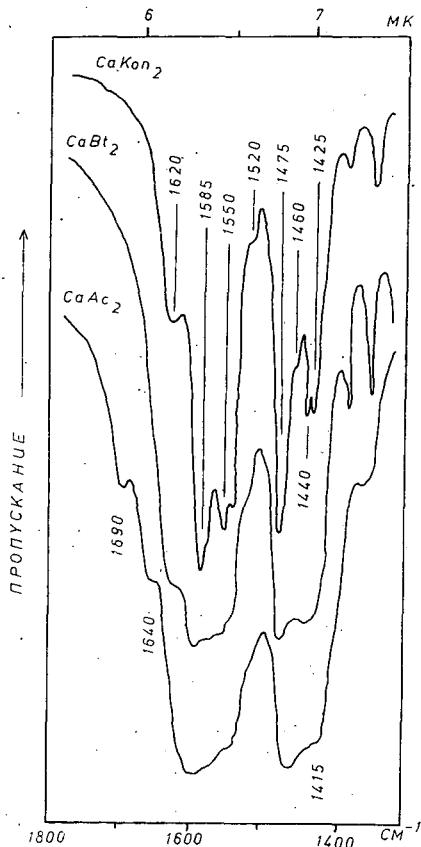


Рис. 1. ИК-спектры моногидратов CaAc_2 , CaBt_2 и CaKon_2 в интервале длин волн от 5,6 до 7,5 мк.

ной цепи примыкающей к полярной группе, так, например, члены цепи находящиеся за двойной связью не проявляются в прогрессии полос как продолжение цепи.

Максимумы полос поглощения в полученных нами спектрах представлены в таблице II.

Таблица II

Смещение максимумов полос поглощения в ИК-спектрах кристаллических образцов $\text{CaAn}_2 \cdot \text{H}_2\text{O}$ в области частот 1400—1150 см^{-1}

Отнесение Соль	$\delta_s \text{CH}_3$	$\gamma_{as} \text{CH}_2 + \gamma_s \text{CH}_2 + \text{—C—C—}$ скелетные	$\nu \begin{array}{c} \\ \text{C} \\ \end{array} \begin{array}{c} ? \\ \text{—CH}_3 \end{array}$
CaAc_2	1360		1270 1240
CaBt_2	1380	1345 1305	1260 1225
CaKon_2	1380	1345 1300 1260	1230 1205
CaKil_2	1380 1370	1345 1280 1260 1240	1215 1190
CaKin_2	1380 1360	1340 1310 1280 1245 1220	1205 1180
CaLr_2	1380 1360	1340 1320 1290 1265 1230 1200	
CaMir_2	1380 1355	1340 1320 1300 1275 1250 1220 1195	
CaPm_2	1380 1355	1340 1320 1300 1280 1260 1240 1215 1195	
CaSi_2	1380 1355	1340 1325 1310 1290 1270 1250 1230 1210 1190	

На основании анализа изменений интенсивности полос и характера их смещений в гомологическом ряду, нам представляется наиболее вероятным рассматривать их отнесение к характеристическим частотам, как это показано в таблице II.

Исходя из того, что в CaAc_2 нет CH_2 -групп очень слабо проявляющиеся плечи при 1270 и 1240 см^{-1} мы не отнесли к области прогрессии полос. В этом случае более верно отражается логика смещения полос и правило Джонса [15] о числе эквидистантных полос удовлетворяется не только для высших членов гомологического ряда, но для всех солей содержащих алкильную цепь. Имеющиеся у нас данные еще не позволяют сделать достаточно обоснованное предложение к отнесению двух слабых полос, берущих своё начало при 1270 и 1240 см^{-1} и постепенно смещающихся в сторону меньших частот, пока более интенсивные полосы области прогрессии не перекрывают их, однако, представляется весьма вероятным, что эти полосы могут соответствовать валентному колебанию углерода метильной группы с соседним углеродным атомом.

В области прогрессии полос достаточно четко наблюдается появление новых полос поглощения от 1305 до 1190 см^{-1} при увеличении длины цепи кислотных остатков на две метиленовые группы. Все члены прогрессии полос закономерно смещаются в сторону меньших частот и дают приблизительно эквидистантную серию полос средней и малой интенсивности, в соответствии с литературными данными [3].

Весьма сложно и мало надежно отнесение полос поглощения спектров в области 1150—800 см^{-1} [6]. Полученные нами данные представлены в таблице III.

При рассмотрении спектров этой области длин волн, мы ставили перед собой цель, в основном, только определения закономерностей смещения наблюдающихся полос при увеличении длины углеводородного радикала солей, а не отнесения их к определенным видам колебаний. Большинство полос в этой области слабый или даже очень слабый.

Таблица III

Смещение максимумов полос поглощения в ИК-спектрах кристаллических образцов $CaAn_2 \cdot H_2O$ в области частот 1150—800 cm^{-1}

Отнесение Соль	$\begin{array}{c} \alpha \quad \beta \quad \gamma \\ \text{—C—C—C—} \\ \text{скелетн.} \end{array}$	$\begin{array}{c} \text{—C—C—} \\ \text{скелетн.} \end{array}$	$\begin{array}{c} \text{—C—C—} \\ \text{скелетные} \end{array}$	A	$\beta_{as} CO_2^-$	B	C	D
	+ деформационные кол. CH_2							
$CaAc_2$			1050	1025	960 945	930		880
$CaBt_2$	1100	1060	1050		965 955	930	900	880
$CaKon_2$	1115	1065	1050	1015	965 950	920	895	850
$CaKl_2$	1115	1065	1050	1005	960 940	920	985	835
$CaKin_2$	1115	1070	1060 1050 1035	995	960 940		890	825
$CaLr_2$	1115	1085	1050	990	960 940		875	820
$CaMir_2$	1115	1090	1040	990	960 940	910	860	820
$CaPm_2$	1115	1110	1070 ↔ 1035 1010	975	960 940	895	850	815
$CaSt_2$	1115		1080 ↔ 1030 990	975	960 940	880	845	815

Наиболее интенсивная полоса рассматриваемой области находится при 1115 cm^{-1} . Эта полоса отсутствует в спектре $CaAc_2$, но появляется в виде острого и достаточно сильного поглощения в спектре $CaBt_2$. В работе [17] полоса, найденная в спектре метилового эфира лауриновой кислоты (снятом в CCl_4) при 1112 cm^{-1} отнесена к C—C скелетным колебаниям алкильной цепи, связанной с концевой группой. Такое отнесение нам представляется весьма вероятным в виду того, что например, в спектре HLr отсутствует, вернее, имеется другая слабая острая полоса при 1085 cm^{-1} . Для сравнения нами был снят спектр лаурата натрия, в этом случае обнаруживалась только полоса при 1085 cm^{-1} . Таким образом, кажется достаточно обоснованным отнесение острой сильной полосы при 1115 cm^{-1} к C—C скелетным колебаниям α , β , γ углеродных атомов алкильных цепей солей кальция в твердом состоянии.

Имеющаяся поблизости полоса, смещающаяся от 1060 cm^{-1} $CaBt_2$ до 1110 cm^{-1} в виде плеча у $CaPm_2$ (в спектре $CaSt_2$ перекрывается полосой 1115 cm^{-1}) с большой вероятностью может быть отнесена к C—C скелетным колебаниям алкильных цепей вместе с деформационными колебаниями CH_2 -групп. Эта полоса обнаруживается как в спектрах лаурата натрия и HLr , так и в спектрах [18] кислот и их метиловых эфиров алкильного гомологического ряда.

Диффузная слабая полоса, находящаяся при 1050 cm^{-1} также относится к C—C скелетным колебаниям и, в соответствии с литературными данными [14, 18], наиболее интенсивна и расчленена на отдельные составляющие при 10 углеродных атомах в алкильной цепи. В спектрах $CaAn_2$, начиная от лаурата, для высших членов ряда происходит сначала уменьшение интенсивности, затем увеличение диффузности полосы.

Кроме перечисленных выше, найдены еще четыре очень слабые полосы, представленные в таблице III (А, В, С, D), максимумы которых с увеличением длины алкильной цепи смещаются в сторону меньших частот в среднем на 50—60 см⁻¹. Эти полосы могут быть пригодны только для установления идентичности отдельных солей.

В рассматриваемой области частот, кроме полосы при 1115 см⁻¹ в гомологическом ряду не смещаются максимумы только двух весьма слабых полос, находящихся при 960 и 940 см⁻¹. Эти полосы, вероятно, являются резонантами $\beta_{as}CO_2^-$ колебаний, имеющих основное поглощение в области частот 480—460 см⁻¹ [6, 9].

В области частот 800—650 см⁻¹ надежно установленной является полоса соответствующая асимметричным деформационным колебаниям в плоскости метиленовых групп $\beta_{as}CH_2$ алкильных цепей. Представленные в таблице IV данные, полученные нами, показывают, что в соответствии со взглядами изложенными в [2], только с большой осторожностью можно принимать в качестве характеристики кристалличности, расщепление полосы при 720 см⁻¹. Интенсивность этой полосы, как и следовало ожидать, возрастала с увеличением длины алкильной цепи.

Таблица IV

Смещение максимумов полос поглощения в ИК-спектрах кристаллических образцов $CaAn_2 \cdot nH_2O$ в области частот 800—650 см⁻¹

Отнесение Соль	Е	$\beta_{as}CH_2$	γ_{as} и/или $\gamma_s CO_2^-$
$CaAc_2$			680 ← 660
$CaBt_2$	780*	760 ← 740	660
$CaKon_2$	780	760 → 730	670
$CaKil_2$	780	740 → 725	670
$CaKin_2$	780	740 → 725	680
$CaLr_2$	780	730 → 720	680
$CaMir_2$	785 760	720	680 ← 670
$CaPm_2$	785 765	720	680 ← 670
$CaSt_2$	785 765	720	700 680 ← 665

* в виде плеча на указываемой стрелкой полосе

Слабая полоса поглощения, обнаруживаемая при 780 см⁻¹ и расщепляющаяся для высших гомологов ряда, также относится к числу трудно устанавливаемых полос (полоса Е в табл. IV).

Несомненно представляет интерес полоса, появляющаяся в спектре $CaAc_2$ в виде резкого дублета при 680 и 660 см⁻¹. При увеличении длины цепи полоса становится все более диффузной. Согласно работам [19, 20], эта полоса должна быть отнесена к внеплоскостным деформационным колебаниям карбоксилата γ_{as} и/или $\gamma_s CO_2^-$, но, повидимому, на основные колебания накладывается влия-

ние колебаний алкильной цепи. Отнесение этой полосы нельзя считать надежным ввиду того, что и в спектре *HLr* наблюдается полоса при 690 см^{-1} . Отметим, что в спектре лаурата натрия нами найдена острая полоса поглощения при 700 см^{-1} .

Таким образом, из вышеизложенного, на основании анализа полученных экспериментальных данных по гомологическому ряду, можно сделать некоторые заключения относительно ИК-спектров кальциевых солей алифатических одноосновных кислот.

Полоса поглощения ν_{OH} , находящаяся при 3400 см^{-1} , для количественного определения содержания воды в изученных солях, с применением *KBr*-ных таблеток, непригодна.

Гидратная вода солей, обычно дающая полосу поглощения β_{H-O-H} при $1630\text{—}1615\text{ см}^{-1}$, вследствие перекрывания с карбоксилатными колебаниями у короткоцепных солей, также трудно устанавливаемая.

В области проявления $\nu_s CO_2^-$, вследствие наложения полосы $\beta_s \alpha-CH_2$ для изученного ряда слей *CaAn₂* только начиная от капроната и выше представляется возможность отнести полосу, находящуюся при 1425 см^{-1} , к симметричным валентным колебаниям карбоксилатной группы. Однако, необходимо отметить, что если симметричные деформационные колебания в плоскости $\alpha-CH_2$ групп дают в солях *CaAn₂* расщепленную на дублетную достаточно сильную полосу, то возможно, что полоса соответствующая $\nu_s CO_2^-$ перекрывается и не обнаруживается.

Анализ области прогрессии полбс позволил нам предположить, что две слабые полосы, берущие свое начало при 1270 и 1240 см^{-1} в спектре *CaAc₂*, и постепенно смещающиеся в сторону меньших частот, могут быть отнесены к валентным колебаниям углеродных атомов конца цепей. Отделение двух вышеупомянутых полос от обычно принятой области прогрессии полос обусловленных $\gamma_{as} CH_2 + \gamma_s CH_2 + C-C_{\text{скелетн.}}$ колебаниями алкильных цепей связанных с полярной группой показало, что количество приблизительно эквидистантных полос для исследованного ряда солей *CaAn₂* находится в соответствии с правилом Джонса, начиная уже от *CaBt₂*, а не только для высших членов гомологического ряда [3, 16].

В области «отпечатки пальцев» спектров найден ряд полос, кроме известных уже из литературы «серии 1050 см^{-1} » [14] и $\beta_{as} CH_2$, которые показывают закономерное смещение в сторону меньших частот на $50\text{—}65\text{ см}^{-1}$ в исследованном ряду: полосы А, В, С, и D.

Характер полбс, находящихся при 1115 см^{-1} и около 670 см^{-1} , позволяет предположить, что они могут быть после дальнейшего более точного их отнесения, использованы для идентификации и установления структуры различных солей карбоновых кислот.

Литература

- [1] Nakamoto, K.: *Infrared Spectra of Inorganic and Coordination Compounds*, J. Wiley and Sons, New York. 1963.
- [2] Беллами, Л.: Новые данные по ИК-спектрам сложных молекул «Мир», Москва. 1971.
- [3] Meiklejohn, R. A., R. J. Meyer, S. M. Aronovic, H. A. Schuette, V. W. Meloch: *Anal. Chem.* 29, 329 (1957).

- [4] *Андор, И. А., Я. Киш.*: Acta Phys. et Chem. Szeged **21**, 143 (1975).
- [5] *Gyenes, I.*: Titrationen in Nichtwässrigen Medien, Akadémiai Kiadó, Budapest. 1970. S. 245.
- [6] *Holly, S., P. Sohár.*: Infravörös spektroszkópia (Инфракрасная спектроскопия), Műszaki Könyvkiadó, Budapest. 1968.
- [7] *Андор И., Я. Балаж, С. В. Фелдьман.*: Acta Phys. et Chem. Szeged **20**, 157 (1974).
- [8] *Gmelins Handbuch, Calcium Teil B 1, Syst. Num. 28.* Verlag Chemie, GmbH., Weinheim. 1956. S. 162.
- [9] *Ellis, B., H. Pyszora.*: Nature **181**, 181 (1958).
- [10] *Nakatomo, K., P. J. McCarthy.*: Spectroscopy and Structure of Metal Chelate Compounds, J. Wiley and Sons, New York. 1968.
- [11] *Fodor, G.*: Szerves Kémia, I. köt. (Органическая химия, т. I.), Tankönyvkiadó, Budapest. 1960. ст. 183.
- [12] *Наканиси, К.*: Инфракрасные спектры и строение органических соединений, «Мир», Москва. 1965. ст. 72.
- [13] *Spinner, E.*: J. Chem. Soc. **1964**, 4217.
- [14] *Brown, J. K., N. Sheppard.*: Trans. Faraday Soc. **50**, 535 (1954).
- [15] *Jones, R. N., A. F. McKay, R. G. Sinclair.*: J. Amer. Chem. Soc. **74**, 2575 (1952).
- [16] *Childers, E., G. W. Struthers.*: Anal. Chem. **27**, 737 (1955).
- [17] *Jones, R. N.*: Canad. J. Chem. **40**, 301 (1962).
- [18] *Jones, R. N.*: Canad. J. Chem. **40**, 321 (1962).
- [19] *Hummel, D.*: Identification and Analysis of Surface-Active Agent (Text Volume), Intersci. Publ. 1962., p. 46.
- [20] *Салимов, М. А., В. А. Пчелин, А. В. Керимбеков.*: Ж. физ. химии **37**, 2285 (1963).

INVESTIGATION OF THE STRUCTURE AND CHARACTERISTICS OF LONG CHAIN FATTY ACID SALTS, II.

Infrared Spectroscopy of the Calcium Salts of Aliphatic Monoacids

J. A. Andor, Z. Kiss and J. Balázs

It was pointed out that calcium salts of monoacids having even carbon number can be produced for caproic acid to stearic acid by interface reaction of dynamic emulsions (IFR). The composition of formed salts by IFR was determined by TG, X-ray and IR and the crystal structure was proved. IR spectra of calcium salts formed from acetic acid to stearic acid in the region from 3800 to 650 cm^{-1} were discussed in detail.

INVESTIGATIONS ON ISOQUINOLINES

Preparation of Carboxamides with Potential Pharmacological Activity, III* Synthesis of 6,7-Dimethoxy-1,2,3,4-tetrahydro-1-isoquinolineacetamides

By

J. KÓBOR

Chair of Chemistry, Gyula Juhász Pedagogical High School, Szeged

and

G. BERNÁTH

Institute of Organic Chemistry, Attila József University, Szeged.

(Received February 3, 1975)

The preparation of fifteen 6,7-dimethoxy-1,2,3,4-tetrahydro-1-isoquinolineacetamides is described. The mixed anhydride of 2-carbobenzyloxy-6,7-dimethoxy-1,2,3,4-tetrahydro-1-isoquinolineacetic acid with isobutyl chloroformate was reacted with the corresponding amines at -10 to -15°C . The carbobenzyloxy protecting group was removed from the 2-carbobenzyloxy-6,7-dimethoxy-1,2,3,4-tetrahydro-1-isoquinolineacetamides by means of HBr in acetic acid:

In the course of our work aiming at the preparation of carboxamides with pharmacological activity, we earlier synthesized numerous *N*-acyl aminomethylcyclopentane and cyclohexane derivatives [1—3]. Similarly to related derivatives [4], these compounds proved to act on the central nervous system. Among the alicyclic β -amino carboxamides prepared subsequently [5, 6], numerous compounds proved to exert antypiretic, analgetic or narcosis enhancing effects. This circumstance prompted us to synthesize for pharmacological purposes some related carboxamide derivatives of 6,7-dimethoxy-1,2,3,4-tetrahydro-1-isoquinolineacetic acid, a β -amino acid used also in our earlier investigations [7].

With the aim of preparing tranquilizing and hypotensive azabenzopyridocolines and related compounds, LOMBARDINO *et al.* synthesized some 6,7-dimethoxy-1,2,3,4-tetrahydro-1-isoquinolineacetamides (6) [8, 9]. They obtained the isoquinolineacetamides from 1-carbethoxymethyl-6,7-dimethoxy-1,2,3,4-tetrahydroisoquinolines (1) by refluxing under nitrogen protecting blanket with a high excess of the corresponding amine for 24 hrs. However, the yield, *e.g.* in the case of the 6,7-dimethoxy-1,2,3,4-tetrahydro-1-isoquinoline-*N*-*n*-butylacetamide, was only 50%. Though the yields reached with amines of higher boiling points were somewhat higher and also a recent application of the method is known [10], it seemed desirable to attempt the application of another way of synthesis.

* Part II: G. Bernáth, L. Gera, Gy. Göndös, I. Pánovics, Z. Ecsery: Acta Chim. (Budapest) 89, 61 (1976).

Table I

 α -[1-(2-Carbobenzyloxy-6,7-dimethoxy-1,2,3,4-tetrahydroisoquinolyl)]-acetamides (5a-o)

No.	R	Formula, Molecular weight	M.p. (°C); Solvent of crystallization	Analysis (%)		
				C	H	N
5a		$C_{24}H_{30}N_2O_5$ 426.50	158—160 Benzene—ether	67.58 67.83	7.09 7.23	6.57 6.28
5b		$C_{27}H_{34}N_2O_5$ 466.56	164—166 Benzene	69.50 69.15	7.35 7.24	6.01 6.25
5c		$C_{27}H_{26}N_2O_5$ 460.51	104—106 Benzene—ether	70.41 69.91	6.13 6.05	6.08 6.17
5d		$C_{28}H_{30}N_2O_5$ 474.54	168—169 Ethanol	70.86 70.81	6.37 6.41	5.90 6.16
5e		$C_{27}H_{27}FN_2O_5$ 478.50	142—144 Benzene—ether	67.77 67.47	5.69 5.75	5.86 6.00
5f		$C_{27}H_{27}BrN_2O_5$ 539.41	152—154 Ethanol—ether	60.11 59.86	5.04 5.00	5.19 5.09
5g		$C_{28}H_{30}N_2O_6$ 490.54	145 Benzene—petro- leum ether	68.55 68.87	6.16 6.55	5.71 5.85
5h		$C_{29}H_{30}N_2O_6$ 502.55	185—186 Benzene	69.30 69.64	6.02 6.63	5.58 6.02

Table I (Continued)

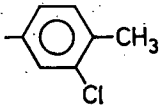
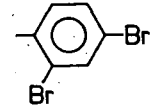
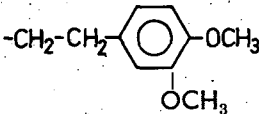
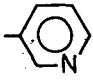
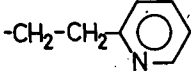
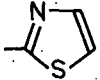
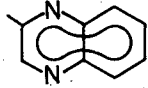
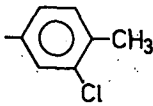
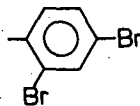
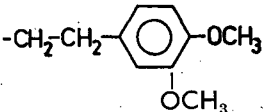
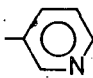
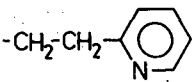
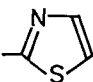
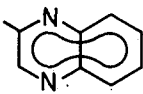
No.	R	Formula, Molecular weight	M.p. (°C); Solvent of crystallization	Analysis (%)		
				Calcd./Found C	H	N
5i		$C_{28}H_{29}ClN_2O_5$ 508.99	125—126 Benzene—ether	66.07 66.40	5.74 6.01	5.51 5.74
5j		$C_{27}H_{29}Br_2N_2O_5$ 618.33	168—169 Benzene	52.44 52.55	4.24 4.46	4.53 4.41
5k		$C_{31}H_{36}N_2O_7$ 548.61	132—134 Benzene—ether	67.86 68.02	6.61 6.55	5.10 5.85
5l		$C_{26}H_{27}N_3O_5$ 461.50	113—115 Benzene—ether	67.66 67.32	5.90 6.15	9.11 8.92
5m		$C_{28}H_{31}N_3O_5$ 489.56	119—121 Benzene—ether	68.69 68.85	6.38 6.46	8.58 8.46
5n		$C_{24}H_{25}N_3O_5S$ 467.47	Oil	61.66 62.02	5.39 5.56	8.99 8.75
5o		$C_{29}H_{27}N_4O_5$ 512.55	166—167 Ethanol—ether	67.91 67.89	5.50 5.95	10.93 10.85

Table II

 α -[1-(6,7-Dimethoxy-1,2,3,4-tetrahydroisoquinolyl)]-acetamides (6a - o)

No.	R	Formula, Molecular weight	M.p. (°C); Solvent of crystalliza- tion	Analysis (%)				Note
				C	H	N	Br	
6a		$C_{10}H_{25}BrN_2O_3$ 273.29	192—193 Ethanol— water 4:1	51.47 50.94	6.75 6.91	7.50 7.60	21.40 21.62	a)
6b		$C_{19}H_{29}BrN_2O_3$ 413.36	184—186 Ethanol	55.20 55.23	7.07 7.20	6.78 6.71	19.33 18.99	a)
6c		$C_{19}H_{23}BrN_2O_3$ 407.31	232—233 Ethanol— water 3:2	56.02 55.92	5.69 5.67	6.88 6.49		
6d		$C_{20}H_{25}BrN_2O_3$ 421.34	253—254 Ethanol— water 3:2	57.01 57.25	5.98 6.10		18.97 18.67	a)
6e		$C_{19}H_{22}BrFN_2O_3$ 425.30	232—234 Ethanol— water 4:1	53.65 54.02	5.21 5.35	6.59 6.14	18.19 18.18	a)
6f		$C_{19}H_{22}BrN_2O_3$ 486.22	234—236 Ethanol— water 3:2	46.93 46.80	4.56 4.50		32.87 32.90	b)
6g		$C_{20}H_{25}BrN_2O_4$ 437.33	238—239 Ethanol— water 2:3	54.92 55.12	5.76 5.69	6.40 6.63		
6h		$C_{21}H_{25}BrN_2O_4$ 449.35	206—208 Ethanol— water 7:3	56.13 55.98	5.61 5.85	6.24 6.17		

Table II (Continued)

No.	R	Formula, Molecular weight	M.p. (°C); Solvent of crystalliza- tion	Analysis (%)				Note
				Calcd./Found	C	H	N	
6i		$C_{20}H_{24}BrClN_2O_3$ 455.79	224—225 Ethanol— water 4:1	52.70 53.01	5.31 5.48	6.15 6.11	17.53 17.40	a)
6j		$C_{19}H_{21}Br_3N_2O_3$ 565.13	207—208 Ethanol— water 9:1	40.38 40.79	3.75 3.93	4.96 4.91	14.13 14.57	a)
6k		$C_{23}H_{31}ClN_2O_5$ 450.95	194—195 Ethanol— ether	61.26 61.10	6.93 6.78	6.21 6.39		c)
6l		$C_{18}H_{23}Br_2N_3O_3 \cdot H_2O$ 507.24	224—226 Ethanol— water 9:1	42.61 42.36	4.96 5.12	8.28 8.66	31.51 30.98	e)
6m		$C_{20}H_{25}N_3O_3$ 355.43	104 Benzene — ether	67.58 68.02	7.09 7.17		11.82 11.99	d)
6n		$C_{16}H_{20}BrN_3O_3S$ 414.27	238—240 Ethanol— water 1:1	46.39 46.53	4.87 5.03		19.29 19.12	a)
6o		$C_{21}H_{23}BrN_4O_3 \cdot H_2O$ 477.36	192—194 Ethanol— water 7:3	52.83 52.83	5.28 5.23	11.74 11.38	16.76 16.48	e)

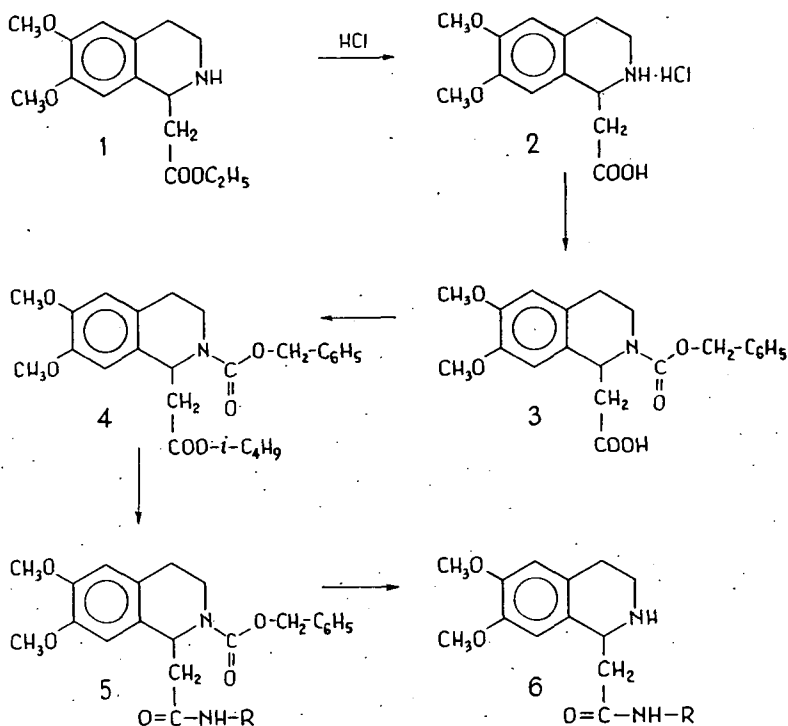
Note: a) Ionic bromide.

b) Ionic + covalent bromide.

c) Hydrochloride. Cl^- Calcd.: 7.86%. Found: 7.90%. Base: $C_{23}H_{30}N_2O_3$ (414.49). Calcd.: C 66.64; H 7.29; N 6.76. Found: C 66.70; H 7.56; N 6.86%.

d) Base.

e) Analysis for this compound with one mole crystal water is satisfactory.



The mixed anhydride method [11] used in peptide chemistry appeared suitable for this purpose. The secondary amino group of the 1-carboxymethyl-6,7-dimethoxy-1,2,3,4-tetrahydroisoquinoline (2) obtained by HCl hydrolysis of 1-ethoxycarbonylmethyl-6,7-dimethoxy-1,2,3,4-tetrahydroisoquinoline (1) was protected by benzyl chloroformate. The mixed anhydride of 2-carboxybenzyl-6,7-dimethoxy-1,2,3,4-tetrahydro-1-isoquinolineacetic acid with isobutyl chloroformate (4), formed in THF solution in the presence of triethylamine, was reacted with the corresponding amines at -10 to -15°C . The carbobenzyloxy-6,7-dimethoxy-1,2,3,4-tetrahydro-1-isoquinolineacetamides (5a—o) (Table I) were obtained with a very good yield (about 80—90%). The carbobenzyloxy protecting group was removed by HBr in acetic acid.

It has to be mentioned, that the use of the *p*-toluenesulfonyl protecting group in preparing the amides of related β -amino acids is also found. In a recent paper [12] ARMAREGO pointed out that the reaction of *cis*-hexahydroantranilic acid with alcoholic methyl amine or ammonia solution being slow, he prepared the desired amides from acid chlorides using *p*-toluenesulfonyl protecting group. Removal of the *p*-toluenesulfonyl protecting group is, however, possible only by sodium in liquid ammonia. Protection of the amino acid by benzyloxycarbonyl group proved not suitable because debenzoylation occurred during the preparation of the acid

chloride. The method described in our paper is similar to that found suitable also by ARMAREGO.

The results of pharmacological testing of the 6,7-dimethoxy-1,2,3,4-tetrahydro-1-isoquinolineacetamides (**6a—o**) prepared will be dealt with elsewhere.

Experimental

2-Carbobenzyloxy-6,7-dimethoxy-1,2,3,4-tetrahydro-1-isoquinolineacetic acid (**3**)

28.7 g (0.1 mole) 6,7-Dimethoxy-1,2,3,4-tetrahydro-1-isoquinoline acetic acid hydrochloride (**2**) was solved under stirring in 50 ml aqueous solution of 4 g sodium hydroxide; and 17 g (0.1 mole) benzyl chloroformate was added dropwise in 30 minutes under cooling. Then the cooled reaction mixture was stirred for further 3 hrs and acidified with 40 ml 20% HCl solution. The white crystals obtained were recrystallized from benzene—ether mixture. M.p. 153—154 °C, yield 32.5 g (84.4%).

$C_{21}H_{23}O_6N$ (385.40). Calcd. C 65.44; H 6.01; N 3.63. Found C 65.26; H 5.90; N 3.46%.

2-Carbobenzyloxy-6,7-dimethoxy-1,2,3,4-tetrahydro-1-isoquinoline acetamides (**5a—o**)

0.02 mole 2-Carbobenzyloxy-6,7-dimethoxy-1,2,3,4-tetrahydro-1-isoquinolineacetic acid (**3**) solved in 80 ml abs. tetrahydrofuran was cooled in an ice—salt cooling mixture to -10 to -15 °C, then 5 ml each of the tetrahydrofuran solutions of 0.02 mole triethylamine and 0.02 mole isobutyl chloroformate were added simultaneously in 5 minutes under intensive stirring. After further 5 minutes stirring 0.02 mole of the corresponding amine solved in 20 ml tetrahydrofuran was added dropwise to the reaction mixture, stirred for further 5 hrs and left to stand overnight. The triethylamine hydrochloride precipitated was filtered, washed twice with 5 ml tetrahydrofuran, then the combined tetrahydrofuran solution was evaporated in vacuum. The residue was dissolved in 70 ml ethyl acetate, washed with 2×6 ml water and with 1% sodium hydroxide solution, finally washed to neutrality with 4×5 ml water. After drying over sodium sulfate, the ethyl acetate was evaporated in vacuum and the residue was crystallized. The data of the products obtained (**5a—o**) are summarized in Table I.

6,7-Dimethoxy-1,2,3,4-tetrahydro-1-isoquinolineacetamides (**6a—o**)

To 0.015 mole 2-carbobenzyloxy-6,7-dimethoxy-1,2,3,4-tetrahydro-1-isoquinoline acetamides (**5a—o**) 4 to 5 equivalents of a 30% HBr solution in glacial acetic acid was added. Shaking the mixture, a homogeneous solution was obtained which solidified after 30 to 50 minutes. The precipitation of the carboxamide hydrobromide was completed by adding ether. The crystalline product obtained was washed thoroughly with ether, then with acetic acid and recrystallized after drying. The compounds synthesized (**6a—o**) are listed in Table II.

References

- [1] Bernáth, G., E. Csókási, I. Hevér, L. Gera, K. Kovács: Acta Chim. (Budapest) 70, 271 (1971).
- [2] Bernáth, G., K. Kovács, E. Pálosi, P. Görög, L. Szporny: Hung. Pat. 156.542, 25. Apr., 1969.
- [3] Bernáth, G., K. Kovács, E. Pálosi, P. Görög, L. Szporny: Austrian Pat. 286.959, 11 Jan., 1971.
- [4] Lee, J., Ziering, A., Berger, L., Heineman, S. D.: The Synthesis of Analgesic Compounds. Jubilee Volume Emile Barel, 1946, p. 264—305; C. A. 41, 6246 (1947).
- [5] Bernáth, G., L. Gera, Gy. Göndös, K. Kovács, Z. Ecsery, L. Tardos: Hung. Pat. appl., 1975.
- [6] Bernáth, G., L. Gera, Gy. Göndös, I. Pánovics, Z. Ecsery: Acta Chim. (Budapest) 89, 61 (1976).
- [7] Kóbor, J.: Szegedi Tanárképző Főiskola Tudományos Közleményei. 1967, 41.
- [8] Lombardino, J. G., J. I. Bodin, C. F. Gerber, W. M. McLamore, G. D. Laubach: J. Med. Pharm. Chem. 3, 505 (1961).
- [9] Lombardino, J. G., W. M. McLamore, G. D. Laubach: U.S. Pat. 3.021.331, 13 Feb., 1962; C. A. 57, 786d (1962).
- [10] Montzka, T. A., J. D. Matiskella: U.S. Pat. 3.654.281, 4 Apr. 1972; C. A. 77, 19.688a (1972).
- [11] Wieland, T., B. Heinke, K. Vogeler, H. Morimoto: Annalen 655, 189 (1962).
- [12] Armarego, W. L. F., P. A. Reece: J.C.S. Perkin I. 1974, 2313.

ИССЛЕДОВАНИЕ ПРОИЗВОДНЫХ ИЗОХИНОЛИНА, III.
СИНТЕЗ ПОТЕНЦИАЛЬНЫХ ФАРМАКОНОВ АМИДНОГО ХАРАКТЕРА.
СИНТЕЗ 6,7-ДИМЕТОКСИ-1,2,3,4-ТЕТРАГИДРО-1-ИЗОХИНОЛИНАЦЕТАМИДОВ

Е. Кобор и Г. Бернат

Сообщается о синтезе производного 6,7-диметокси-1,2,3,4-тетрагидро-1-изохинолин-ацетамида. Из 2-карбобензилокси-6,7-диметокси-1,2,3,4-тетрагидро-1-изохинолинуксусной кислоты и изобутил-хлорформата образовавшийся смешанный ангидрид был введен в реакцию с соответствующими аминами при температурах -10 и -15 °C. Из полученных 2-карбобензилокси-6,7-диметокси-1,2,3,4-тетрагидро-1-изохинолинацетамидов защитную карбобензилоксидную группу удаляли с помощью бромистого водорода в среде ледяной уксусной кислоты.

BOOK REVIEW

RADIATION DAMAGE PROCESSES IN MATERIALS

edited by

C. H. S. DUPUY

The book, containing the proceedings of the Summer School on Radiation Damage Processes in Materials, held on Corsica, France, August 27—September 9, 1973 was published in 1975.

The problem of radiation damages in materials became of high importance with the sharp development of nuclear physics in the last decades. After earlier studies essentially connected to the mechanism of defect creation, a better understanding of the processes seemed necessary. Approaches to the theory of damage processes led to a sharp increase in the number of such studies and as a result of strong development in the physics of the defect, the „saturation effect” caused by the wealth of new information prompted J. H. Crawford and the Editor to consider the necessity of organizing a Summer School in the field of „Radiation Damage Processes in Materials”, in order to summarize recent research work on this subject and, by discussions, to impulse new ideas to find new ways for research.

The lectures of the Summer School were classed in terms of mechanisms instead of being classed in terms of models. This resulted in very good review articles on theory and application of different processes by authors eminent in the study of the problems concerned.

The papers of the conference are grouped in three parts. In Part 1 dealing with general principles, we find a comprehensive paper on energy loss of charged particles in solids by P. Sigmund, and on the states of ions penetrating solids by S. Dats.

To illustrate the wide range of problems encompassed, may it suffice to give a list of the topics of Part 2. This part, dealing with different radiation damage processes, contains papers of M. N. Kabler in ionisation damage processes in inorganic materials, D. L. Griscom on color centers in oxide glasses, R. N. Nelson on radiation damage in metals and semiconductors, two papers of D. Pooley on collision damage processes in transparent materials and in ionic solids, respectively, papers of J. C. Bourgoin concerning ionisation effects on damage production in semiconductors, of M. Monin on track processes, E. Dartyge on formation of amorphous material, L. Slifkin on the photographic processes, and on radiolysis.

Part 3; devoted to applications, contains papers of J. C. Pfister on ion implantation, R. S. Nelson on damage to nuclear materials, and two papers of D. Pooley on application of radiation damage effects in dosimetry and in information storage, respectively.

The attractive presentation of the most instructive book of 534 pages, informing about the recent state of knowledge concerning the problems involved is the result of the care of the publisher, the Nordhoff International Publishing Company, Leyden.

M. I. TÖRÖK
*(Institute of Experimental Physics,
Attila József University, Szeged)*



A kiadásért felelős: Dr. Tandori Károly
1976

A kézirat nyomdába érkezett: 1976. március. Megjelenés 1976. október
Példányszám: 550. Ábrák száma 68. Terjedelem: 11,9 (A/5) ív
Készült monószedéssel, íves magasnyomással, az MNOSZ 5601—50/A szabványok szerint
76-1657 — Szegedi Nyomda — F. v.: Dobó József íg.

TOMI PRIORES

Acta Chemica, Mineralogica et Physica	Tom. I,	Fasc. 1—2,	1028—29.
Acta Chemica, Mineralogica et Physica	Tom. II,	Fasc. 1—2,	1932.
Acta Chemica, Mineralogica et Physica	Tom. III,	Fasc. 1—3,	1934.
Acta Chemica, Mineralogica et Physica	Tom. IV,	Fasc. 1—3,	1934.
Acta Chemica, Mineralogica et Physica	Tom. V,	Fasc. 1—3,	1937.
Acta Chemica, Mineralogica et Physica	Tom. VI,	Fasc. 1—3,	1938.
Acta Chemica, Mineralogica et Physica	Tom. VII,	Fasc. 1—3,	1939.
Acta Chemica et Physica	Tom. I,	Fasc. 1—2,	1942.
Acta Chemica et Physica	Tom. II,	Fasc. 1—6,	1948—50.
Acta Physica et Chemica, Nova series	Tom. I,	Fasc. 1—4,	1955.
Acta Physica et Chemica, Nova series	Tom. II,	Fasc. 1—4,	1956.
Acta Physica et Chemica, Nova series	Tom. II,	Fasc. 1—5,	1957.
Acta Physica et Chemica, Nova series	Tom. IV,	Fasc. 1—2,	1958.
Acta Physica et Chemica, Nova series	Tom. IV,	Fasc. 3—4,	1958.
Acta Physica et Chemica, Nova series	Tom. V,	Fasc. 1—2,	1959.
Acta Physica et Chemica, Nova series	Tom. V,	Fasc. 3—4,	1959.
Acta Physica et Chemica, Nova series	Tom. VI,	Fasc. 1—4,	1960.
Acta Physica et Chemica, Nova series	Tom. VII,	Fasc. 1—2,	1961.
Acta Physica et Chemica, Nova series	Tom. VII,	Fasc. 3—4,	1961.
Acta Physica et Chemica, Nova series	Tom. VIII,	Fasc. 1—2,	1962.
Acta Physica et Chemica, Nova series	Tom. VIII,	Fasc. 3—4,	1962.
Acta Physica et Chemica, Nova series	Tom. IX,	Fasc. 1—2,	1963.
Acta Physica et Chemica, Nova series	Tom. IX,	Fasc. 3—4,	1963.
Acta Physica et Chemica, Nova series	Tom. IX,	Fasc. 3—4,	1963.
Acta Physica et Chemica, Nova series	Tom. X,	Fasc. 1—2,	1964.
Acta Physica et Chemica, Nova series	Tom. X,	Fasc. 3—4,	1964.
Acta Physica et Chemica, Nova series	Tom. XI,	Fasc. 1—2,	1965.
Acta Physica et Chemica, Nova series	Tom. XI,	Fasc. 3—4,	1965.
Acta Physica et Chemica, Nova series	Tom. XII,	Fasc. 1—2,	1966.
Acta Physica et Chemica, Nova series	Tom. XII,	Fasc. 3—4,	1966.
Acta Physica et Chemica, Nova series	Tom. XIII,	Fasc. 1—2,	1967.
Acta Physica et Chemica, Nova series	Tom. XIII,	Fasc. 3—4,	1967.
Acta Physica et Chemica, Nova series	Tom. XIV,	Fasc. 1—2,	1968.
Acta Physica et Chemica, Nova series	Tom. XIV,	Fasc. 3—4,	1968.
Acta Physica et Chemica, Nova series	Tom. XV,	Fasc. 1—2,	1969.
Acta Physica et Chemica, Nova series	Tom. XV,	Fasc. 3—4,	1969.
Acta Physica et Chemica, Nova series	Tom. XVI,	Fasc. 1—2,	1970.
Acta Physica et Chemica, Nova series	Tom. XVI,	Fasc. 3—4,	1970.
Acta Physica et Chemica, Nova series	Tom. XVII,	Fasc. 1—2,	1971.
Acta Physica et Chemica, Nova series	Tom. XVII,	Fasc. 3—4,	1971.
Acta Physica et Chemica, Nova series	Tom. XVIII,	Fasc. 1—2,	1972.
Acta Physica et Chemica, Nova series	Tom. XVIII,	Fasc. 3—4,	1972.
Acta Physica et Chemica, Nova series	Tom. XIX,	Fasc. 1—2,	1973.
Acta Physica et Chemica, Nova series	Tom. XIX,	Fasc. 3,	1973.
Acta Physica et Chemica, Nova series	Tom. XIX,	Fasc. 4,	1973.
Acta Physica et Chemica, Nova series	Tom. XX,	Fasc. 1—2,	1974.
Acta Physica et Chemica, Nova series	Tom. XX,	Fasc. 3,	1974.
Acta Physica et Chemica, Nova series	Tom. XX,	Fasc. 4,	1974.
Acta Physica et Chemica, Nova series	Tom. XXI,	Fasc. 1—2,	1975.
Acta Physica et Chemica, Nova series	Tom. XXI,	Fasc. 3—4,	1975.

INDEX

<i>I. K. Gyémánt, M. G. Benedict, Gy. Papp and B. Vasvári: Multiple Scattering Xα Treatment of Scattering States of Clusters</i>	3
<i>V. Maráz: Integral Expressions for $(nl n'l')$ with $n, n' = 3, 4$</i>	7
<i>E. Vozáry and L. Szalay: Transfer of Electronic Excitation Energy in Protein-Detergent Solutions</i>	17
<i>C. Bojarski and R. Bujko: Concentration Depolarization by Excitation Transfer. Selfquenching Considerations</i>	25
<i>Л. Козма, З. Фаркаш, И. Кечкемети и М. Молнар: О природе фотопродуктов генерирующих красителей</i>	33
<i>Л. Козма, К. Чернаи, И. Кечкемети, Б. Рац и Ж. Бор: Исследование генерации потушенных растворов флуоресцеина</i>	41
<i>A. Süli, S. D. Kurmashev, L. Michailovits and I. Hevesi: Photoconductivity of V₂O₅-Si Sandwich System</i>	45
<i>M. Tölgyesi, T. Bérces and A. Nacsá: The Role of Excited States in the Photolysis of <i>n</i>-Butyraldehyde, I. Triplet State Quenching by Piperylene</i>	57
<i>F. Solymosi: Kinetics and Mechanism of the Thermal Decomposition of Metal Chlorites, Chlorates, and Perchlorates (Review)</i>	75
<i>И. А. Андор, З. Киш и Я. Балажс: Исследование структуры и свойств мыл, II. Инфракрасные спектры кальциевых солей алифатических одноосновных кислот</i>	117
<i>J. Kóbór and G. Bernáth: Investigations on Isoquinolines. Preparation of Carboxamides with Potential Pharmacological Activity, III. Synthesis of 6,7-Dimethoxy-1,2,3,4-tetrahydro-1-isoquinolineacetamides</i>	127
<i>M. I. Török: Book review</i>	135

